NASA/CR–2010-216854

Flexible Material Systems Testing

John K. Lin, Lauren S. Shook, Joanne S. Ware, and Joseph V. Welch
ILC Dover, LP, Frederica, Delaware

October 2010

NASA STI Program . . . in Profile

Since its founding, NASA has been dedicated to the advancement of aeronautics and space science. The NASA scientific and technical information (STI) program plays a key part in helping NASA maintain this important role.

The NASA STI program operates under the auspices of the Agency Chief Information Officer. It collects, organizes, provides for archiving, and disseminates NASA's STI. The NASA STI program provides access to the NASA Aeronautics and Space Database and its public interface, the NASA Technical Report Server, thus providing one of the largest collections of aeronautical and space science STI in the world. Results are published in both non-NASA channels and by NASA in the NASA STI Report Series, which includes the following report types:

- TECHNICAL PUBLICATION. Reports of completed research or a major significant phase of research that present the results of NASA programs and include extensive data or theoretical analysis. Includes compilations of significant scientific and technical data and information deemed to be of continuing reference value. NASA counterpart of peer-reviewed formal professional papers, but having less stringent limitations on manuscript length and extent of graphic presentations.

- TECHNICAL MEMORANDUM. Scientific and technical findings that are preliminary or of specialized interest, e.g., quick release reports, working papers, and bibliographies that contain minimal annotation. Does not contain extensive analysis.

- CONTRACTOR REPORT. Scientific and technical findings by NASA-sponsored contractors and grantees.

- CONFERENCE PUBLICATION. Collected papers from scientific and technical conferences, symposia, seminars, or other meetings sponsored or co-sponsored by NASA.

- SPECIAL PUBLICATION. Scientific, technical, or historical information from NASA programs, projects, and missions, often concerned with subjects having substantial public interest.

- TECHNICAL TRANSLATION. English-language translations of foreign scientific and technical material pertinent to NASA's mission.

Specialized services also include creating custom thesauri, building customized databases, and organizing and publishing research results.

For more information about the NASA STI program, see the following:

- Access the NASA STI program home page at *http://www.sti.nasa.gov*

- E-mail your question via the Internet to help@sti.nasa.gov

- Fax your question to the NASA STI Help Desk at 443-757-5803

- Phone the NASA STI Help Desk at 443-757-5802

- Write to:
  NASA STI Help Desk
  NASA Center for AeroSpace Information
  7115 Standard Drive
  Hanover, MD 21076-1320

NASA/CR–2010-216854

Flexible Material Systems Testing

John K. Lin, Lauren S. Shook, Joanne S. Ware, and Joseph V. Welch
ILC Dover, LP, Frederica, Delaware

National Aeronautics and
Space Administration

Langley Research Center
Hampton, Virginia 23681-2199

Prepared for Langley Research Center
under Contract NNL09AC89D

October 2010

Acknowledgments

The work presented herein was performed for NASA Langley Research Center and NASA Ames Research Center, under task order NNL09AC89D, in support of the Flexible Materials Systems Testing program. The authors would like to thank Charles Player from NASA Langley Research Center and Scott Murman from NASA Ames Research Center for their support.

Available from:

NASA Center for AeroSpace Information
7115 Standard Drive
Hanover, MD 21076-1320
443-757-5802

Table of Contents

List of Tables

List of Figures

1. Introduction

An experimental program has been undertaken to better characterize the stress-strain characteristics of flexible material systems to support a NASA ground test program for inflatable decelerator material technology. A goal of the current study is to investigate experimental methods for the characterization of coated woven material stiffness. This type of experimental mechanics data would eventually be used to define the material inputs of fluid-structure interaction simulation models. The test methodologies chosen for this stress-strain characterization are presented along with the experimental results.

This report covers work performed by ILC Dover, LP (ILC) in support of the Flexible Materials Systems Testing program toward the investigation and characterization of the material properties of various coated woven materials which may be appropriate for use in inflatable decelerators. This task order (NNL09AC89D) consists of the materials testing and experimental results from four candidate materials. These activities were performed during the time frame of September 2009 to May 2010.

2. Objective

A limited volume of mechanical property data is typically available when undertaking the structural analysis of inflatable aerodynamic structures fabricated with textile materials. The objective of this study is to provide a more comprehensive set of measured stress-strain behavior that will be used to support continued experimental and analytical work in this area.

The particular stress-strain behaviors of interest for this work are shown below.

- Normal stress versus strain
- Transverse contraction versus axial strain
- Shear stress versus shear strain

Figure 1 is an illustration of these stress terms relative to the warp and fill axes of the woven fabric. With these two orthogonal axes of the weave we have limited our focus to that of an orthotropic lamina.

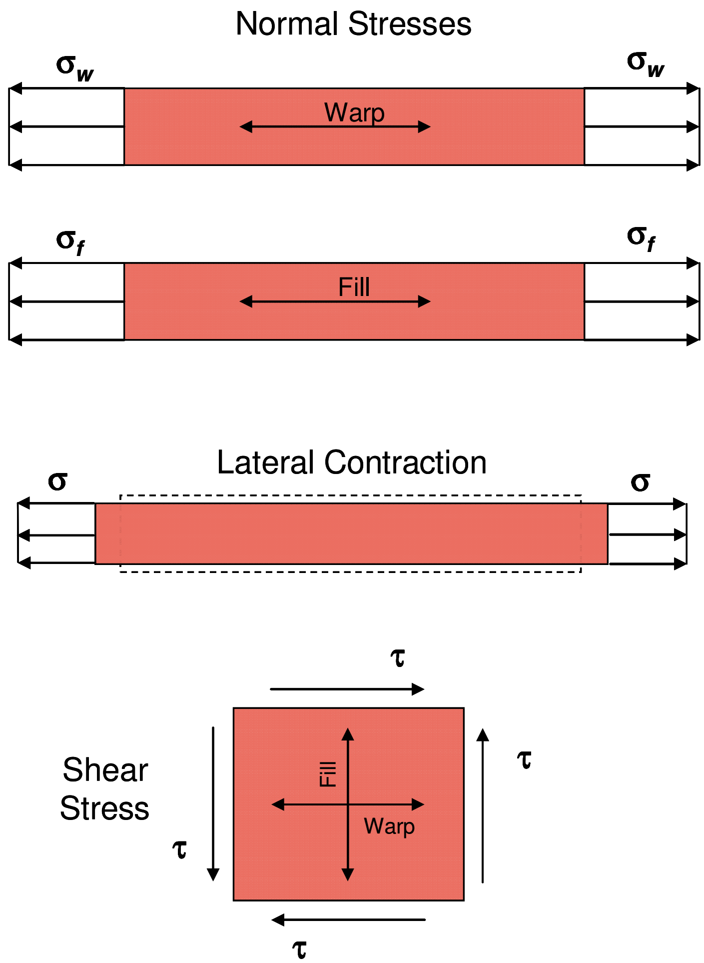

Figure 1: Textile stress and strains.

Some degree of both inelastic and non-linear behavior is expected in the stress-strain behavior of textiles. We are interested in observing the differences between the load ramp up and load ramp down portions of stress-strain curves. We also have the objective to observe the strain which persists after the stress that produced it is removed. In mechanics this is typically referred to as permanent set. Although for textile materials, this apparent set may not necessarily be permanent. The set up of the experiments for this task placed an emphasis on assigning a magnitude to these tendencies.

3. Materials

3.1 Material Descriptions

The number of materials selected for this experimental study was defined in the statement of work, which called for mechanical behavioral testing of six different coated fabrics. The fabrics ultimately selected were considered either "flight-like" materials or representative of materials used in wind tunnel experiments. The fabrics selected were Nylon, Nomex, and Kevlar. The coatings selected were chosen based on similar operational conditions for flight and wind tunnel testing. Silicone and urethane were selected to reduce the baseline porosity of the fabrics both for performance in anticipated wind tunnel studies and to represent the use of a coated fabric as the gas retaining layer of an inflated structural bladder in a flight article. The end-item fabrics specified for study are shown in Table 1.

Table 1: Textile material selection and rationale.

Textile Material	Rationale for Use
Zero-Porosity Parachute Nylon (F-111)	The fabric used for the 2009 Isotensoid Wind Tunnel Article, (Tanner and Cruz PAI-DAE study) and corresponding stress-strain behavioral testing, was the nylon basecloth manufactured IAW PIA44378D with a urethane scrape coat applied to one face.
Silicone Coated Plain Weave Nomex (2)	Nomex was selected for study for its high temperature, flame resistant and self-extinguishing capabilities when removed from the flame source.
Silicone Coated Plain Weave Kevlar (2)	The two materials used for study were used in the IRVE-II Flight Article. Both materials were used in the structural bladder skin, with the heavier material used to create the structural spars
Unbalanced, Silicone Coated, Fiber Type Not Specified	An unbalanced fabric was desired to open the trade space of the materials used and obtain some performance properties.

3.2 Baseline Fiber Properties

Although the materials to be tested during this effort were intended to be coated, the base fiber is the primary contributor to structural performance of the end item. Therefore, from a comparative point of view, it is important to understand the differences between the types of base fiber used in this study.

One of the main differences is that the polyamide (Nylon) is a flexible "melt" polymer, while the aramid fibers (Kevlar, Nomex) are more rigid, "non-melt" liquid crystalline polymers. The flexible chain polymers possess a random coil configuration and do not obtain a higher degree of order with increasing concentration. Conversely, the rigid polymers begin to align with increasing concentration and become structurally highly oriented polymer chains. Due to these random, flexible polymer chains, the Nylon has a significantly higher elongation than the Kevlar fibers. For the same reason, the rigid polymer chain materials have a higher tenacity and modulus than the Nylon.

Table 2: Fiber property comparison.

Fiber Type	Material Type	Density *(g/cc)*	Moisture Regain *(%)*	Elongation *(%)*	Breaking Tenacity *(g/d)*	Initial Modulus *(cN/tex)*
Nylon (6,6)	Polyamide	1.14	2.8 – 5.0	17-45	2.3 - 9.8	400
Nomex	Meta-aramid	1.38	4.5	28	4.0-5.3	839
Kevlar 29	Para-aramid	1.44	4.8	3.6	23.5	4900
Kevlar 129	Para-aramid	1.45	4.3	3.3	26.8	6810

Though the Nomex (meta-aramid) and the Kevlar (para-aramid) fibers are both in the aramid family, the differences in their properties are striking. These differences are due to the location of the amide linkages on their aromatic rings. This causes the Nomex to have a lower modulus and tensile capacity, as well as a higher percentage of elongation, when compared to the Kevlar as noted in Table 2.

3.3 Uncoated (Baseline) Fabric Properties

Fabrics meeting the fiber, weave balance, and thickness targets that were outlined in the statement of work were identified and traded so as to provide a reasonable subset of materials for study. The baseline characteristics of the uncoated fabrics selected for study, including Nylon, Nomex, and Kevlar, are found in Table 3.

Though many of a fabric's performance characteristics are directly related to the amount of yarns packed into a given area, a fabric's shear stiffness is directly dependent upon both the amount of yarns, as well as the weave type. Fabric properties can be tailored in a woven fabric development effort to the specific physical performance needs through the selection of yarn size twist, density, etc. for any or all of the $0^o/90^o/45^o$ directions. In this effort, the fabric construction properties of $0^o/90^o$ fabrics were considered when selecting materials for study. Choice of fabric construction properties were limited to those of existing, off-the shelf materials. The properties listed in Table 3 indicate the baseline properties of the all the uncoated fabrics, prior to coating.

Table 3: Baseline fabric properties of uncoated materials.

	ID	Denier (w x f)	Thread Count (yarns per inch)		Weave Type	Areal Density (oz/yd²)	Uncoated Fabric Thickness (inches)	Fabric Break Strength (lbs/in)	
			warp	fill				warp	fill
Nylon	F-111	30	126	132	ripstop	1.2	0.003	50	50
Nomex	HT1	200	101	92	basket	5.2	0.0096	229	216
	HT48	200	99	86	2x2 chain	5.1	0.0114	258	234
Kevlar	740	200	40	40	plain	2.1	0.005	337	327
	726	840	26	26	plain	5.8	0.010	760	770

3.4 Coating Effort

The requirements developed for testing were that the Nomex and Kevlar fabrics be tested with a silicone coating and the Nylon be tested with a urethane coating. Different coating processes were used for the materials selected, based on the fabric and the coating being applied.

The Kevlar materials used in the IRVE II flight article were available in the coated condition, so no additional coating effort was required. Both of the Kevlar fabrics (Style 740 and Style 726) fabrics had been primed with a silicone infused solution to promote adhesion and then calendered with a Dow Corning Silicone Rubber. The silicone coating effort planned for the Nomex fabric was different in that it was performed not by calendering, which presses the rubber into the fabric filling the interstices under extreme load, but via a solution coating process. In this instance, there was sufficient adhesion without a prime coat (which can stiffen the fabrics by locking in yarns). The rubber was put into solution with solvent and then coated onto the fabric while passing under a knife with a predetermined gap; this pushes the rubber solution into the interstices as the fabric passes under the knife. The same base silicone was used to coat both fabrics, is relatively soft in comparison to many other rubbers and has a minimum elongation of 400%.

The urethane coating of the Nylon fabric that was planned for this effort was to have replicated the coating process used to coat the Isotensoid IAD wind tunnel model tested at the LaRC Transonic Dynamics Tunnel in 2009. That coating process applied a very thin (scrape coat) layer of an aromatic polyether urethane to the surface of the fabric to further reduce the porosity through the fabric. In the scrape coating process, the fabric passes under a blade, but there is no measurable gap between the fabric and the blade. Here, the solution is essentially scraped over the surface as the fabric passes under the blade. Using this process with the very thin Nylon ripstop applied only a very thin layer of coating to the fabric.

Unfortunately, during the first run of the all the coating efforts that were planned, the allowable limit of volatile organic compounds (VOC's) found in the solvent solutions for that 24 hour period was exceeded, though only slightly. State and Federal statutes require that production stop while an investigation was conducted. This delay impacted the planned coating efforts and as a result only the HT1 construction of the Nomex fabrics was coated. The program schedule/funding source expired prior to receiving authorization to resume coating from State officials. Therefore, the testing matrix was revised and testing occurred only on the materials identified in Table 4.

Table 4: Test fabric properties.

Fiber Type	ID	Uncoated Areal Density *(oz/yd²)*	Uncoated Fabric Thickness *(inches)*	Coating Add-On *(oz/yd²)*	Final Areal Density *(oz/yd²)*	Final Thickness *(inches)*	Mean Fabric Density *(g/cm³)*
Nylon	F-111	1.2	0.003	NA	1.2	0.003	1.1534
Nomex	HT1	5.2	0.096	3.5	8.7	0.0124	1.1456
Kevlar*	740 (ST11-4545)	2.1	0.005	5.9	8.0	0.008	1.1099
Kevlar*	726 (ST11-4600)	5.8	0.010	4.4	10.2	0.014	1.0730

* The ST numbers assigned to the Kevlar fabrics are ILC's P/Ns of the coated goods

The decision to leave the uncoated Nylon Ripstop, F-111 in the test matrix while the other uncoated Nomex fabric, HT48 was eliminated was made due to the baseline porosities of the fabrics, and the intended use of the F-111 in NASA Ames wind tunnel testing that was to be conducted at a later date. The F-111 is considered to have an extremely low porosity according to ASTM D 737 (0.5-3.0 ft^3/minute at 0.5" water) compared to the Nomex HT48 (18.0 ft^3/minute at 0.5" water). The porosity of these fabrics is directly dependent upon their fabric constructions. The Nylon is a tightly packed plain weave/ripstop construction. The yarns used in both the warp and fill directions use 30 denier yarns which accommodates a tight packing condition with a 126 x 132 yarns per inch. This fabric has proven repeatedly that it can take shape when in an air stream, and would function in the planned wind tunnel tests at NASA Ames. The Nomex HT-48 chain weave is a much less dense construction made of 200 denier yarns in both the warp and filling directions and has a yarn density of 99 x 86 yarns per inch. This construction is much more porous and would not perform as needed in the wind tunnel experiments without the coating.

3.5 Fabric Density Determinations

Density determinations were made for each of the fabrics in this study using a Mettler Density Determination Kit, ME-33360. Three replicates of each of the four different fabrics evaluated in this study were used to obtain a mean density for that fabric. Considered a solid body, the density of the fabric was determined using a liquid of known density; this is also known as density measurements by hydrostatic weighing[i]. That liquid was distilled water and is considered a standard test liquid.

To calculate each value per replicate, each sample was first weighed in air and then immersed into the distilled water bath. Then, from a series of weightings, the density (ρ) was calculated. Two variables, bath temperature and air buoyancy, were included in the calculations to obtain the most accurate result. In general, temperature has only a slight effect on any density change of a solid body and as such is often disregarded in density determinations; however, in the case of liquids, the density may change on the order of 0.1 - 1.0% per C°. Therefore, in this evaluation, the temperature of the water (24.5°C) in which the sample was immersed was included. The buoyancy of solids also has an effect on the density of a solid as each cubic centimeter of air weighs 1.0 - 1.2 milligrams. Any object that is being weighed in air is subject to buoyancy for each cm^3 of its volume, meaning that with a density of 1 gm/cm^3, an error of 0.1% could occur if buoyancy was not taken into consideration. Therefore, buoyancy was included in these calculations.

Procedure:

1. Using the density determination kit, distilled water was poured into the beaker so that a sample would be covered with at least 10mm of the liquid.
2. The thermometer was inserted into the beaker and the entire set-up was placed on a bridge within in the balance.
3. The sample holder was attached to the set-up while ensuring that there were no air bubbles created within the bath or along the holder.
4. The balance tare read 0.0 grams
5. A sample was weighed in air (W_1)
6. The wire holder was weighed in air (W_2)
7. The balance is tared again (W_3)
8. The weighed sample was placed on the wire holder and immersed in the bath
9. Balance displays buoyancy (negative number) of the sample, (W_4)
10. Note the temperature to determine density of distilled water
11. Density of water at 23.5°C is 0.9972 g/cm^3

The equation used to calculate the density of each sample was:

$$\frac{W_1 - W_2}{W_1 + W_3 - W_4} * 0.9972$$

Therefore, the densities listed below are the mean values densities of the fabric samples.

Table 5: Fabric density.

	Fiber Density *(g/cm³)*	**Denier**	**Yarn Density** *(yarns/inch)*	**Coating Add-On** *(oz/yd²)*	**Mean Fabric Density** *(g/cm³)*
Uncoated Nylon (F-111)	1.14	30	126 x 132	NA	**1.1534**
Silicone Coated Nomex (Style HT1)	1.38	200	101 x 92	3.5	**1.1456**
Silicone Coated Kevlar (ST11-4545)	1.44	200	40 x 40	5.9	**1.1099**
Silicone Coated Kevlar (ST11-4600)	1.44	840	26 x 26	4.4	**1.0730**

4. Test Methods

4.1 Introduction

Four different test methods were used in this program to measure and characterize the normal stress-strain and shear stress-strain behavior of textile materials for the inflatable aerodynamic decelerators. Two of the test methods, namely Uni-axial and Cylindrical Biaxial tests, have been used in previous programs[ii]. These two tests were again used here, but with slight modification to include the capability of photogrammetry to capture additional data for comparison and correlation. In addition, two other shear stress-strain test methods, namely Trellis-Frame Test[iii iv] and Bias Extension Test[v], have been refined with photogrammetry capability to measure shear stress-strain behavior for comparison and correlation with the Cylindrical Biaxial test method. The goal of using several test methods to measure the same mechanical behavior is to determine which shear modulus test method will be best suited for future wind tunnel test correlation.

General test procedures were clearly defined in the internal Test Information Sheet with required test equipment and specimen preparation information. For test methods with special requirements, which are the case for this program, an additional test specimen was used to determine loading conditions. In the current test program, all tests were performed under laboratory ambient condition with standard room temperature, pressure and humidity. All test specimens, their quantity and quality (e.g. environmental conditioning), were prepared according to ASTM standards and/or best laboratory practices.

Samples for the uni-axial, trellis-frame, and bias extension tests were performed using an INSTRON test machine, model number 1125. Calibration data showed the machine results to be within ±0.2%. Two extensometers from MTS Systems Corporation were used during testing, a 9% extensometer (model number 632.11E-90) and a 50% extensometer (model number 634.12F-24.) The data showed that the 9% extensometer was within ±0.2% and the 50% extensometer was within ±0.4%.

Units of stress are reported in lbs/in, where the fabric thickness has been removed from the calculation. For fabrics, the stress is typically reported in units of load per width. The thicknesses for each of the fabrics are given in Table 6.

Table 6: Fabric Thickness.

Fabric	Thickness (in)
Kevlar, 200 denier	0.008
Kevlar, 840 denier	0.013
Nomex	0.013
F-111 Nylon	0.003

4.2 Uni-axial Test Method

The uni-axial test, see Figure 2, is one of the most common test methods for determining the stress-strain characteristics of textile materials. This test method is performed according to ASTM

D5035 -06(2008) e1 "Standard Test Method for Breaking Force and Elongation of Textile Fabrics (Strip Method)". In the strip tensile test, a narrow strip of fabric specimen is used. For this particular test program, the test specimens, five samples per material per condition, were three inches wide by 6 inches long with raveled uni-axial threads along the edges. This width was chosen so that an extensometer could be mounted horizontally on the strip sample so that transverse strain could be measured in addition to the axial strain. INSTRON test machine with grips wider than the test sample width was used to pull the specimen. In this study, the test has been modified with additional features to include measurement of the transverse strain. Pin mounted extensometer was used to measure the strain. The INSTRON load cell was used to provide the measurement for stress. Since the stress-strain characteristics of a textile are typically different in the orthogonal warp and fill fiber directions. Two sets of test samples are prepared for the uni-axial strip tensile method. One set of samples has the warp fibers running parallel to the axis of load application. A second set has the fill fibers running parallel to the axis of load application.

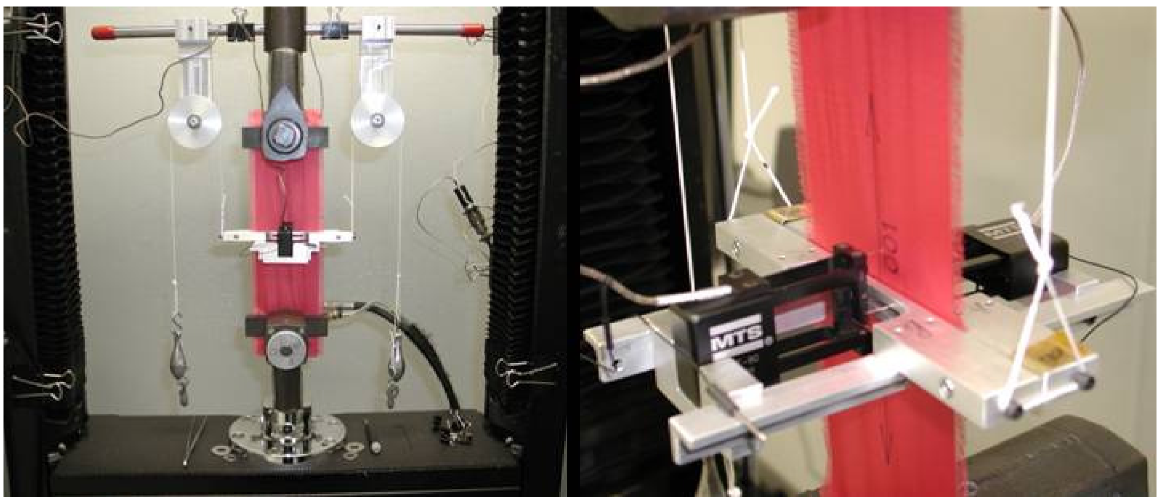

Figure 2: Uni-axial test setup in INSTRON test machine.

4.3 Shear Stress-Strain Test Methods

Several inter-laboratory approaches have been developed and used by industry and academia to measure the shear stress-strain behavior of textile materials. In this study, three methods, namely Trellis-Frame Test (also known as Picture-Frame Test), Bias Extension Test and Cylindrical Biaxial Test, were performed on several textile materials for comparison and correlation. As mentioned above, all three test methods have been enhanced to include the use of photogrammetry.

4.3.1 Trellis-Frame Test

The objective of the Trellis-Frame Test, see Figure 3, is to measure the in-plane shear stress response to shear strain and shear strain rate by using a trellis-frame or picture-frame apparatus actuated by a tensile testing machine. The trellis-frame consists of four pinned corners and four clamped edges. Clamping mechanisms hold the cross-shaped fabric sample rigidly in the frame with no slippage. One corner of the frame is equipped with a locking pin to ensure proper installation of test specimen into the frame and the assembled fixture onto the INSTRON testing machine. During the test, the distance between the top and bottom corners of the frame is increased by the INSTRON testing machine, and thus reorienting the tows in the specimen in a shearing action. INSTRON crosshead force and motion were recorded for all cycles and photogrammetry pictures captured at specified loading condition as indicated in the Test Information Sheet.

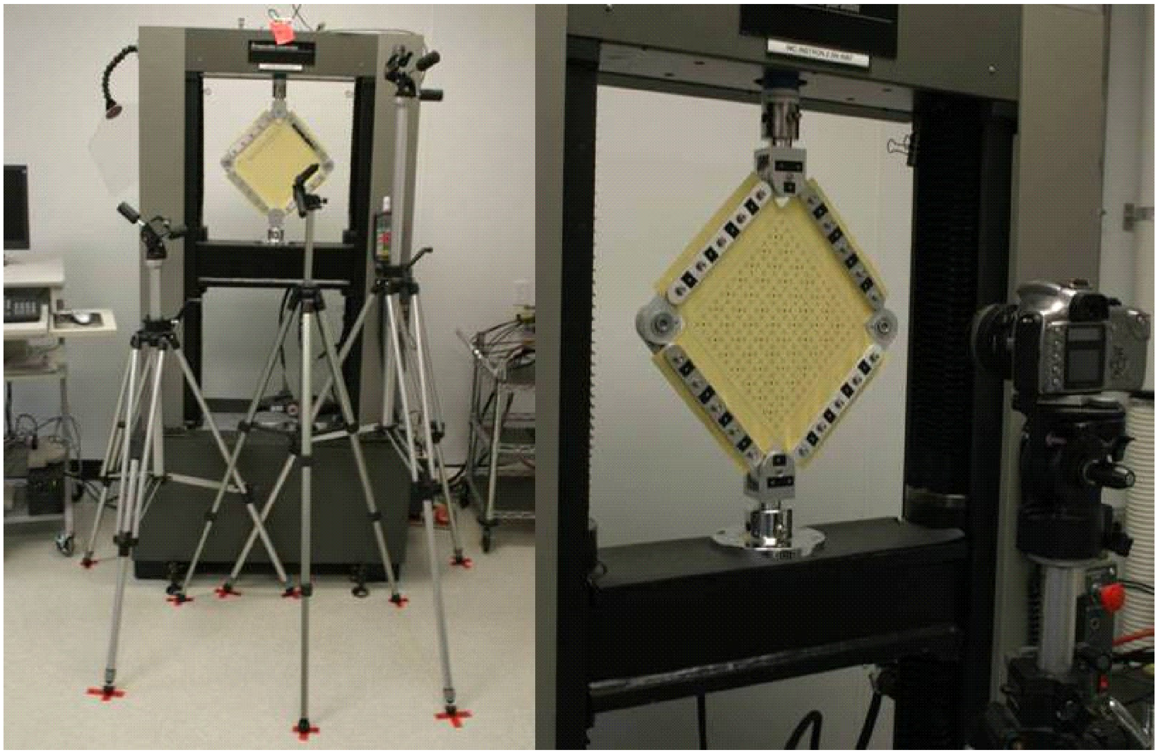

Figure 3: Trellis-Frame test setup in INSTRON test machine.

Three cameras were used to capture photogrammetry data during the testing. As seen in Figure 3, the cameras were placed at different heights and locations across the front of the INSTRON. Figure 4 shows a top view layout of the camera locations.

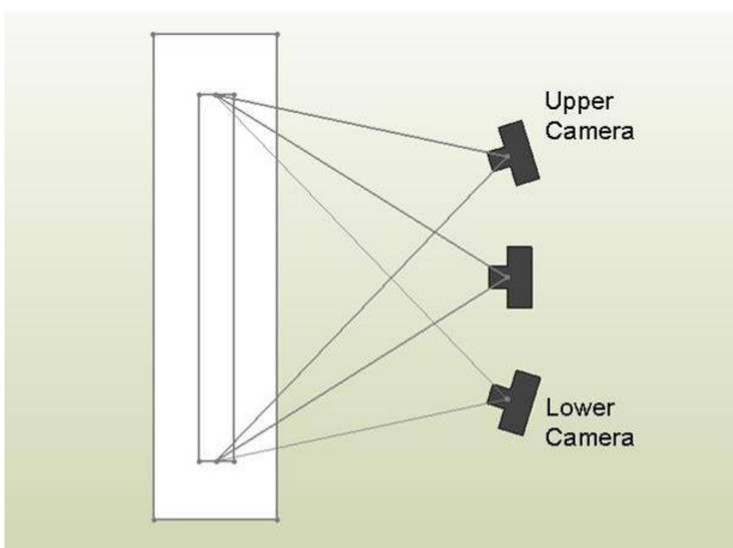

Figure 4: Camera Setup for Trellis Frame Test – Top View

In this study, six test specimens were made for each material and condition. One sample was used for initial set up to determine maximum loading condition. Test specimens were marked and cut from automated cutting equipment using CAD file. Dimensionally the width of the cross is 8 inches and the length is 13 inches. After the specimens have been marked and cut, photogrammetry dots are adhered to the test specimens according to the engineering instruction. The INSTRON crosshead speed for the trellis frame tests was 5 in/min. This gave an average shear strain rate of 0.012 rad/sec.

4.3.2 Bias Extension Test

Bias Extension Test, see Figure 5, is used to measure the in-plane combined shearing and tensile responses of a given textile material sample with a set displacement and cross head speed. This test is considered to be an alternate method to the Trellis-Frame test. In terms of test setup it is similar to ASTM D5035 -06(2008) e1 "Standard Test Method for Breaking Force and Elongation of Textile Fabrics". However, test specimen preparation requires special attention. One critical aspect of the sample preparation in the bias extension test is yarn orientation which must be ±45° to the edges of the grippers. During the test, the specimen is clamped into the grips with zero (i.e. minimum) preload. As the distance of the crossheads of the testing machine separates the tows at the center zone (a pure shear zone) of the sample reorient in shear. The INSTRON crosshead speed for the bias extension tests was 1.25 in/min. This was selected in order to give an average shear strain rate equal to that used for the trellis frame tests.

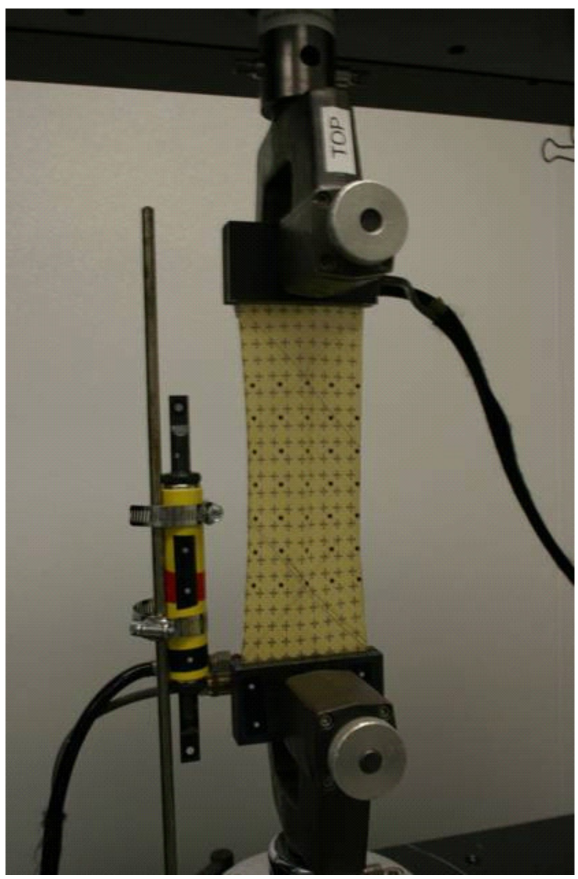

Figure 5: Bias extension sample in INSTRON test machine.

In this study, six test specimens were made for each material and condition. One sample was used for initial set up to determine appropriate values for photogrammetry measurements and the maximum extension. Data will be used to validate the calculations based on the linear length measurements taken as part of this procedure. Data will also be used to report on test article flatness as load is applied. Flatness is an important assumed condition for the bias extension test. These measurements would take place at a set of discrete load points using photogrammetry. Test specimens were marked and cut from automated cutting equipment using CAD file. After the specimens have been marked and cut, photogrammetry dots are adhered to the test specimens according to the engineering instruction. Again, three cameras were placed to capture the photogrammetry data during the testing. Figure 6 shows a side view of the camera locations for the bias extension tests.

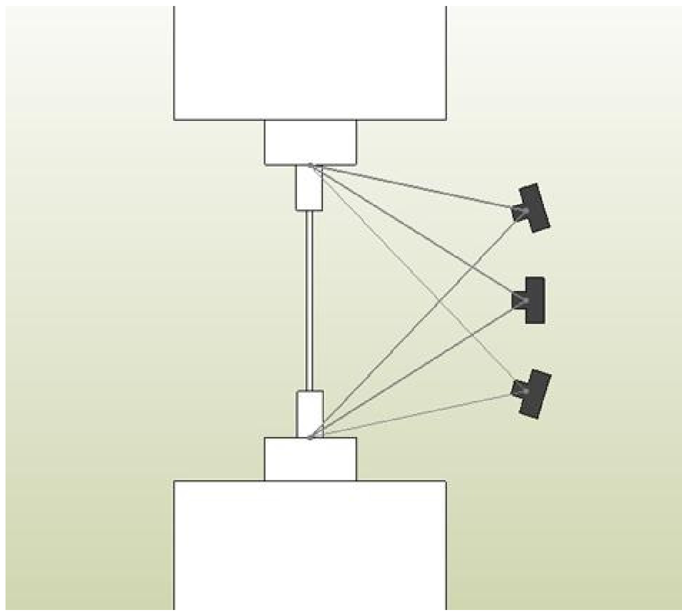

Figure 6: Camera Setup for Bias Extension Tests – Side View

4.3.3 Cylindrical Biaxial Test

In this study the inflated cylinder torsion test, see Figure 7, was the third method selected to characterize the shear stress-strain behavior of the textile materials. In the inflated cylinder torsion test torque versus twist angle is measured for an inflated cylinder where one end cap has a free rotational degree of freedom and the other end cap has a free axial degree of freedom. Photogrammetry measurements were taken at zero and maximum torque values (both directions). Using well known relations from engineering mechanics the applied torque can be converted to the resulting shear stress and the twist angle can be converted to shear strain.

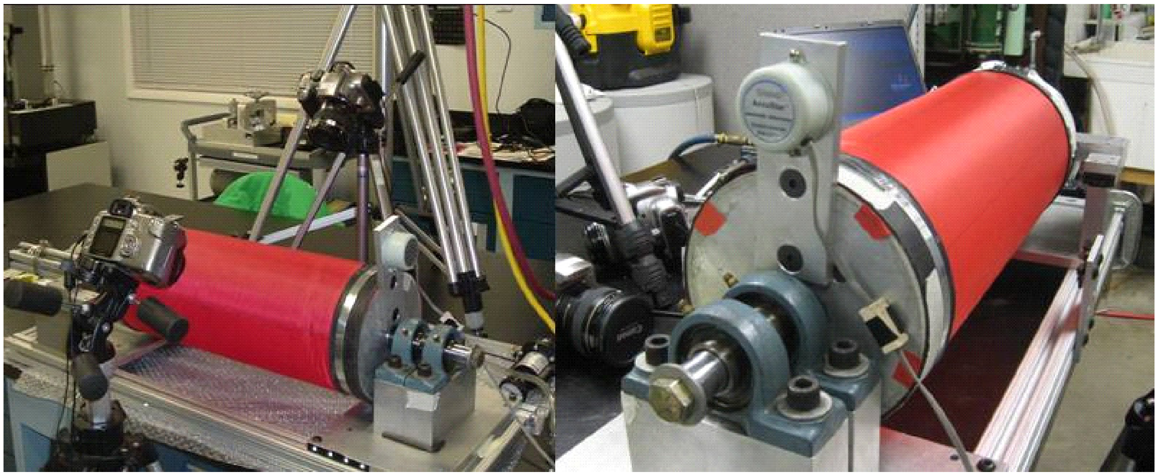

Figure 7: Cylindrical biaxial test setup.

In this study, five test specimens were made for each material and condition. A nominal length to diameter aspect ratio of 3:1 or greater is recommended for the inflated cylinder torsion test. Each sample will run through a break in cycle as its preconditioning. Test specimens were marked and cut from automated cutting equipment using CAD file and then assembled into cylindrical tubes. After the specimens have been assembled, photogrammetry dots are adhered to the test specimens according to the engineering instruction. Each test article will be tested at a given set of discrete internal pressures. These pressures will be selected so that the shear modulus dependence on the biaxial preload state is known. A regression will be performed to estimate the shear modulus at a state of zero biaxial preload.

5. Normal Stress-Strain

5.1 F-111 Nylon Uni-axial testing

5.1.1 Warp Direction Pull Tests

The F-111 Nylon warp direction measured normal stress-strain behavior for the stress interval [0, 37] lbf/in is shown in Figure 8 through Figure 10. Figure 8 shows the first load cycle for all the samples tested. Similarly, Figure 9 shows the stress-strain data for the tenth load cycle. The results for the first load cycle exhibit non-linearity in the ramp up portion of the load curve, where two points of inflection are observed. The first load cycle also exhibits significant inelastic behavior both in hysteresis and strain set. The results for the tenth load cycle showed much less inelastic behavior, but the non-linearity increased. Figure 10 shows all ten load/unload cycles for the test item A.

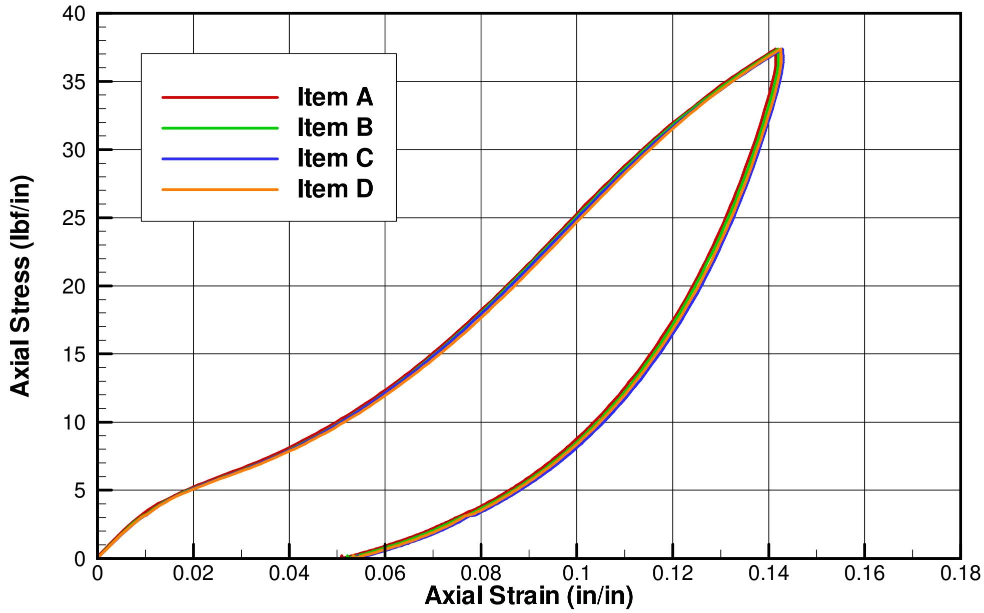

Figure 8: F-111 Nylon warp axial pull test, load cycle 1.

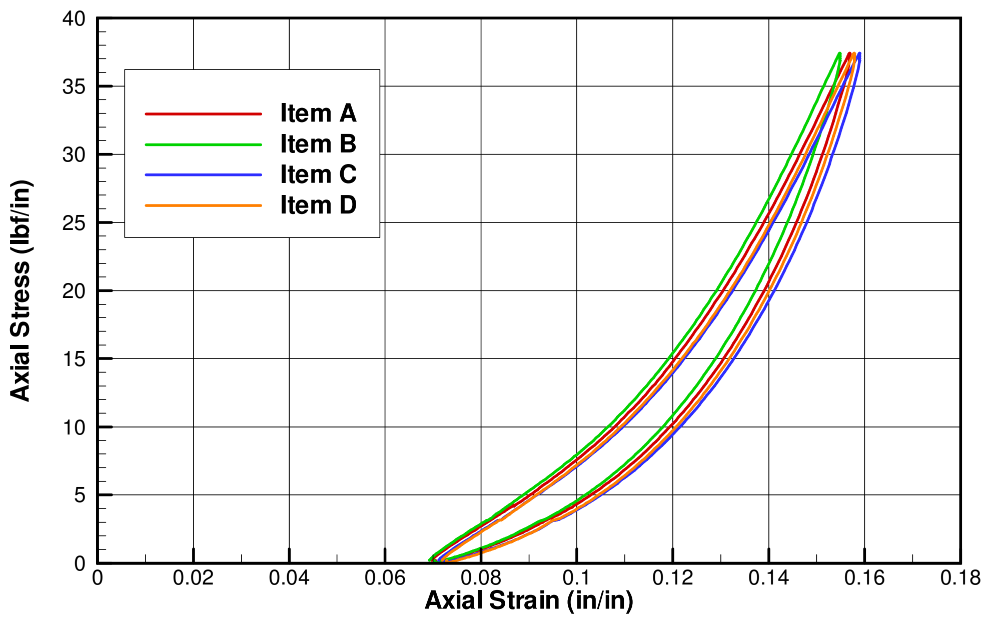

Figure 9: F-111 Nylon warp axial pull test, load cycle 10.

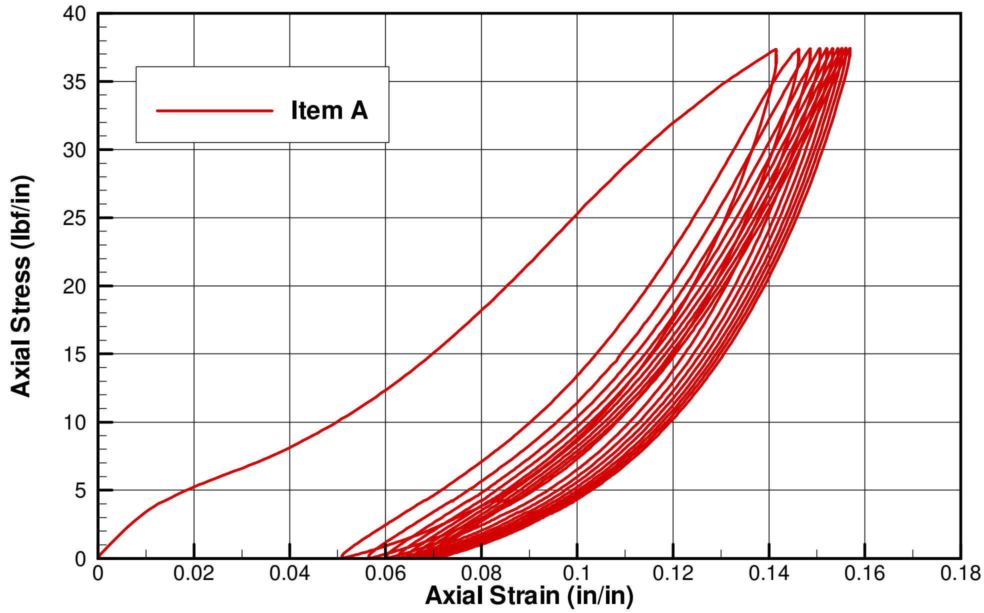

Figure 10: F-111 Nylon warp axial pull test, all ten load cycles.

Figure 11 and Figure 12 show the transverse to axial strain ratios for warp axial pulls of the F-111 Nylon material. The strain ratio is observed to be highly loading dependent in the early portions of the loading histories. The relative sample to sample agreement of the strain ratio data is observed to be less than that observed for the normal stress-strain data. At stresses above 10 lbf/in, the strain ratio was observed to be between 0.25 and 0.40 for the first load cycle. For the tenth load cycle the strain ratio was observed to be between 0.20 and 0.27 for stresses greater than 10 lbf/in.

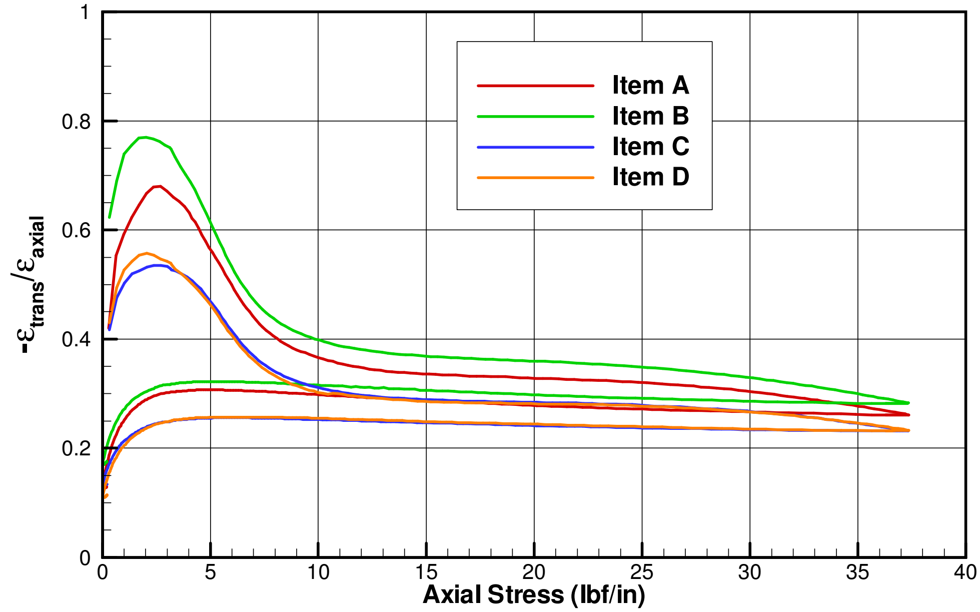

Figure 11: F-111 Nylon warp axial pull test, strain ratio cycle 1.

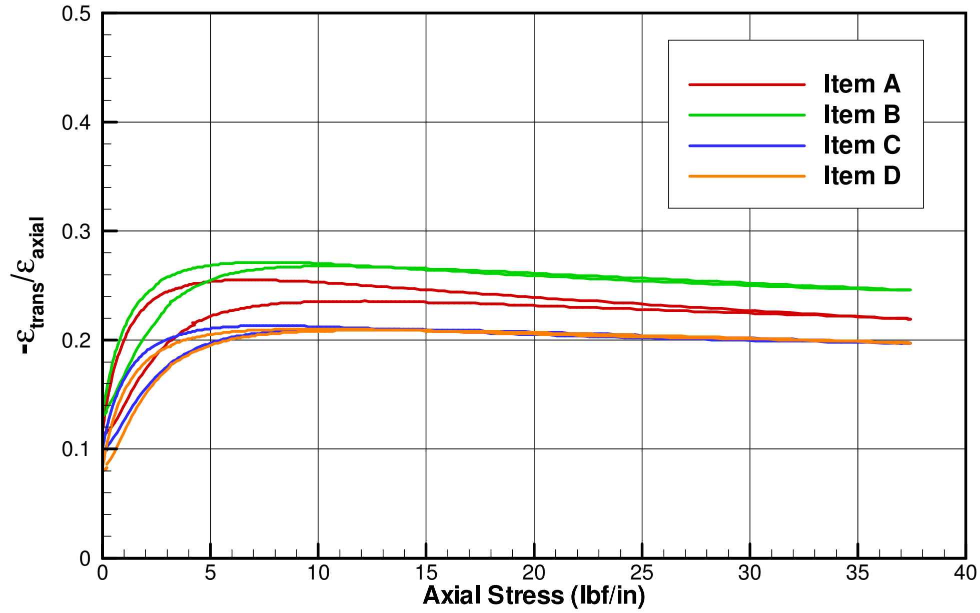

Figure 12: F-111 Nylon warp axial pull test, strain ratio cycle 10.

5.1.2 Fill Direction Pull Tests

The F-111 Nylon fill direction measured normal stress-strain behavior for the stress interval [0, 37] lbf/in is shown in Figure 13 through Figure 15. Figure 13 shows the first load cycle for all the samples tested. Similarly, Figure 14 shows the stress-strain data for the tenth load cycle. The results for the first load cycle exhibit non-linearity in the ramp up portion of the load curve. The first load cycle also exhibits significant inelastic behavior both in hysteresis and strain set. The strain set resulting from the first load cycle was approximately 10%. The results for the tenth load cycle showed much less inelastic behavior. Figure 15 shows all ten load/unload cycles for the test item A.

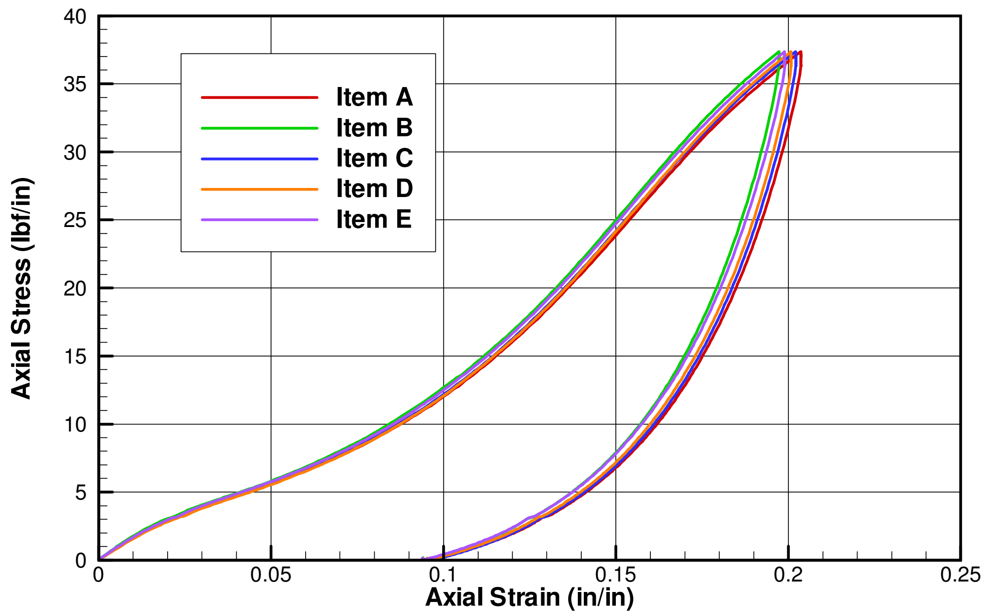

Figure 13: F-111 Nylon fill axial pull test, load cycle 1.

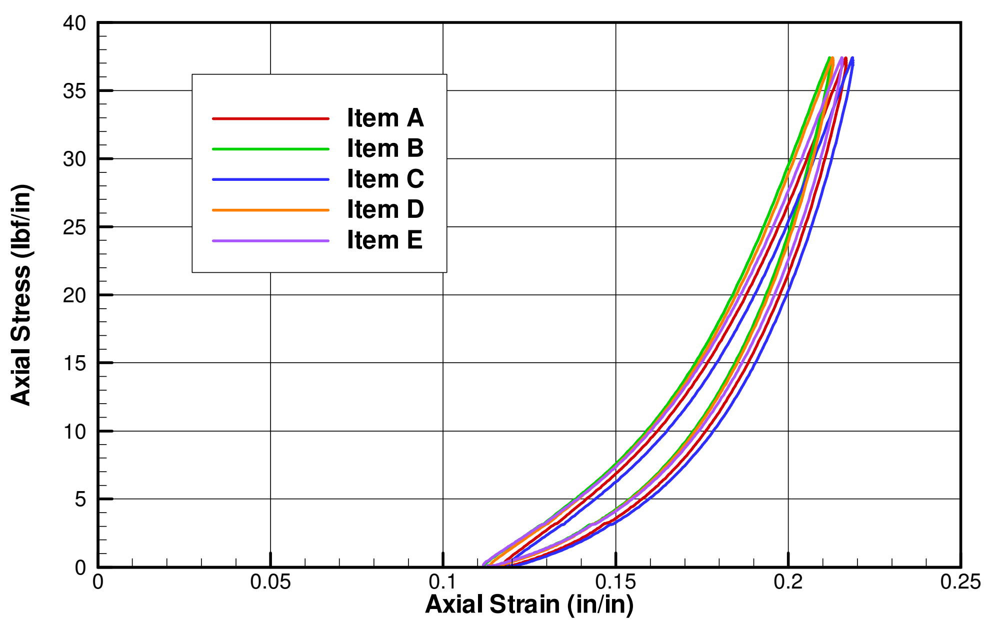

Figure 14: F-111 Nylon fill axial pull test, load cycle 10.

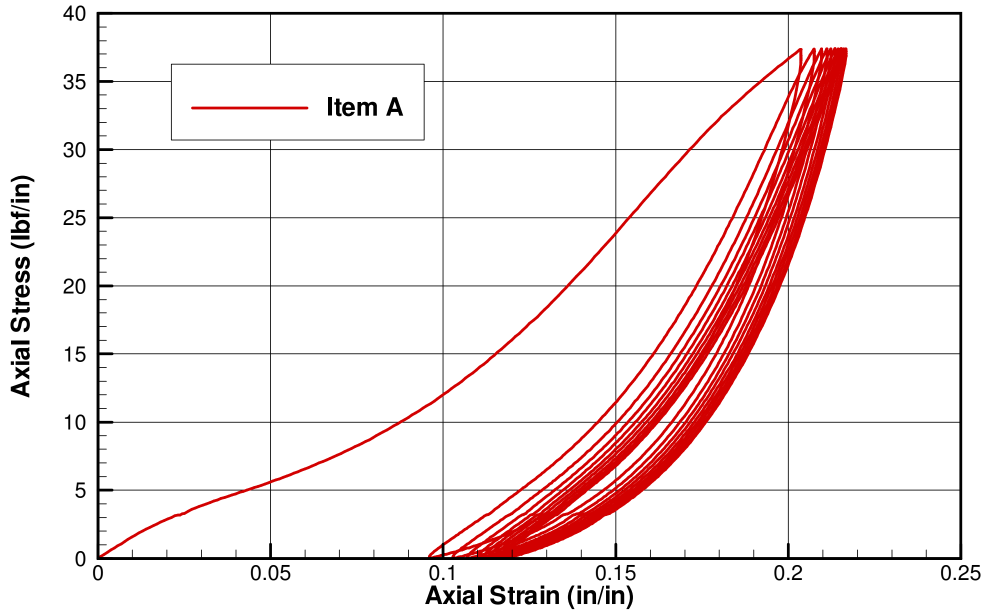

Figure 15: F-111 Nylon fill axial pull test, all ten load cycles.

Figure 16 and Figure 17 show the transverse to axial strain ratios for fill axial pulls of the F-111 Nylon material. The strain ratio is observed to be highly loading dependent in the early portions of the loading histories. The relative sample to sample agreement of the strain ratio data is observed to be less than that observed for the normal stress-strain data. At stresses above 10 lbf/in, the strain ratio was observed to be between 0.24 and 0.34 for the first load cycle. For the tenth load cycle the strain ratio was observed to be between 0.21 and 0.25 for stresses greater than 10 lbf/in.

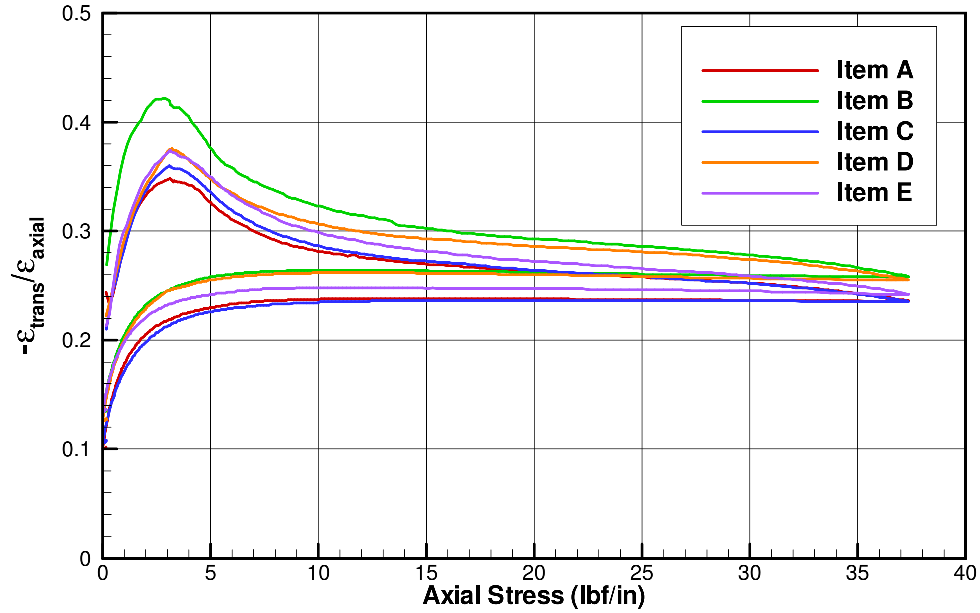

Figure 16: F-111 Nylon fill axial pull test, strain ratio cycle 1.

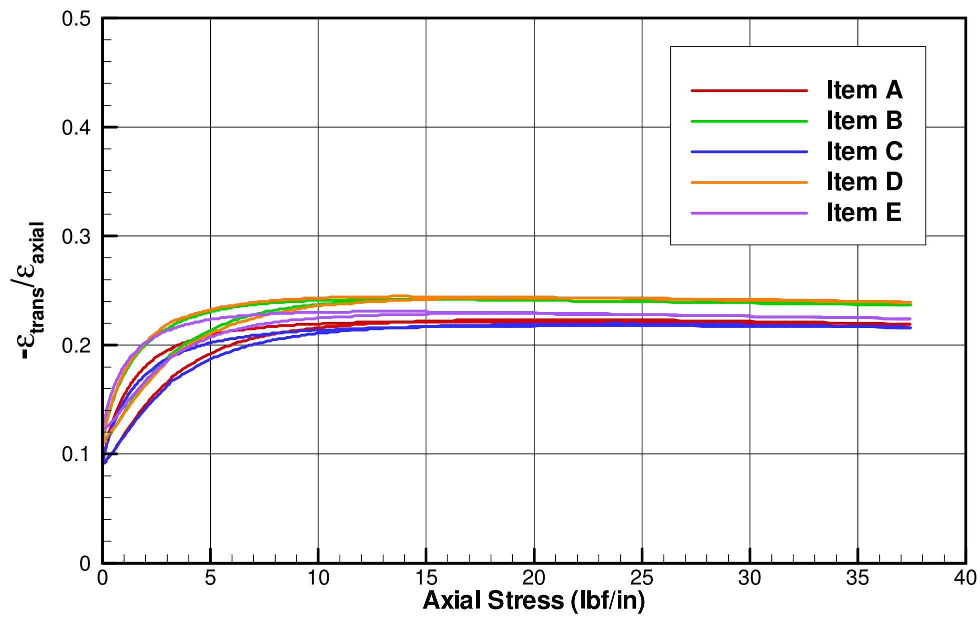

Figure 17: F-111 Nylon fill axial pull test, strain ratio cycle 10.

5.1.3 Warp versus Fill Stiffness Comparison

The F-111 Nylon warp and fill normal stress-strain data for the first load cycle is shown in Figure 18. From this curve we see the relative difference in stiffness in these two principle yarn directions. For the F-111 Nylon material tested, we observed that the warp direction of the material had the higher stiffness in the first load cycle. The warp and fill normal stress-strain data for the tenth load cycle is shown in Figure 19. From this curve we observed only a small stiffness difference in the tenth load cycle.

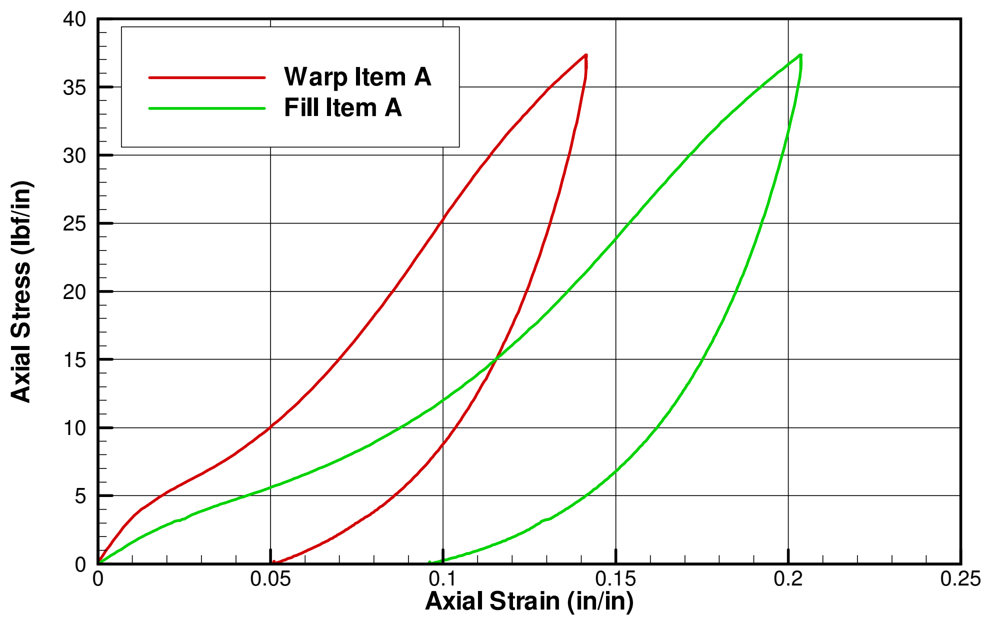

Figure 18: F-111 Nylon axial pull test, cycle 1 warp vs. fill stiffness.

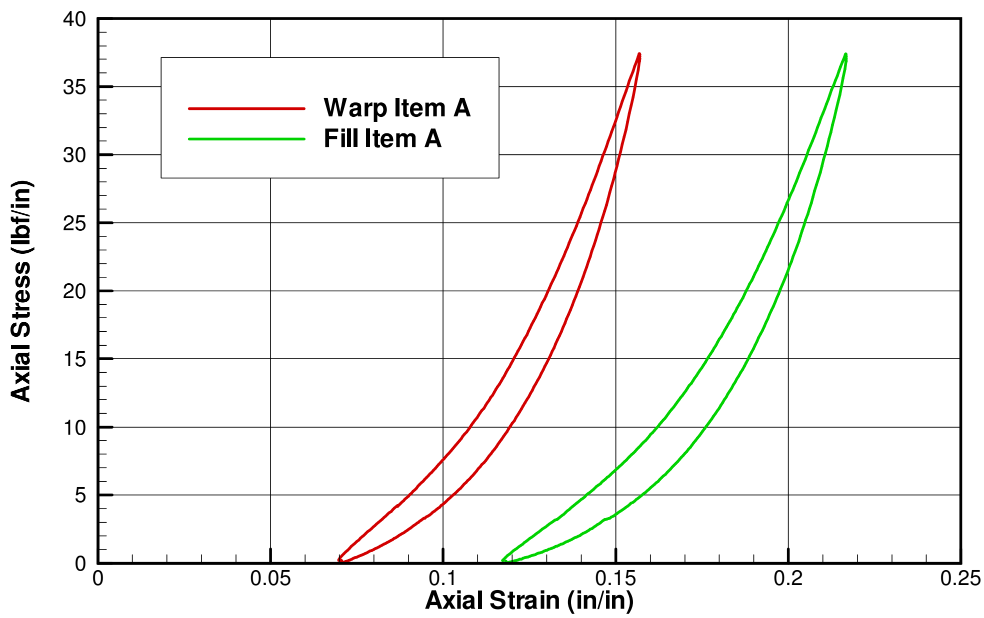

Figure 19: F-111 Nylon axial pull test, cycle 10 warp vs. fill stiffness.

5.2 HT1 Nomex Uni-axial testing

5.2.1 Warp Direction Pull Tests

The HT1 Nomex warp direction measured normal stress-strain behavior for the stress interval [0, 172] lbf/in is shown in Figure 20 through Figure 22. Figure 20 shows the first load cycle for all the samples tested. Similarly, Figure 21 shows the stress-strain data for the tenth load cycle. The results for the first load cycle exhibit non-linearity in the ramp up portion of the load curve, where two points of inflection are observed. Depending on the modeling objectives a linear stress-strain approximation could yield acceptable results for the ramp up portion of cycle 1. The first load cycle also exhibits significant inelastic behavior both in hysteresis and strain set. The strain set was observed to be approximately 50% of the strain maximum for the first load cycle. The results for the tenth load cycle showed much less inelastic behavior. After a small initial region of loading, the tenth cycle stress-strain response was close to linear behavior. Figure 22 shows all ten load/unload cycles for one of the samples tested.

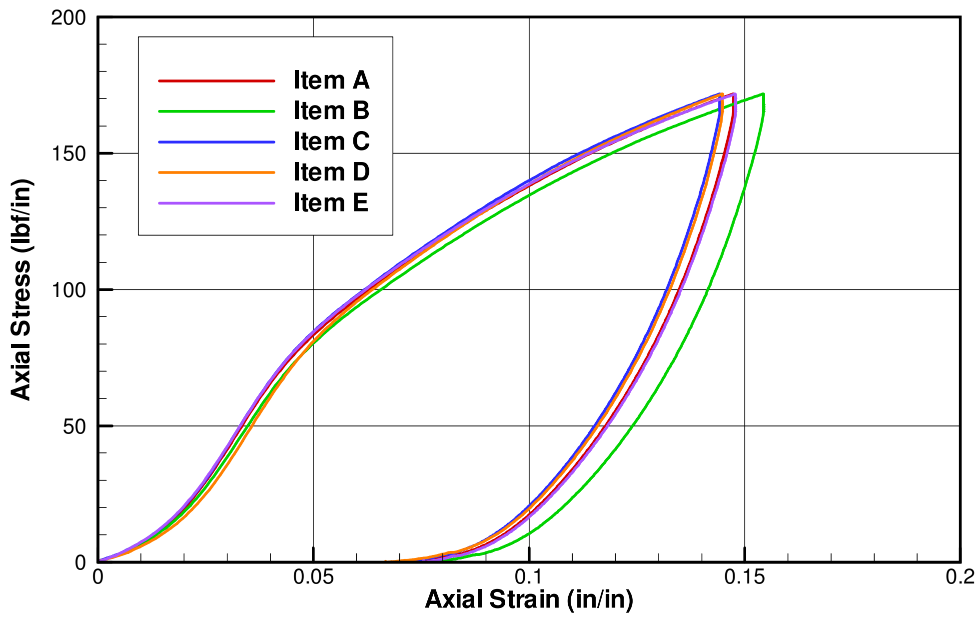

Figure 20: HT1 Nomex warp axial pull test, load cycle 1.

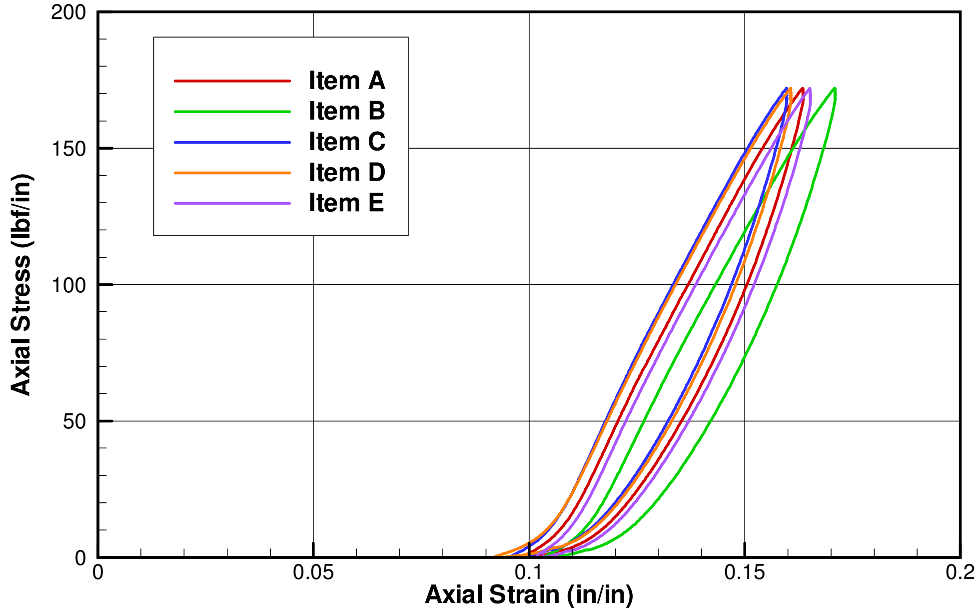

Figure 21: HT1 Nomex warp axial pull test, load cycle 10.

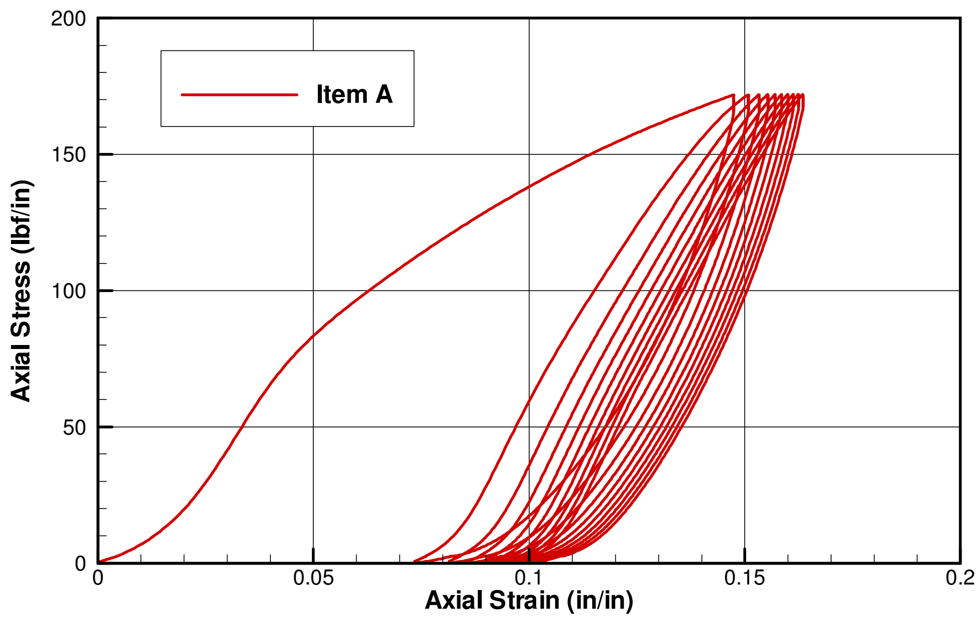

Figure 22: HT1 Nomex warp axial pull test, all ten load cycles.

Figure 23 and Figure 24 show the transverse to axial strain ratios for warp axial pulls of the HT1 Nomex material. The strain ratio is observed to be loading dependent through the entire load range for cycle 1. At stresses above 50 lbf/in, the strain ratio was observed to be between 0.5 and 0.7 for the tenth load cycle. The relative sample to sample agreement of the strain ratio data was not significantly different from that observed for the normal stress-strain data.

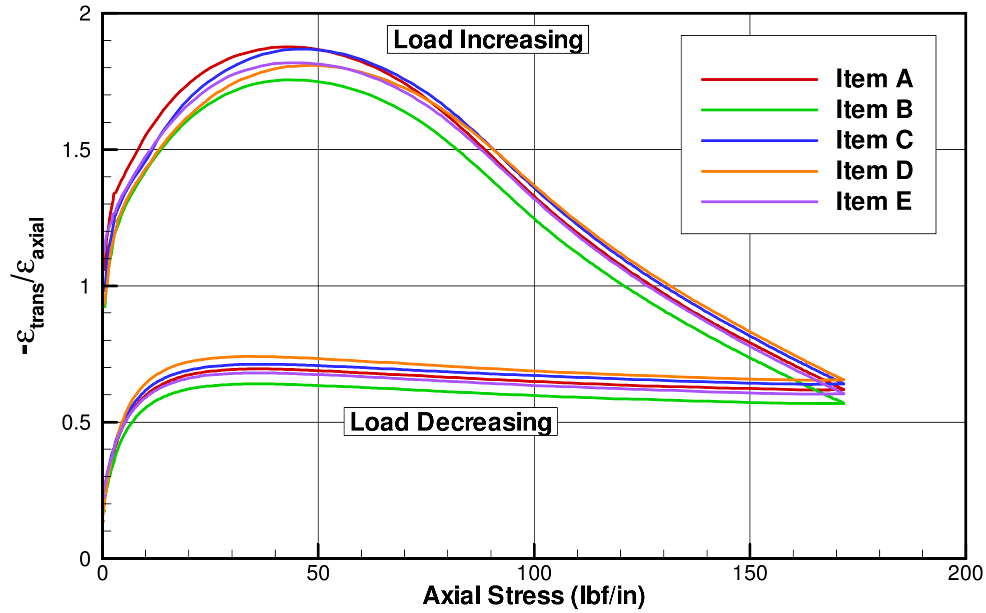

Figure 23: HT1 Nomex warp axial pull test, strain ratio cycle 1.

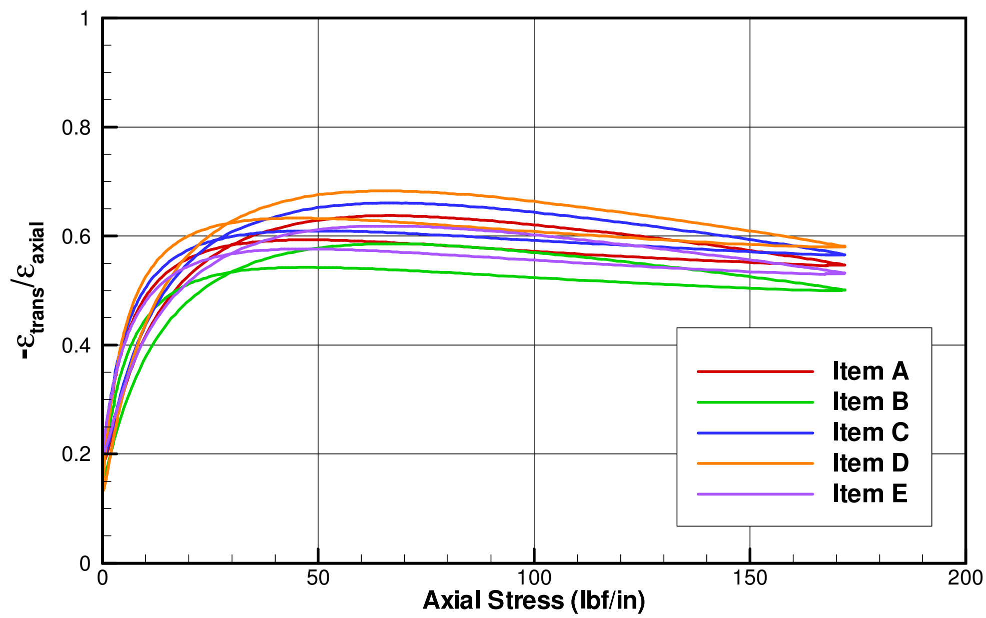

Figure 24: HT1 Nomex warp axial pull test, strain ratio cycle 10.

5.2.2 Fill Direction Pull Tests

The HT1 Nomex fill direction measured normal stress-strain behavior for the stress interval [0, 172] lbf/in is shown in Figure 25 through Figure 27. Figure 25 shows the first load cycle for all the samples tested. Similarly, Figure 26 shows the stress-strain data for the tenth load cycle. The results for the first load cycle exhibit non-linearity in the ramp up portion of the load curve, where two points of inflection are observed. The first load cycle also exhibits significant inelastic behavior both in hysteresis and strain set. For an approximate maximum induced strain of 16%, the strain set was observed to be 9% for the first load cycle. The results for the tenth load cycle showed much less inelastic behavior. Similar to the warp direction, the tenth cycle stress-strain response was close to linear behavior after a small initial region of loading. Figure 27 shows all ten load/unload cycles for one of the samples tested.

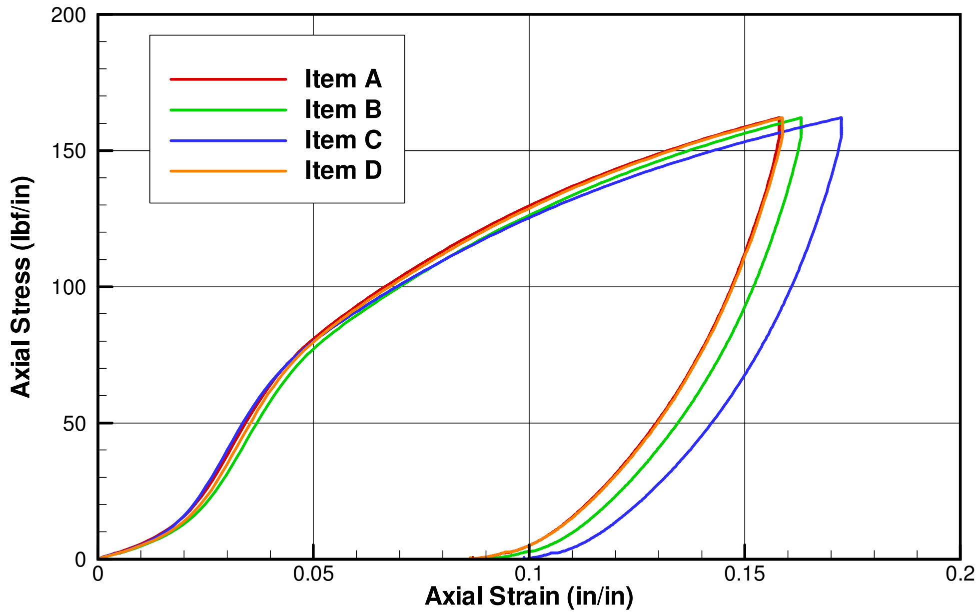

Figure 25: HT1 Nomex fill axial pull test, load cycle 1.

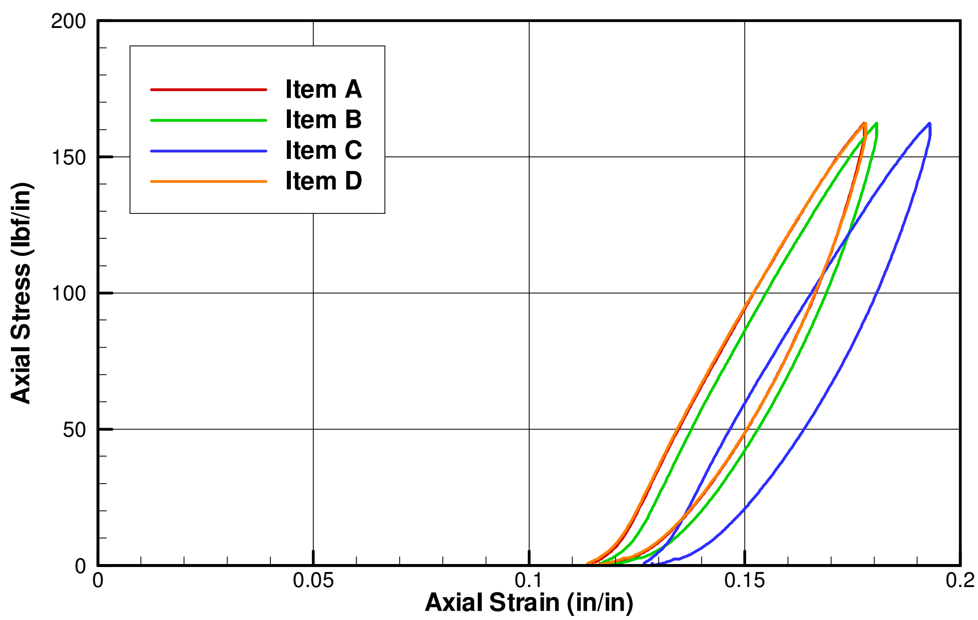

Figure 26: HT1 Nomex fill axial pull test, load cycle 10.

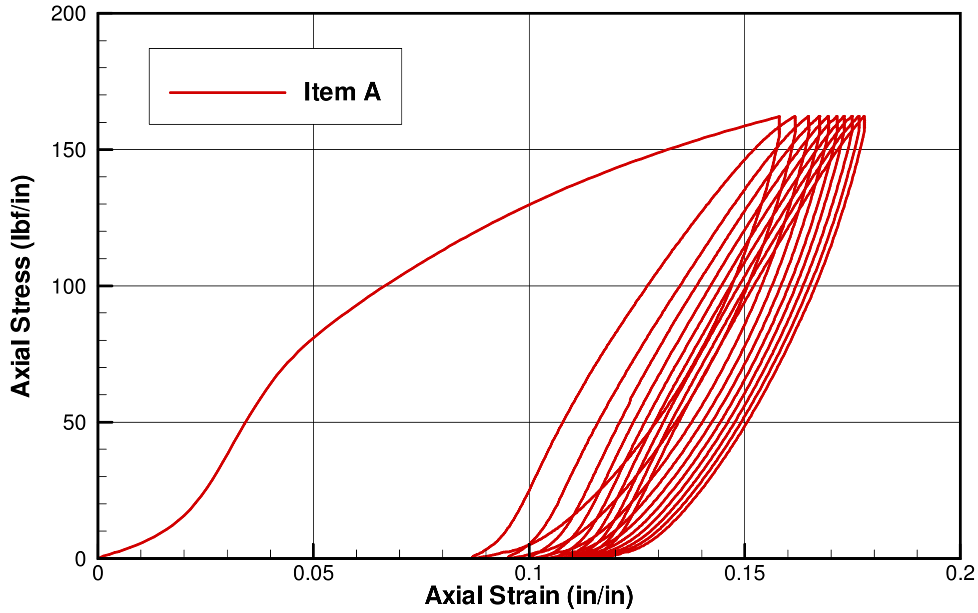

Figure 27: HT1 Nomex fill axial pull test, all ten load cycles.

Figure 28 and Figure 29 show the transverse to axial strain ratios for fill axial pulls of the HT1 Nomex material. The strain ratio is observed to be loading dependent through the entire load range for the first cycle. At stresses above 50 lbf/in, the strain ratio was observed to be between 0.30 and 0.45 for the tenth load cycle.

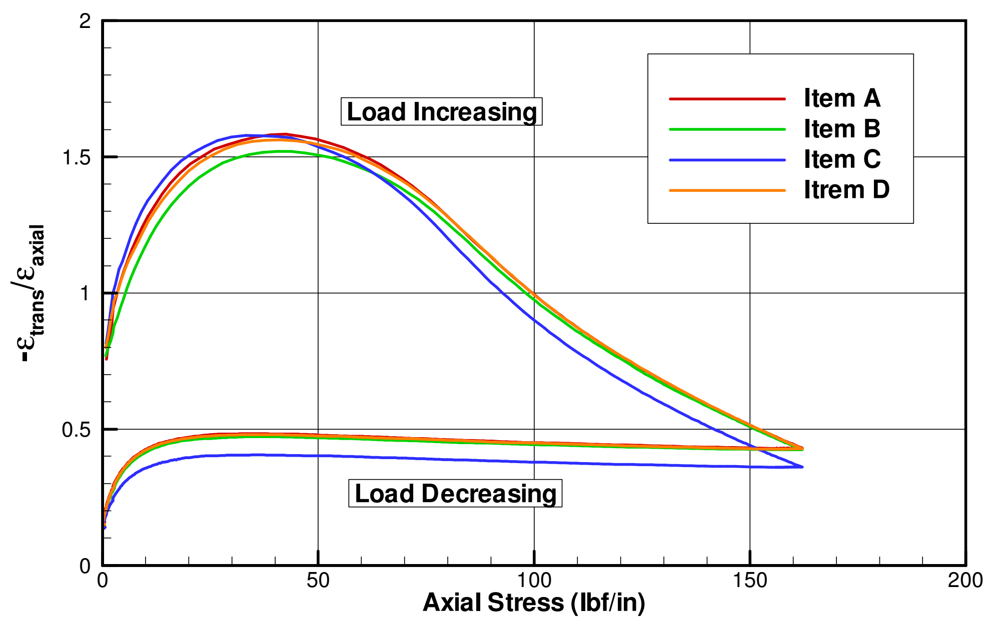

Figure 28: HT1 Nomex fill axial pull test, strain ratio cycle 1.

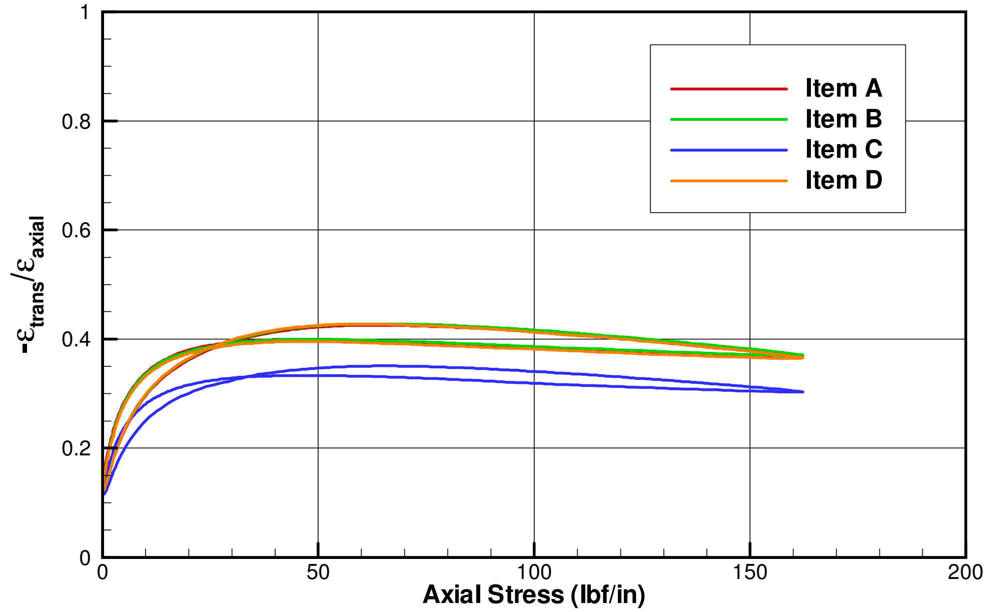

Figure 29: HT1 Nomex fill axial pull test, strain ratio cycle 10.

5.2.3 Warp versus Fill Stiffness Comparison

The HT1 Nomex warp and fill normal stress-strain data for the first load cycle is shown in Figure 30. The warp and fill normal stress-strain data for the tenth load cycle is shown in Figure 31. From this curve we see the relative difference in stiffness in these two principle yarn directions. For the material tested, we observed that the warp and fill stiffness of the material was very similar in both the first and tenth cycles.

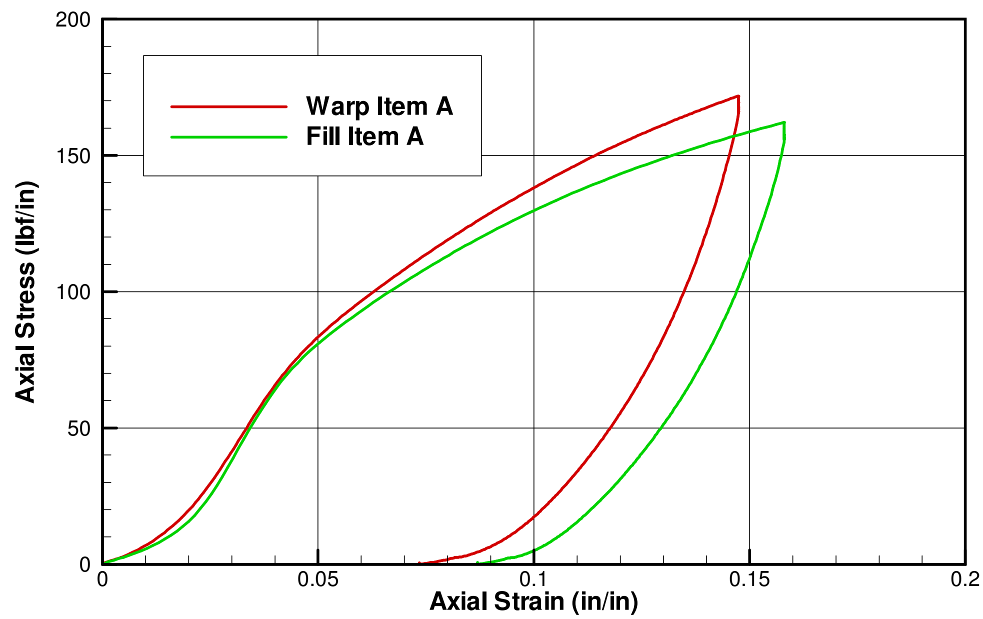

Figure 30: HT1 Nomex axial pull test, cycle 1 warp vs. fill stiffness.

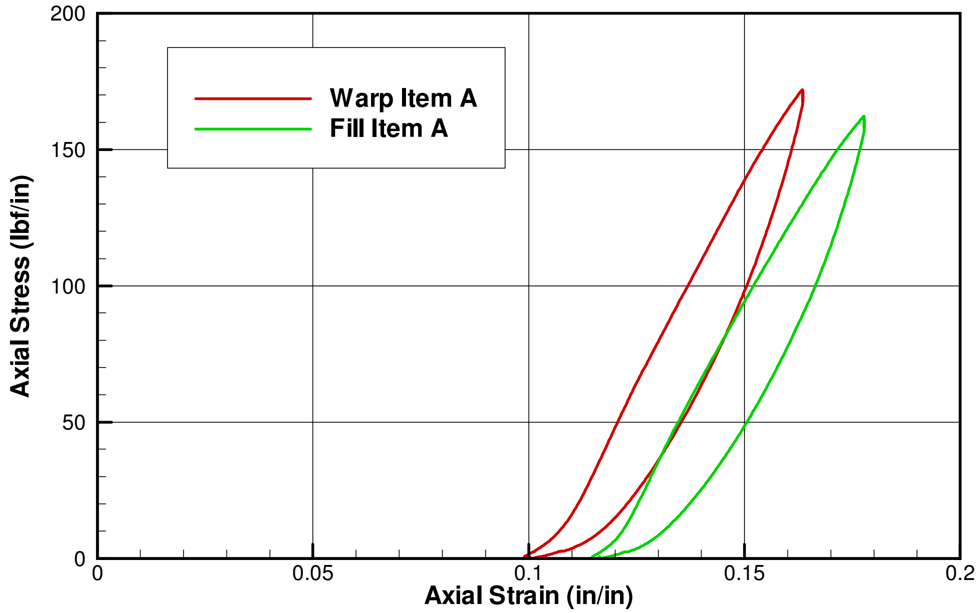

Figure 31: HT1 Nomex axial pull test, cycle 10 warp vs. fill stiffness.

5.3 200 Denier Kevlar

5.3.1 Warp Direction Pull Tests

The 200 denier Kevlar warp direction measured normal stress-strain behavior for the stress interval [0, 189] lbf/in is shown in Figure 32 through Figure 34. Figure 32 shows the first load cycle for all the samples tested. Similarly, Figure 33 shows the stress-strain data for the tenth load cycle. The results for the first load cycle exhibit a smaller degree of non-linearity than was observed in the Nylon and Nomex materials. The first load cycle also exhibits significantly less inelastic behavior that was observed with the Nylon and Nomex materials. The strain set was observed to be approximately 20% of the strain maximum for the first load cycle. Other than the impact of the strain set, the results for the tenth load cycle were very similar to those of the first. Figure 34 shows all ten load/unload cycles for one of the samples tested.

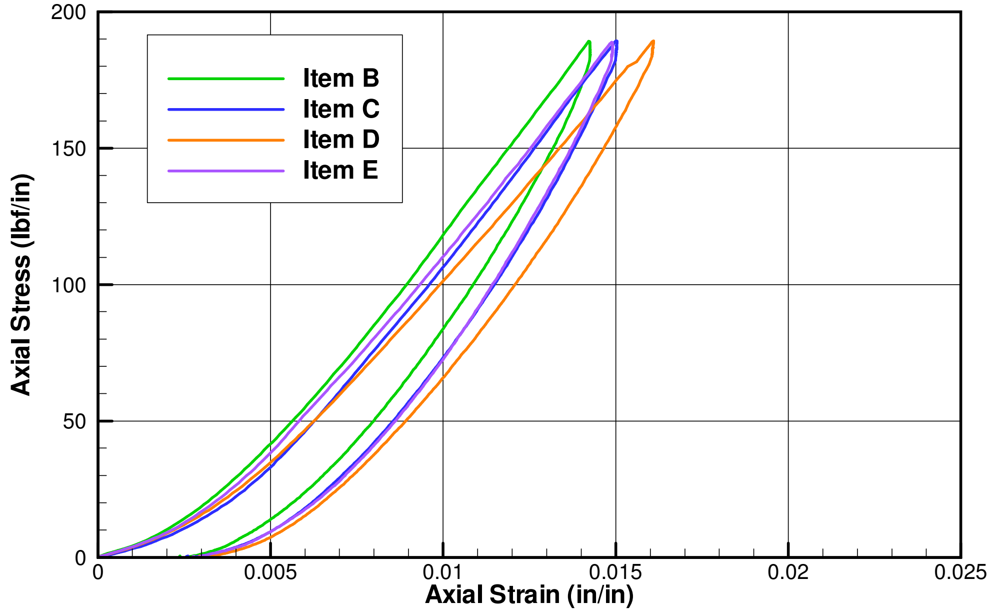

Figure 32: 200 denier Kevlar warp axial pull test, load cycle 1.

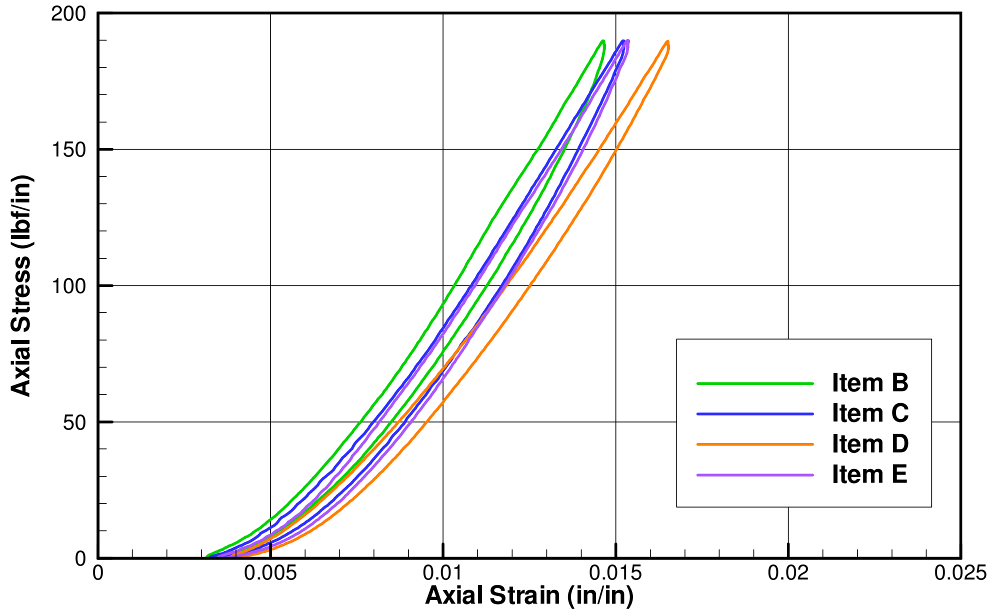

Figure 33: 200 denier Kevlar warp axial pull test, load cycle 10.

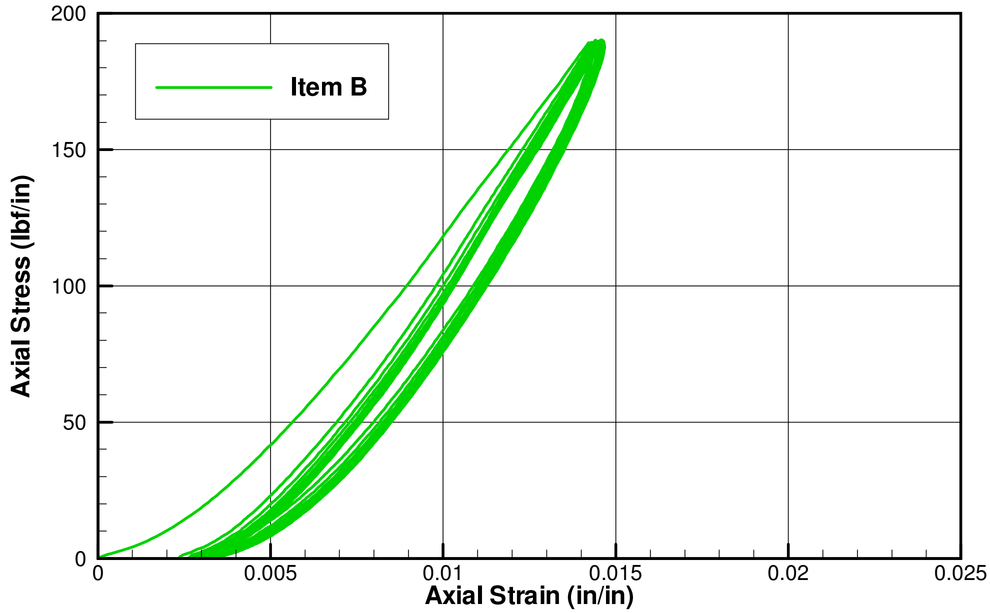

Figure 34: 200 denier Kevlar warp axial pull test, all ten load cycles.

Figure 35 and Figure 36 show the transverse to axial strain ratios for warp axial pulls of the 200 denier Kevlar material. The strain ratio is observed to be loading dependent through the entire load range for all cycles. Other than a minor shift down, the cycling did not have an impact on the ratio. The overall magnitude of the ratio for the 200 denier Kevlar is large in comparison to the Nylon and Nomex materials. In all cases the ratio was greater than 1.0 and under some loads it was greater than 2.0.

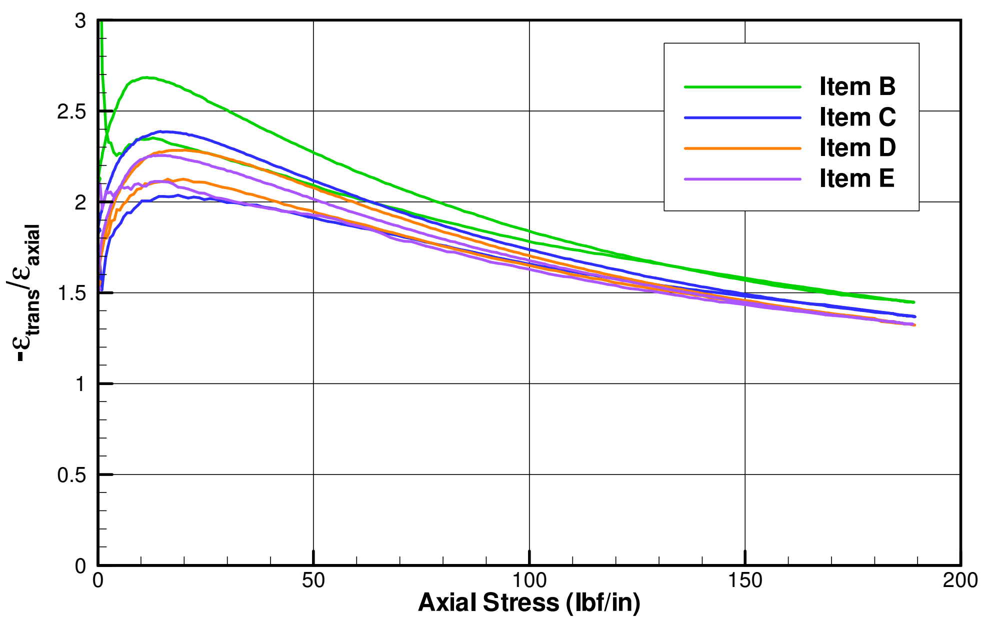

Figure 35: 200 denier Kevlar warp axial pull test, strain ratio cycle 1.

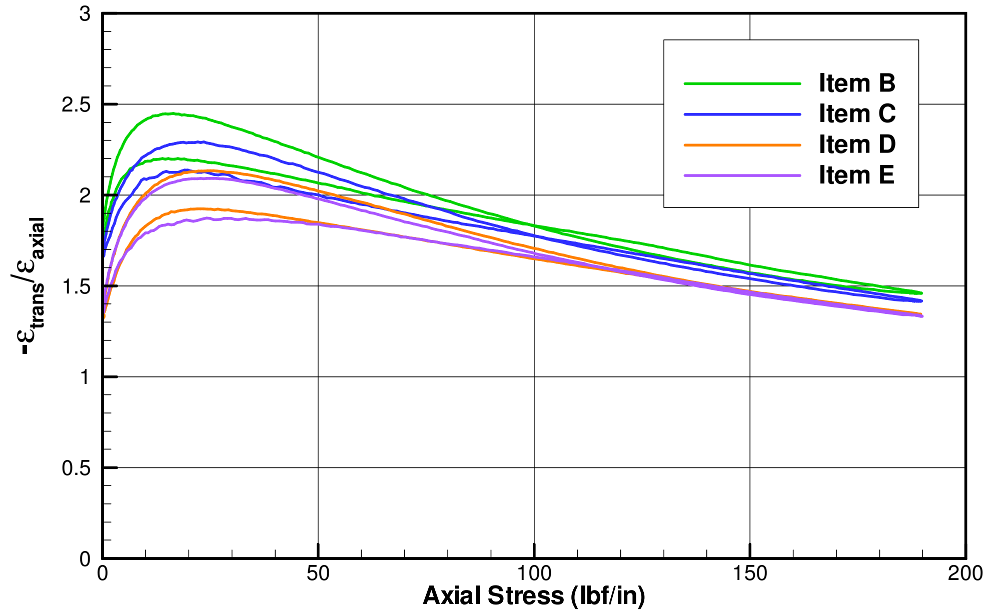

Figure 36: 200 denier Kevlar warp axial pull test, strain ratio cycle 10.

5.3.2 Fill Direction Pull Tests

The 200 denier Kevlar fill direction measured normal stress-strain behavior for the stress interval [0, 189] lbf/in is shown in Figure 37 through Figure 39. Figure 37 shows the first load cycle for all the samples tested. Similarly, Figure 38 shows the stress-strain data for the tenth load cycle. The results for the first load cycle exhibit non-linearity in the ramp up portion of the load curve. The stress-strain response was bi-linear in nature with low stiffness at low loads and then a significantly higher stiffness at higher loads. Similar to the warp direction, the first load cycle exhibits significantly less inelastic behavior than was observed with the Nylon and Nomex materials. The strain set was observed to be approximately 28% of the strain maximum for the first load cycle. The results for the tenth load cycle showed less of a bi-linear response where the initial low stiffness linear region was not present in the stress-strain curve. Figure 39 shows all ten load/unload cycles for one of the samples tested.

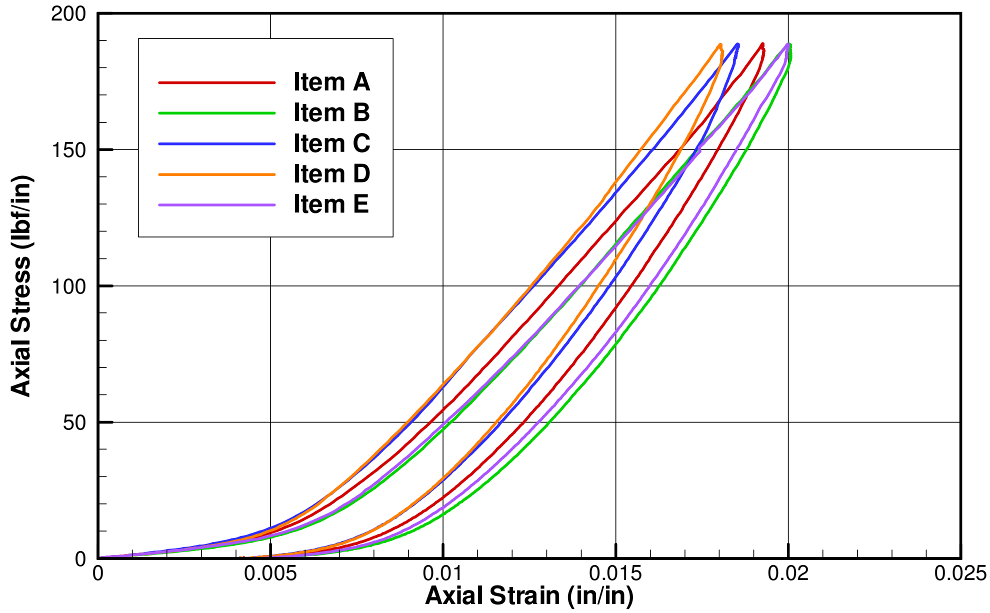

Figure 37: 200 denier Kevlar fill axial pull test, load cycle 1.

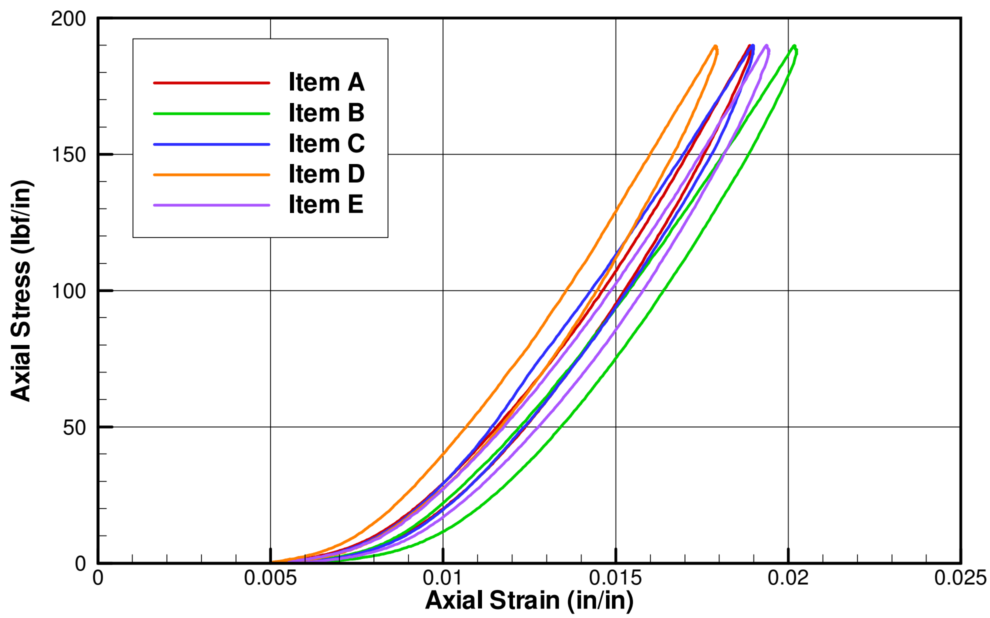

Figure 38: 200 denier Kevlar fill axial pull test, load cycle 10.

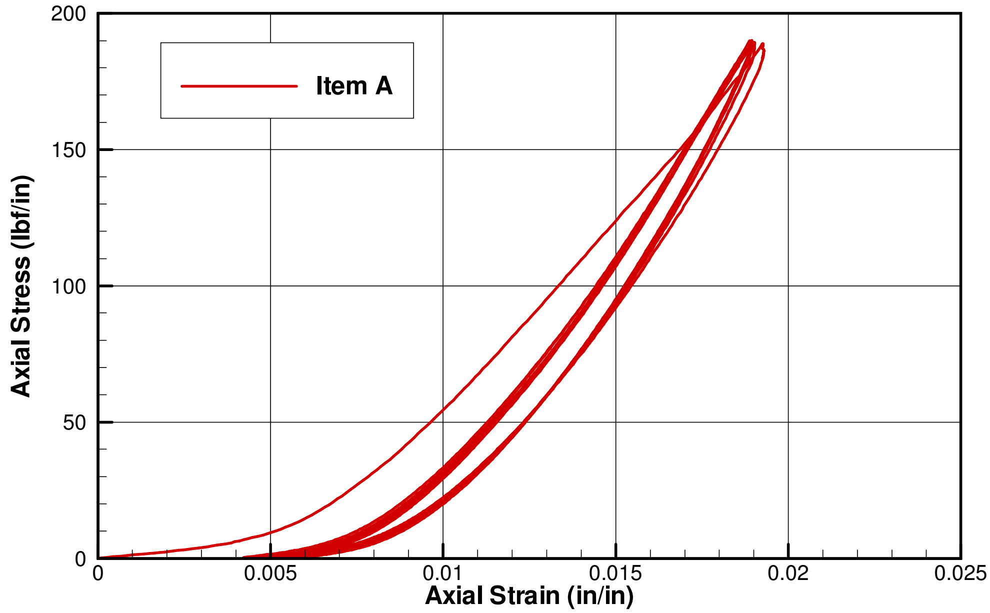

Figure 39: 200 denier Kevlar fill axial pull test, all ten load cycles.

Figure 40 and Figure 41 show the transverse to axial strain ratios for fill axial pulls of the 200 denier Kevlar material. The strain ratio is observed to be loading dependent through the entire load range for all cycles. The cycling did not have an impact on the ratio. Similar to the warp direction, the overall magnitude of the ratio is large in comparison to the Nylon and Nomex materials. In all cases the ratio was greater than 1.0.

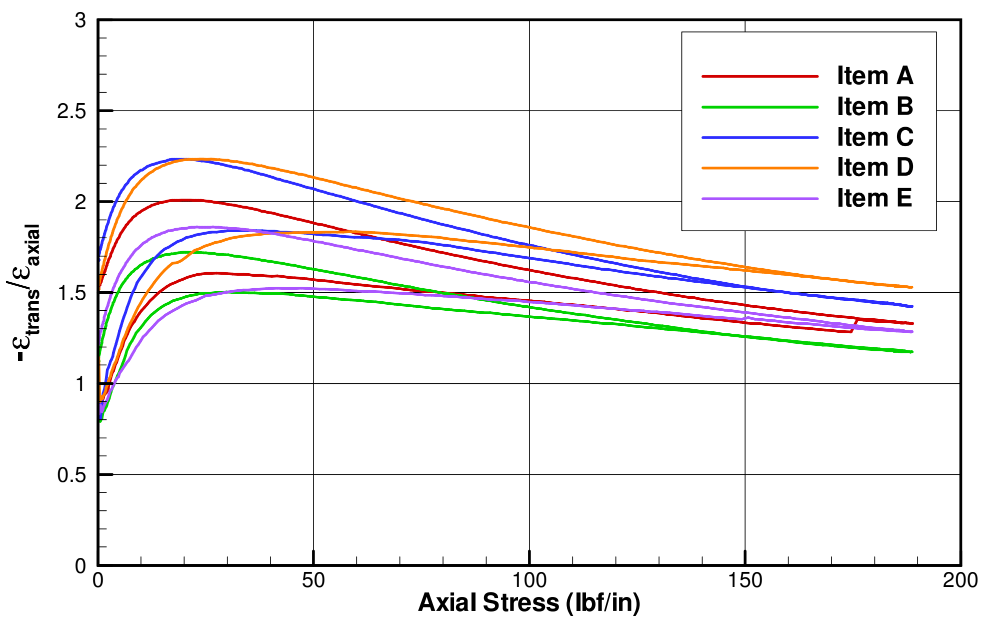

Figure 40: 200 denier Kevlar fill axial pull test, strain ratio cycle 1.

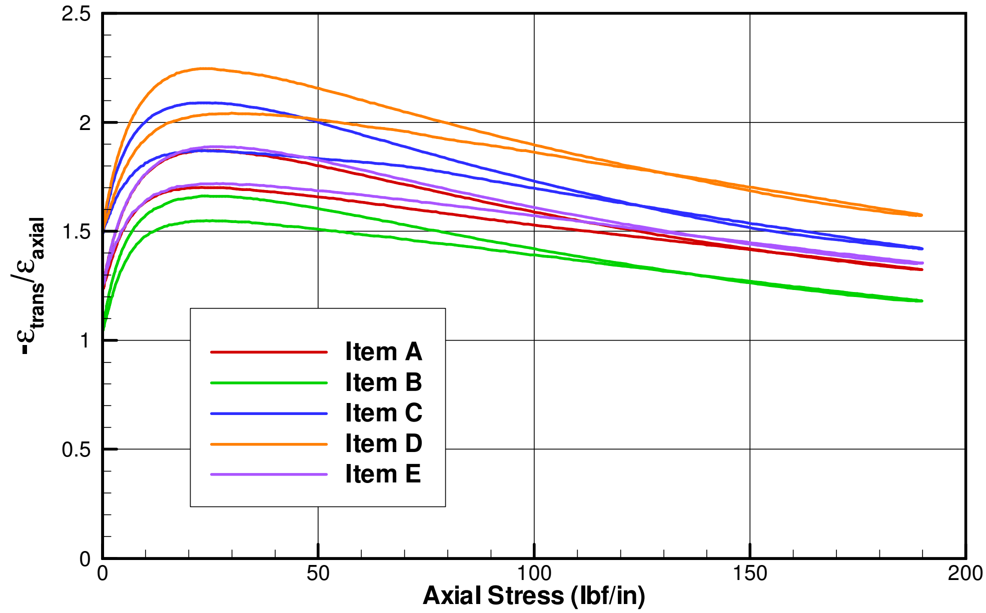

Figure 41: 200 denier Kevlar fill axial pull test, strain ratio cycle 10.

5.3.3 Warp versus Fill Stiffness Comparison

The 200 denier Kevlar warp and fill normal stress-strain data for the first load cycle is shown in Figure 42. The warp and fill normal stress-strain data for the tenth load cycle is shown in Figure 43. For the first load cycle, the warp direction is stiffer than the fill direction. This is due to the initial low stiffness region in the fill direction bi-linear response. Other than an offset resulting from the respective strain sets, the warp and fill stress-strain responses are very similar for the tenth load cycle.

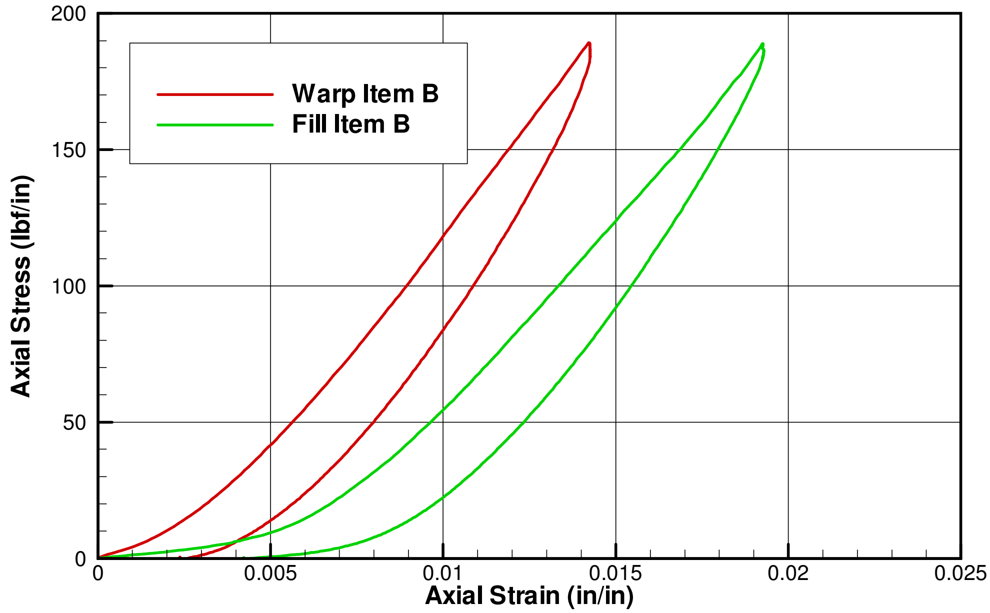

Figure 42: 200 denier Kevlar axial pull test, cycle 1 warp vs. fill stiffness.

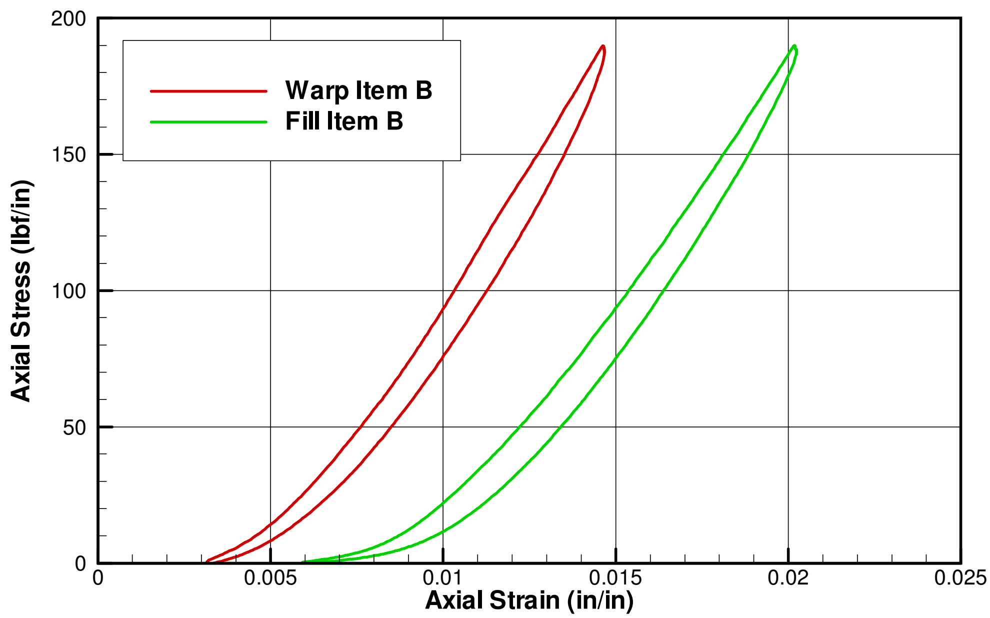

Figure 43: 200 denier Kevlar axial pull test, cycle 10 warp vs. fill stiffness.

5.4 840 Denier Kevlar

5.4.1 Warp Direction Pull Tests

The 840 denier Kevlar warp direction measured normal stress-strain behavior for the stress interval [0, 491] lbf/in is shown in Figure 44 through Figure 46. Figure 44 shows the first load cycle for all the samples tested. Similarly, Figure 45 shows the stress-strain data for the tenth load cycle. The results for the first load cycle exhibit non-linearity in the ramp up portion of the load curve. The stress-strain response was bi-linear in nature with low stiffness at low loads and then a significantly higher stiffness at higher loads. The strain set was observed to be approximately 38% of the strain maximum for the first load cycle. The results for the tenth load cycle showed less of a bi-linear response where the initial low stiffness linear region was not as large in the stress-strain curve. Figure 46 shows all ten load/unload cycles for one of the samples tested.

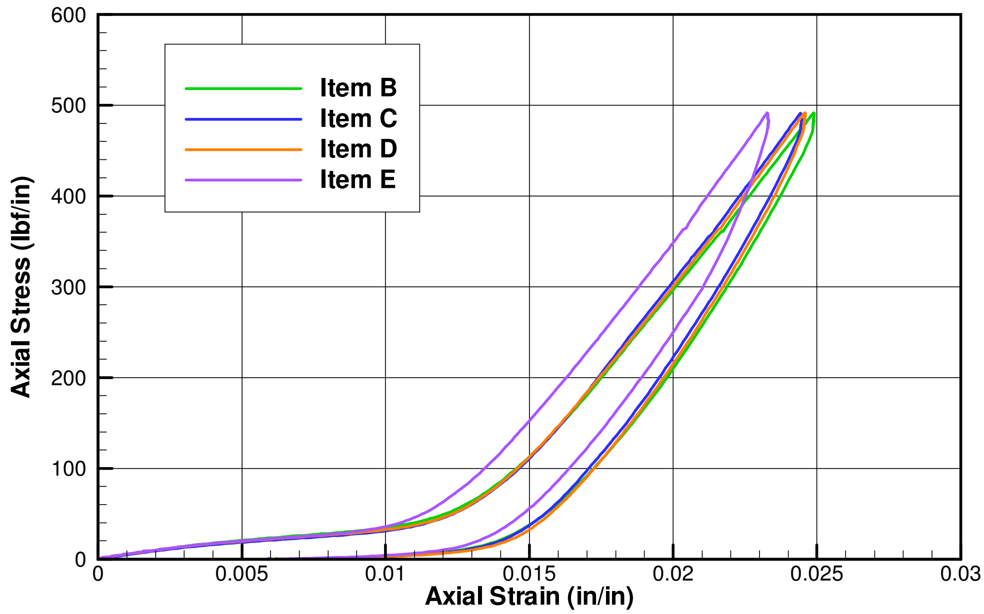

Figure 44: 840 denier Kevlar warp axial pull test, load cycle 1.

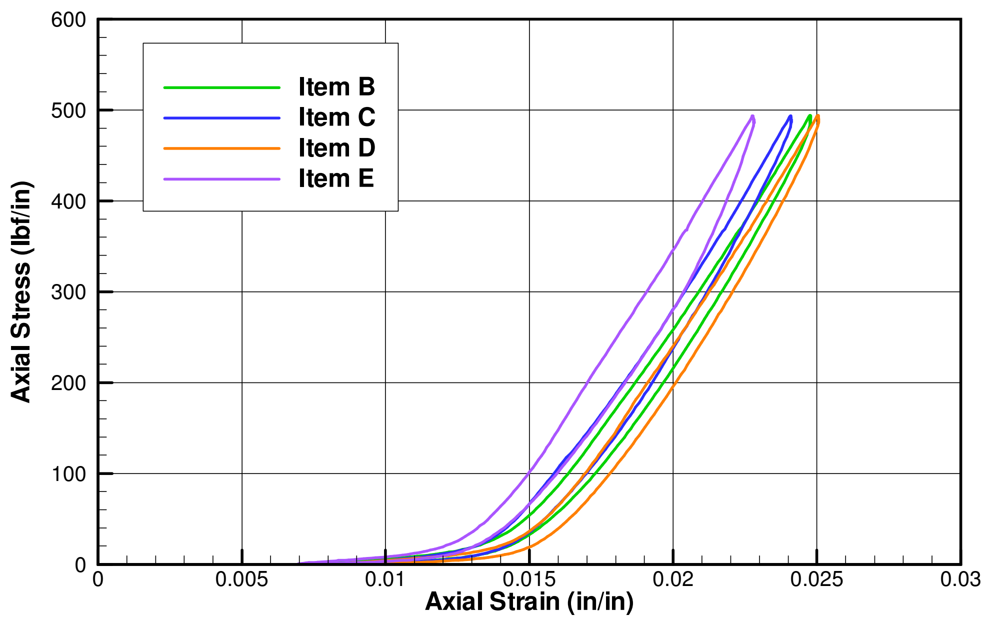

Figure 45: 840 denier Kevlar warp axial pull test, load cycle 10.

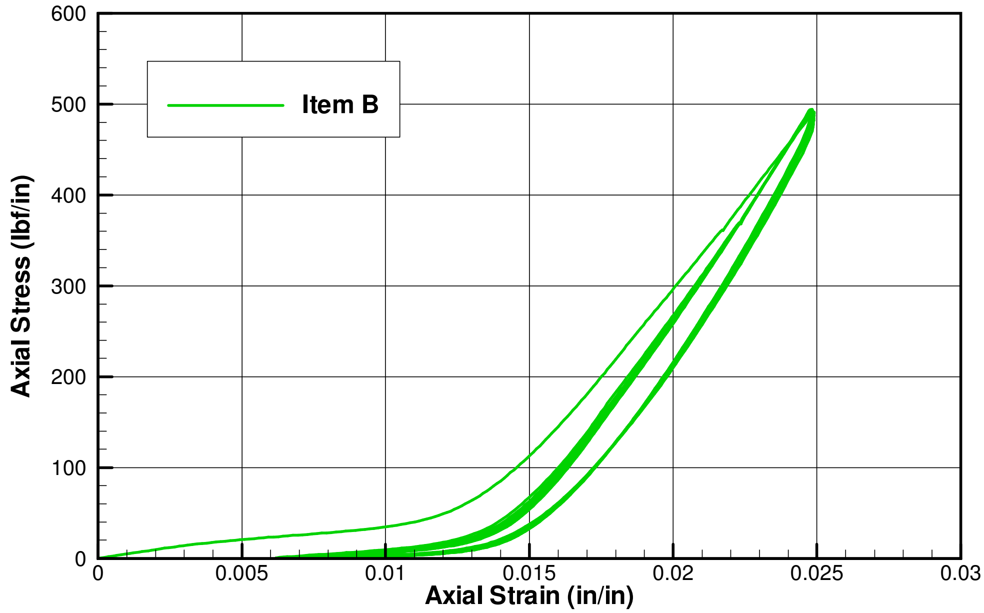

Figure 46: 840 denier Kevlar warp axial pull test, all ten load cycles.

Figure 47 and Figure 48 show the transverse to axial strain ratios for warp axial pulls of the 840 denier Kevlar material. The strain ratio is observed to be loading dependent through the entire load range for all cycles. Other than some differences at low load, the cycling did not have an impact on the ratio. The overall magnitude of the ratio for the 840 denier Kevlar was similar to that of the 200 denier Kevlar. In all cases the ratio was greater than 1.0 and under some loads it was greater than 2.0.

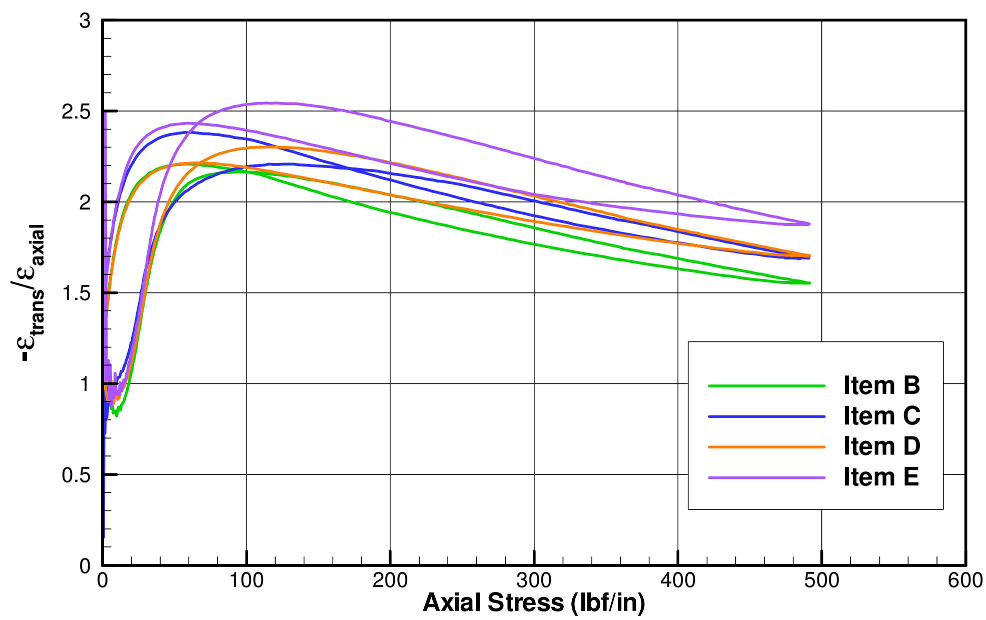

Figure 47: 840 denier Kevlar warp axial pull test, strain ratio cycle 1.

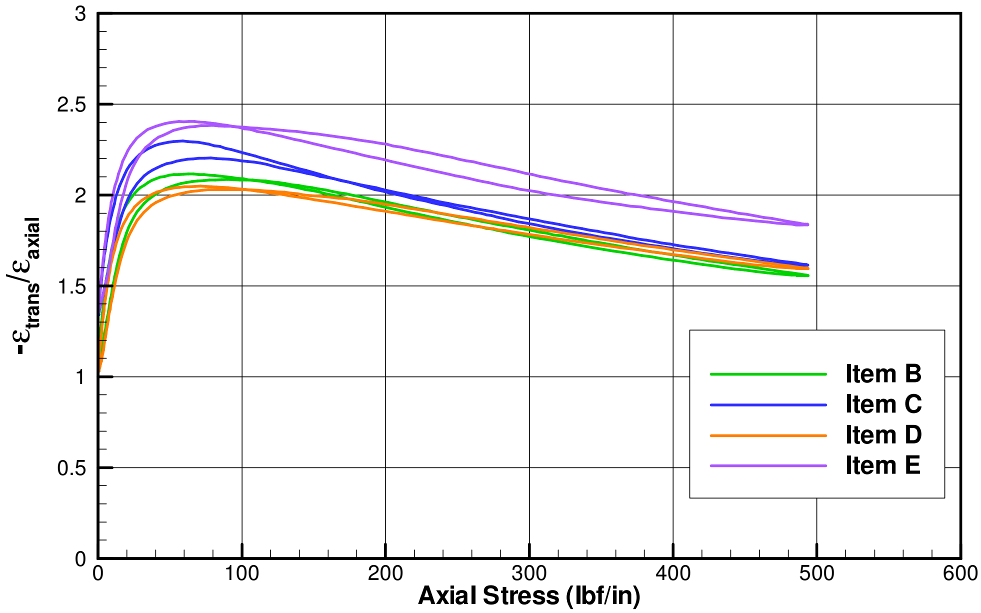

Figure 48: 840 denier Kevlar warp axial pull test, strain ratio cycle 10.

5.4.2 Fill Direction Pull Tests

The 840 denier Kevlar fill direction measured normal stress-strain behavior for the stress interval [0, 491] lbf/in is shown in Figure 49 through Figure 51. Figure 49 shows the first load cycle for all the samples tested. Similarly, Figure 50 shows the stress-strain data for the tenth load cycle.

The results for the first load cycle exhibit non-linearity in the ramp up portion of the load curve. The stress-strain response was bi-linear in nature with low stiffness at low loads and then a significantly higher stiffness at higher loads. The strain set was observed to be approximately 28% of the strain maximum for the first load cycle. The results for the tenth load cycle showed less of a bi-linear response where the initial low stiffness linear region was not present in the stress-strain curve. Figure 51 shows all ten load/unload cycles for one of the samples tested.

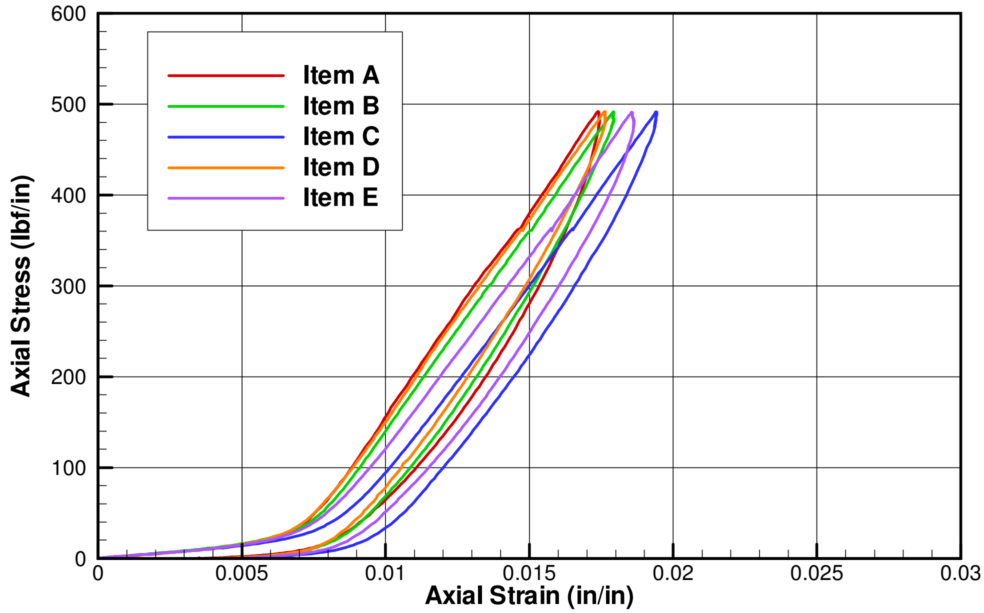

Figure 49: 840 denier Kevlar fill axial pull test, load cycle 1.

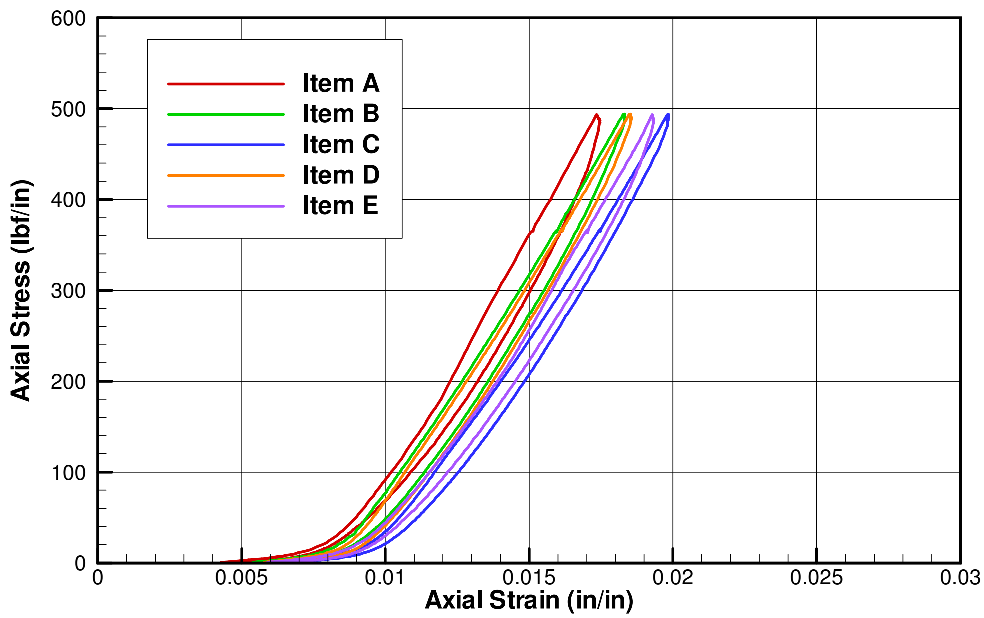

Figure 50: 840 denier Kevlar fill axial pull test, load cycle 10.

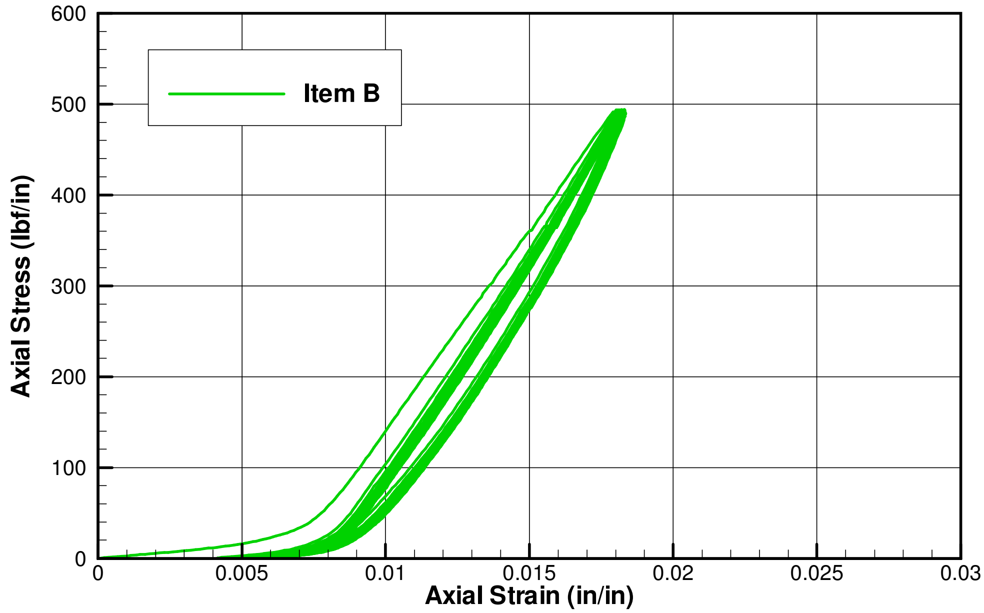

Figure 51: 840 denier Kevlar fill axial pull test, all ten load cycles.

Figure 52 and Figure 53 show the transverse to axial strain ratios for fill axial pulls of the 840 denier Kevlar material. The strain ratio is observed to be loading dependent through the entire load range for all cycles. The cycling did not have an impact on the ratio. The overall magnitude of the ratio for the 840 denier Kevlar was similar to that of the 200 denier Kevlar. In all cases the ratio was greater than 1.0 and under some loads it was greater than 2.0.

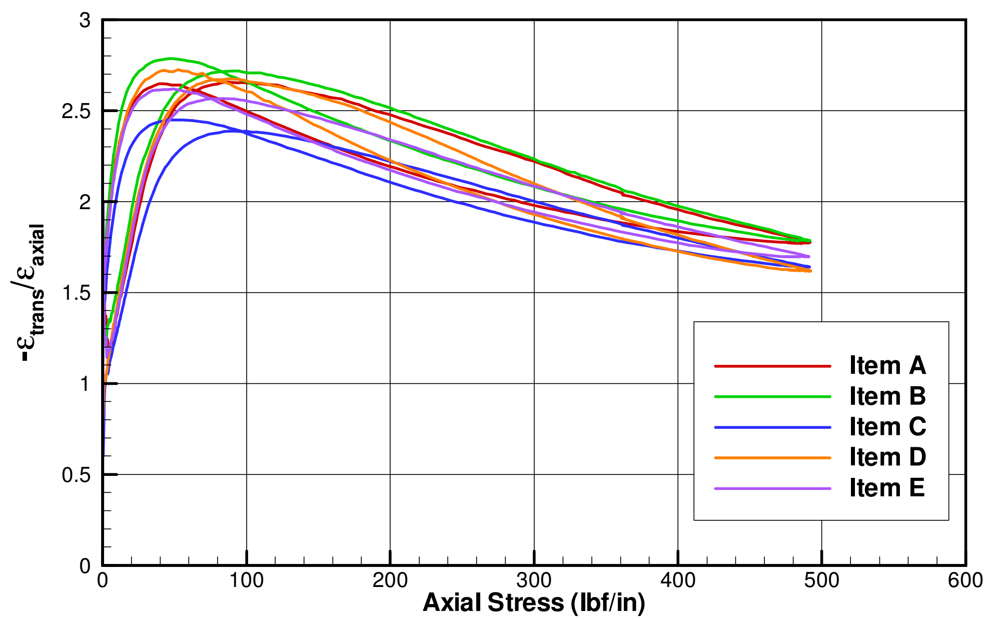

Figure 52: 840 denier Kevlar fill axial pull test, strain ratio cycle 1.

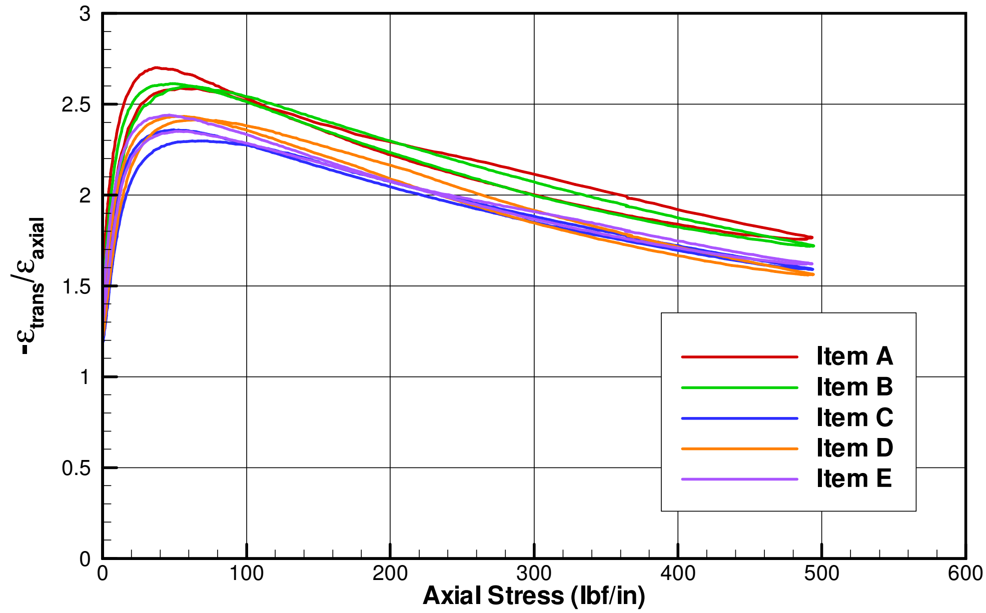

Figure 53: 840 denier Kevlar fill axial pull test, strain ratio cycle 10.

5.4.3 Warp versus Fill Stiffness Comparison

The 840 denier Kevlar warp and fill normal stress-strain data for the first load cycle is shown in Figure 54. The warp and fill normal stress-strain data for the tenth load cycle is shown in Figure 55. For the first load cycle, the fill direction is stiffer than the warp direction. This is due to the initial low stiffness region being larger on the warp direction response. Other than an offset resulting from the respective strain sets, the warp and fill stress-strain responses are very similar for the tenth load cycle.

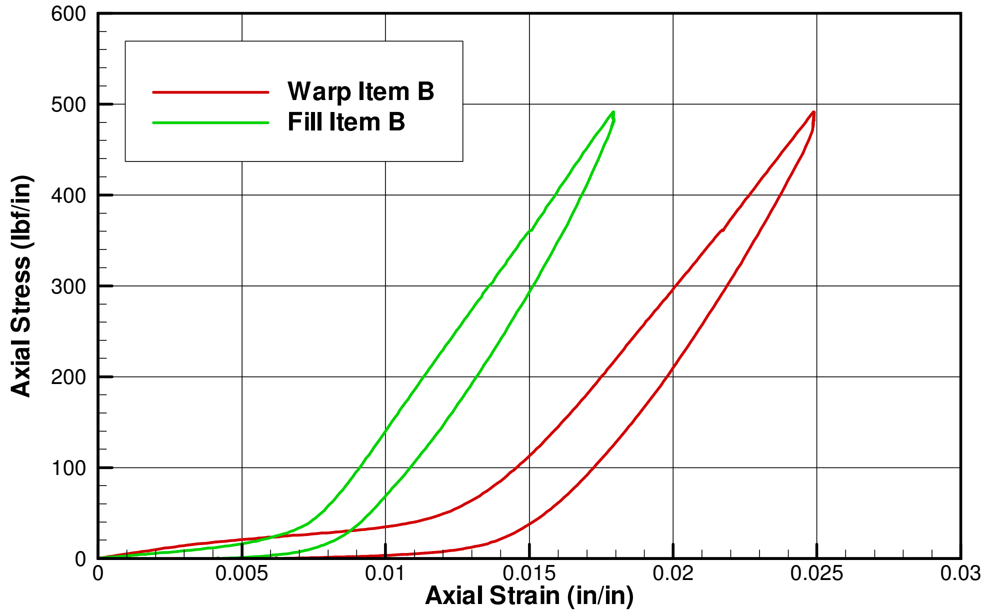

Figure 54: 840 denier Kevlar axial pull test, cycle 1 warp vs. fill stiffness.

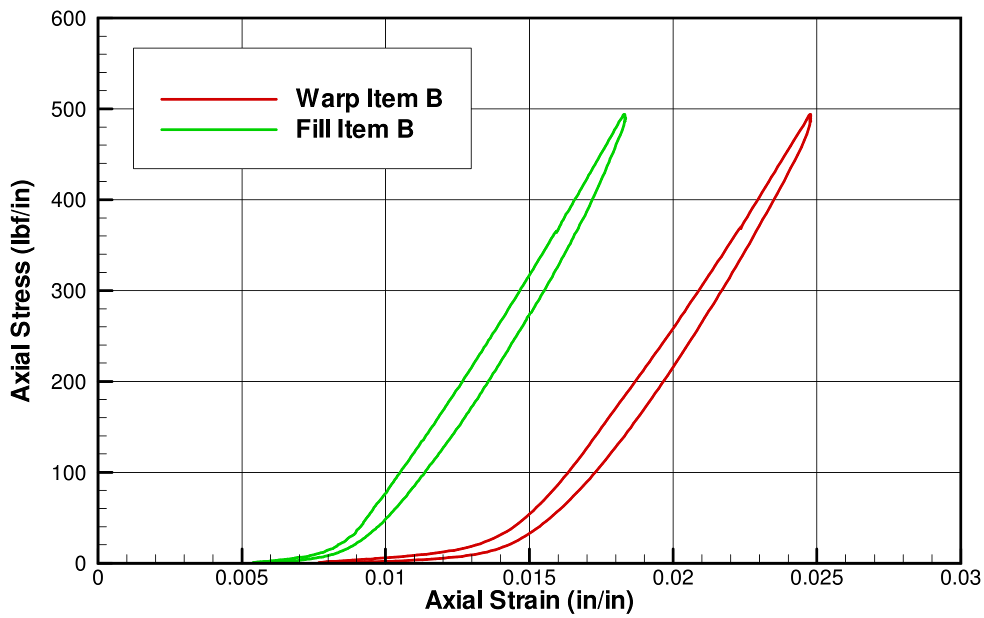

Figure 55: 840 denier Kevlar axial pull test, cycle 10 warp vs. fill stiffness.

6. Shear Stress-Strain

6.1 Picture Frame Testing

The picture frame apparatus used in the testing had a bearing to bearing side length of 10 inches. The test article for the picture frame shear testing had a slightly shorter edge length of 8.0 inches. The apparatus with a test article installed is shown in Figure 3. The INSTRON crosshead extension along with the apparatus side length was used to calculate the shear strain. Shear strain was calculated as $\theta = \frac{\pi}{2} - \phi$, where ϕ is the frame angle as shown in Figure 56.

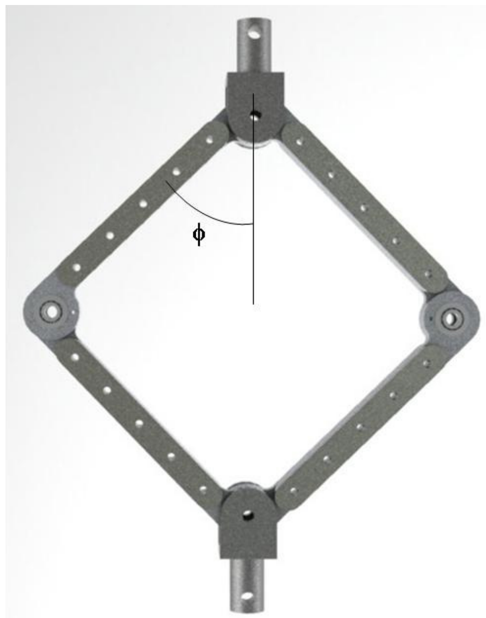

Figure 56: Picture Frame Test Fixture – Frame Angle

The crosshead extension along with the load cell force was used to calculate the shear stress. This included calculating the shear force as $F = \frac{F_L}{2\cos\phi}$ where F_L is the load cell force and the nominal shear stress as $\sigma = \frac{F}{L}$ where L is the side length of the picture frame fixture.

Engineering shear strain versus shear stress is shown plotted in the figures of this section. Shear strain is reported in radians, and is the angle between the warp and fill fibers as the fabric is loaded. The test cycles were defined in terms of maximum/minimum load cell force. The test cycles always started out with a pulling action on the pivot points of the fixture and then a pushing action as shown in Figure 57. The results for the pulling portion of a load cycle were generally positive shear strain and stress. Conversely, the push portions of the load cycle were generally negative shear strain and stress.

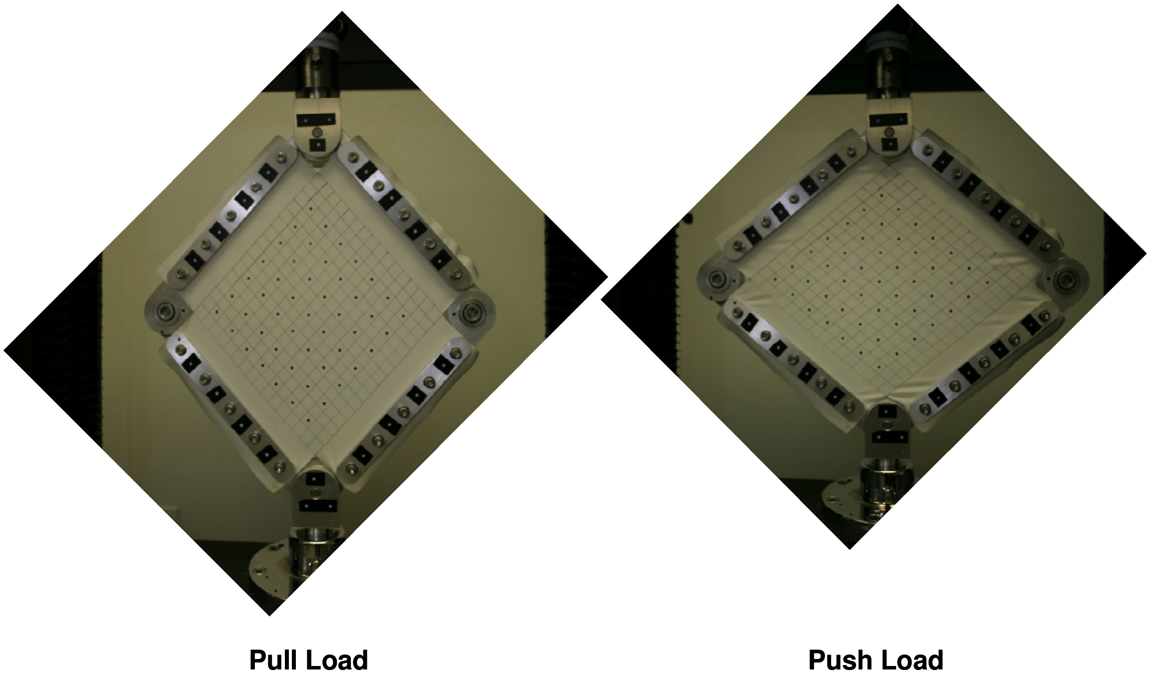

Figure 57: Picture frame test load scenario.

During the first load cycle of this testing, the INSTRON crosshead was paused twice for photogrammetry picture taking. A sample time history plot showing these pauses is shown in Figure 58. Although the strain was held at a constant value for the pictures, the actual load relaxed significantly during the time it took to take the photos. As a result of this, the plots in this section include the 2nd through the 5th cycles.

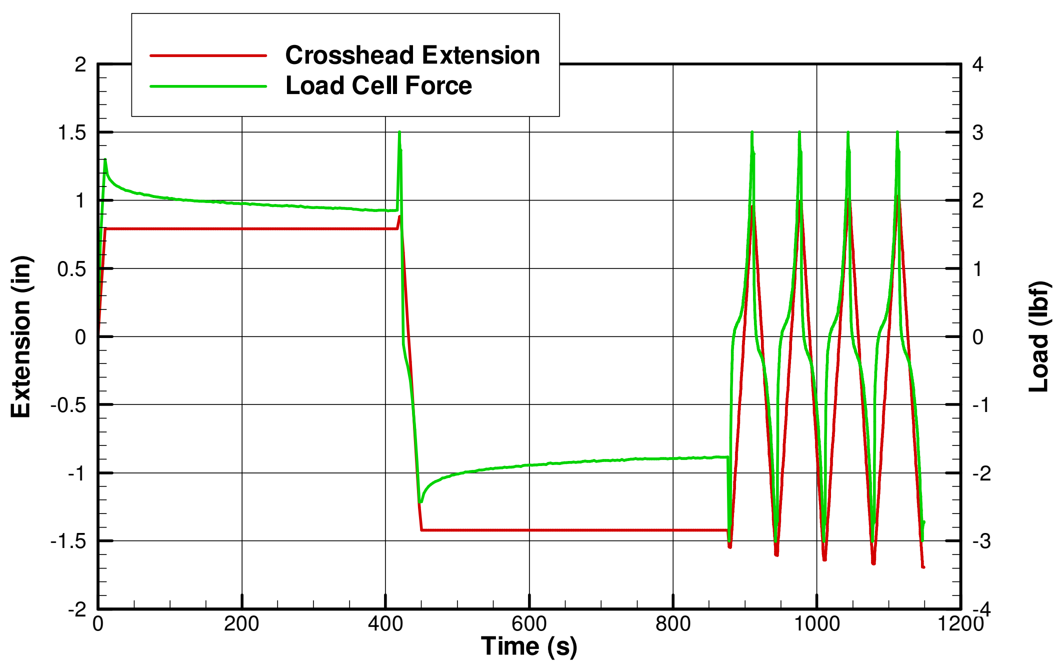

Figure 58: F-111 Nylon Item A time history.

6.1.1 F-111 Nylon Picture Frame Testing

The results for the F-111 Nylon shear stress-strain are shown plotted individually for each test article and then in one plot where all the curves are overlaid. We observe some change in shear stiffness with continued cycling for the Nylon. Other than an offset in shear strain, the response of items A and B were similar. The induced shear strain range for Item C was larger than it was for Items A and B.

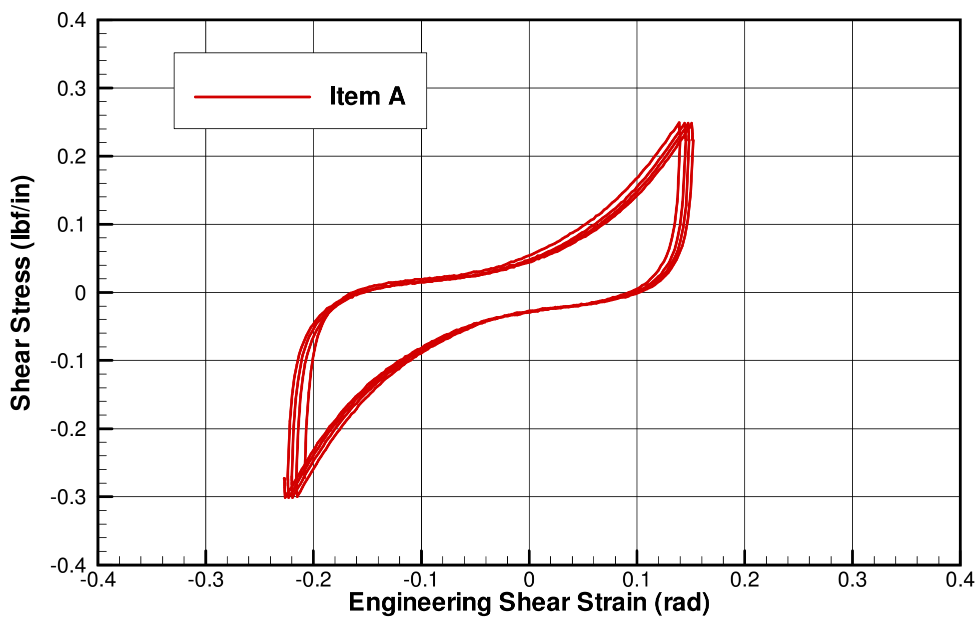

Figure 59: F-111 Nylon picture frame test, Item A shear stress-strain.

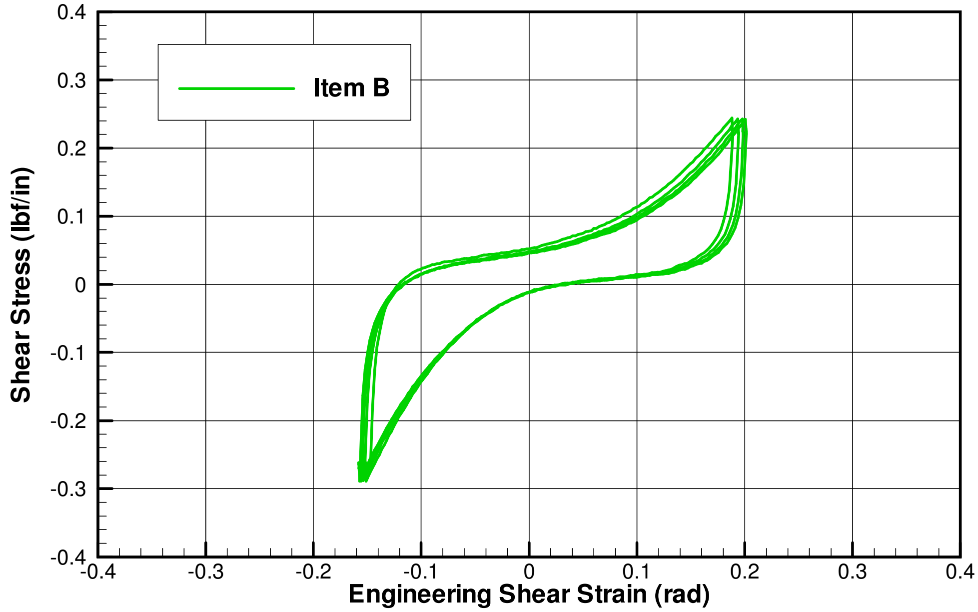

Figure 60: F-111 Nylon picture frame test, Item B shear stress-strain.

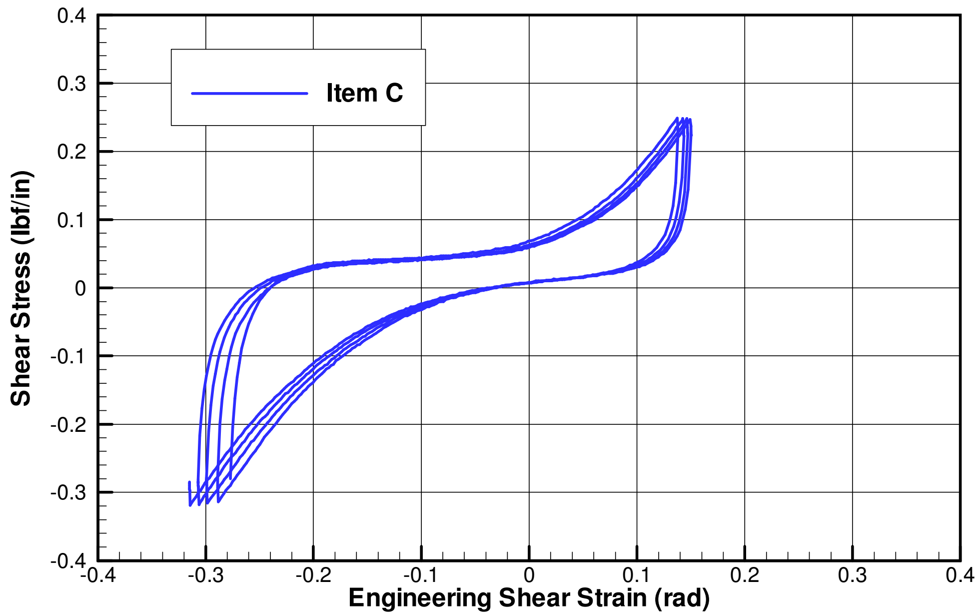

Figure 61: F-111 Nylon picture frame test, Item C shear stress-strain.

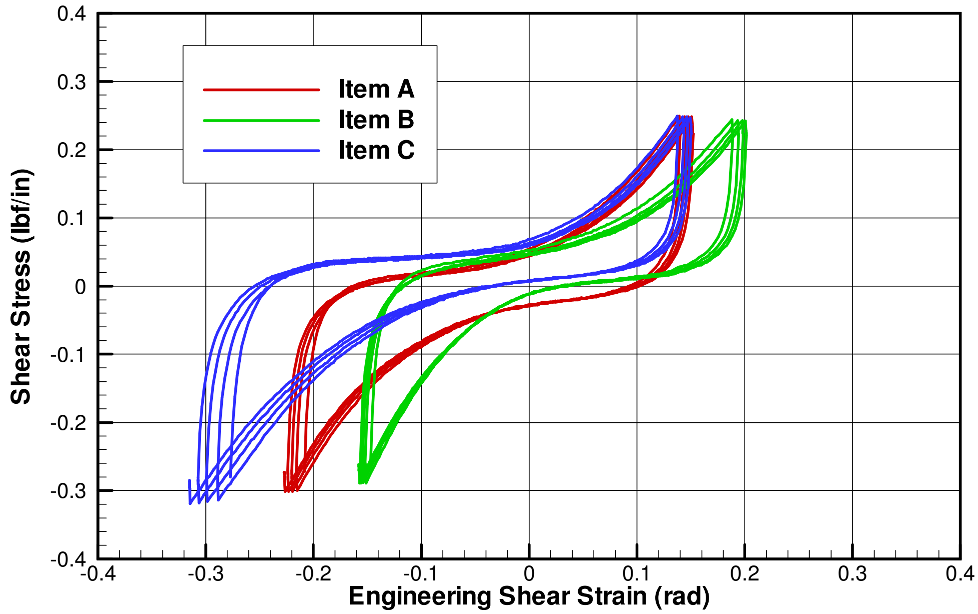

Figure 62: F-111 Nylon picture frame test, shear stress-strain.

6.1.2 HT1 Nomex Picture Frame Testing

Test articles identified as A, B, and C were tested as described in Section 6.1. The results for these test articles are shown in Figure 63 and Figure 64. Figure 63 shows the results for the test article identified as Item A. Similar to the Nylon material, we observe some change in shear stiffness with continued cycling for the HT1 Nomex. In Figure 64 we see that articles A through C are in relatively good agreement with each other. A shear stress strain response was observed that was less stiff in the push portion of the load cycle as it was in the pull section. This result was also observed for the Nylon test articles in the previous sub-section. There was one additional HT1 Nomex test article, identified as Item D, that had a much more consistent response relative to the pull and push portions of the load cycle. All five load cycles are shown for Item D in Figure 65. For Item D there were no pauses in the loading for photogrammetry. Additional testing would be needed to determine if the extended pauses for photogrammetry during the first load cycle impacted the stiffness measured in the push portions of the load cycle.

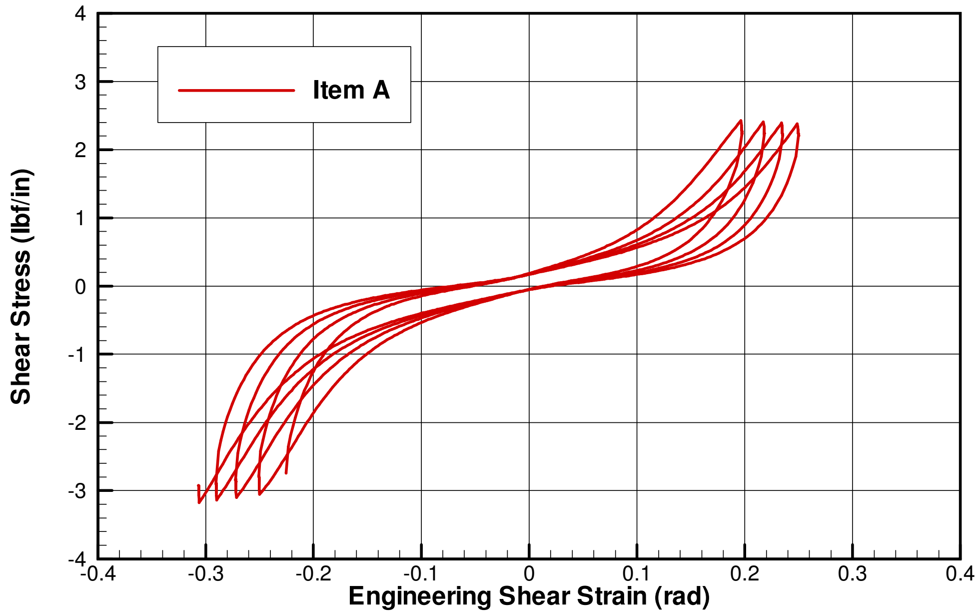

Figure 63: HT1 Nomex picture frame test, Item A shear stress-strain.

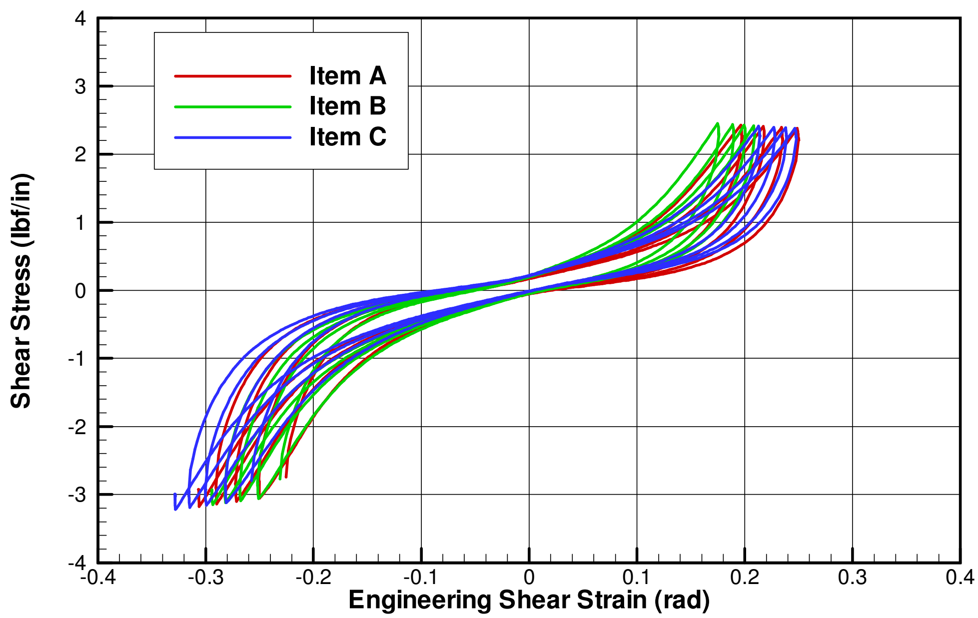

Figure 64: HT1 Nomex picture frame test, Items A, B & C shear stress-strain.

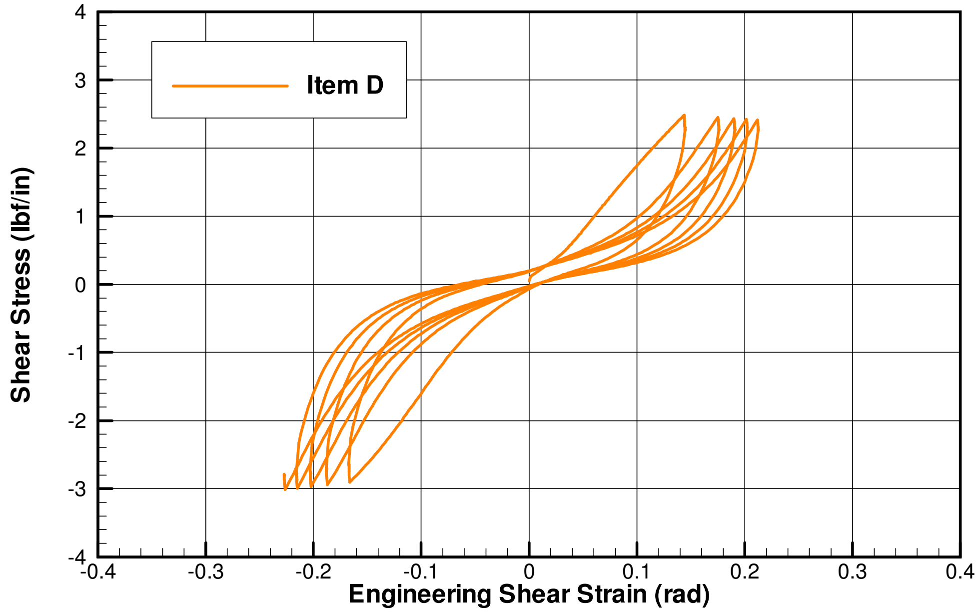

Figure 65: HT1 Nomex picture frame test, Item D shear stress-strain.

6.1.3 200 Denier Kevlar Picture Frame Testing

For the 200 denier Kevlar picture frame testing two of the five test articles were in particularly good agreement as shown in Figure 66. In this figure we see that the shear stress strain response did not change as the load cycling increased. Figure 67 shows the picture frame shear stress-strain response for all the articles tested for the 200 denier Kevlar. The test article identified as Item E had a lower shear stiffness as compared with the other samples.

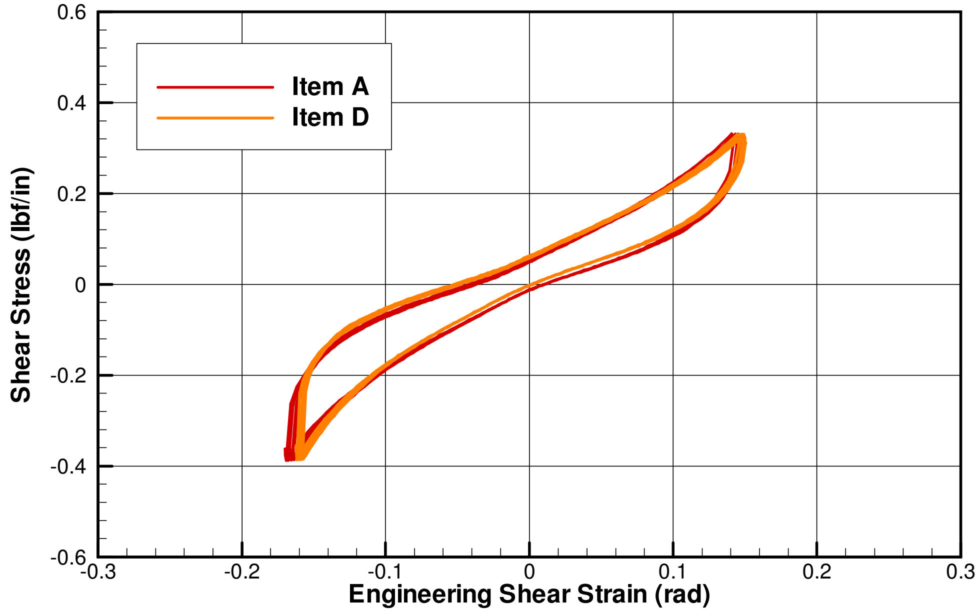

Figure 66: 200 denier Kevlar picture frame test, Item A and D shear stress-strain.

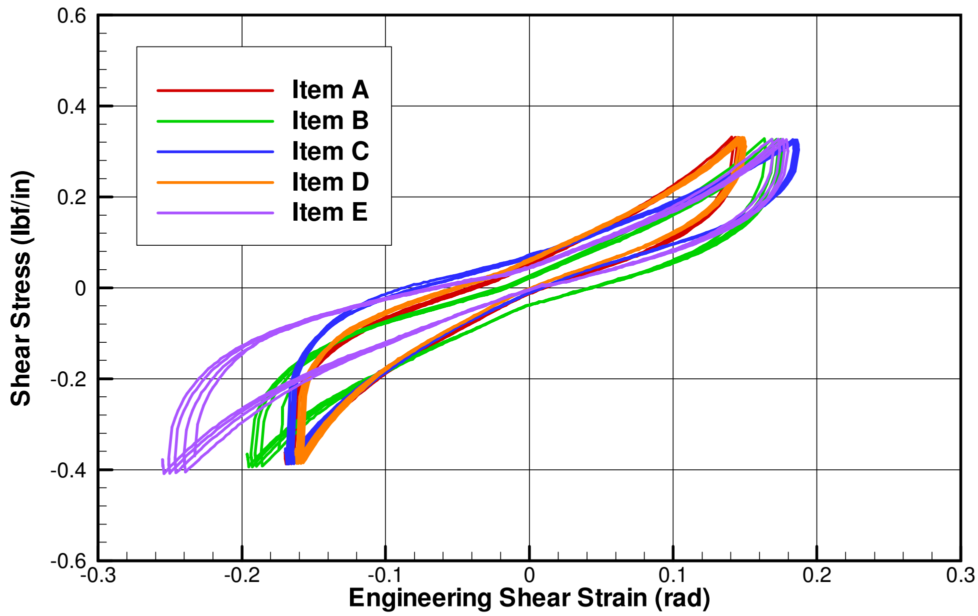

Figure 67: 200 denier Kevlar picture frame test, shear stress-strain.

6.1.4 840 Denier Kevlar Picture Frame Testing

The results for the 840 denier Kevlar picture frame testing are shown in Figure 68 through Figure 70. The tendency for the shear stiffness results to be less stiff in the push direction repeat again for this material. Of the four materials in this study, the 840 denier Kevlar had the largest relative change between the push direction and pull direction shear stiffness. This result can be seen in Figure 68, where the shear stress-strain data is shown plotted for the test article identified as Item

A. For the five 840 denier Kevlar articles tested with the picture frame apparatus, four of the five were in relatively good agreement as shown in Figure 69. Test Item E had a significantly different shear stress-strain response and is shown plotted in Figure 70 with Item A for comparison.

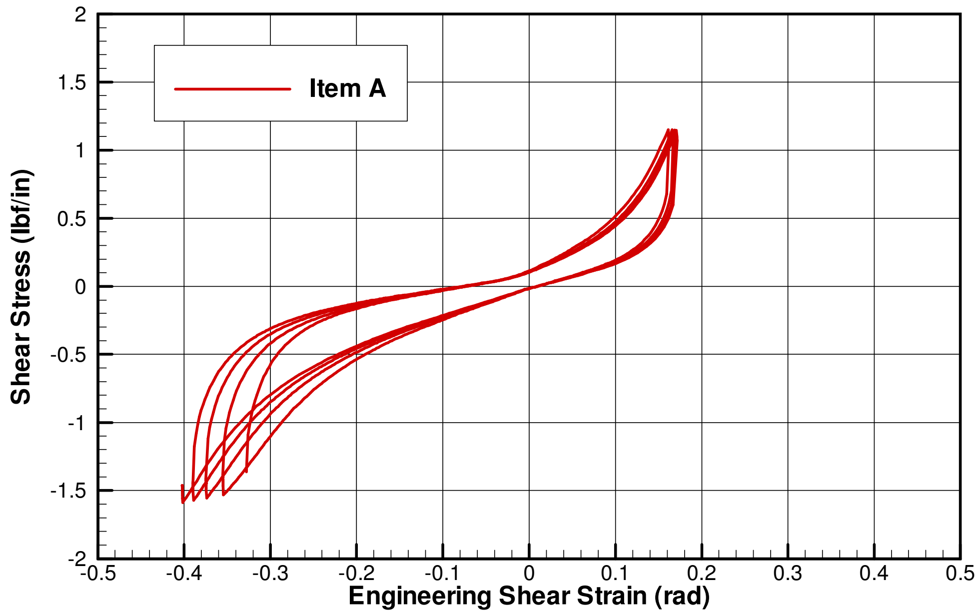

Figure 68: 840 denier Kevlar picture frame test, Item A shear stress-strain.

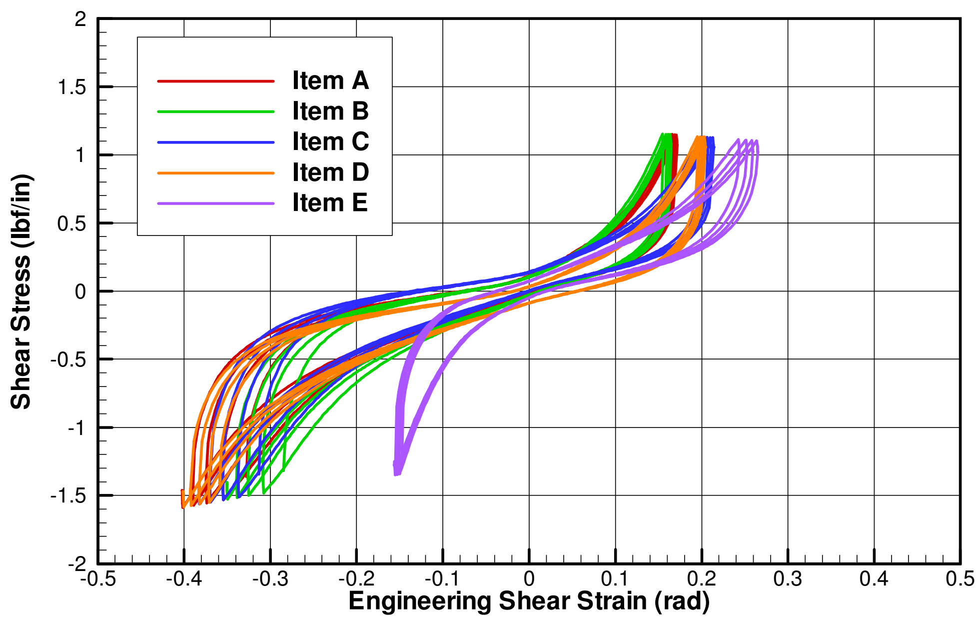

Figure 69: 840 denier Kevlar picture frame test, shear stress-strain.

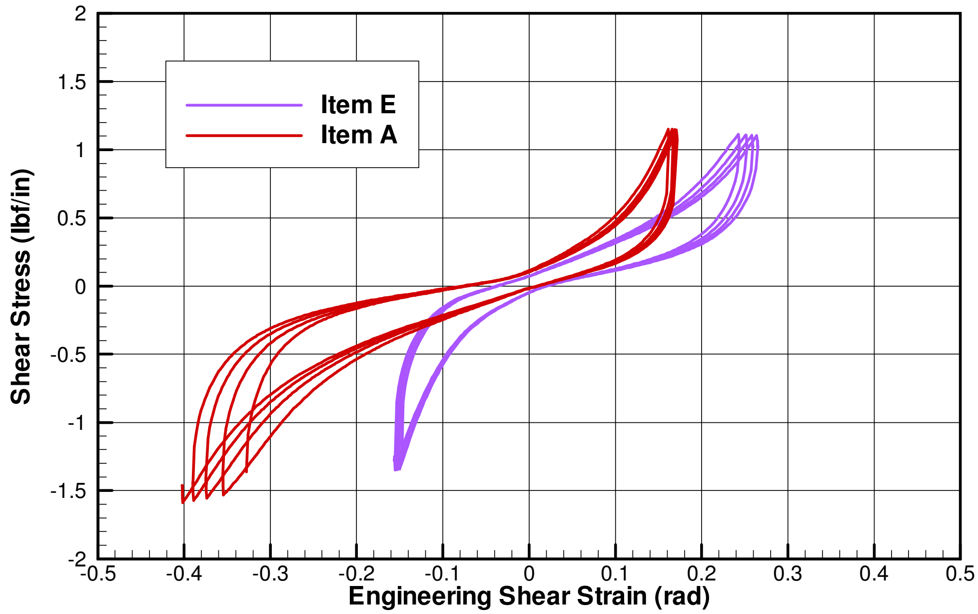

Figure 70: 840 denier Kevlar picture frame test, Item A and E shear stress-strain.

6.2 Bias Extension Testing

Bias Extension test results are presented in the next four sub sections for the four materials under consideration in this task. The sample size used for this testing had a height of 8.6 inches and a width of 3.5 inches. INSTRON load and crosshead extension were the two primary measurements taken during the testing. Cross head extension was converted into engineering shear strain in the pure shear region of the test article. This was calculated as $\theta = \frac{\pi}{2} - 2\phi$ and $\phi = \cos^{-1}\left[\cos\phi_0 + \frac{\delta}{2(H-W)\cos\phi_0}\right]$ where H = sample height, W= sample width, and δ = displacement.

Some iterative numerical analysis is required to convert the load and extension into the shear stress in the pure shear region of the sample. This numerical analysis has not yet been conducted for these results. As a result, the experimental plots in this section will plot load versus engineering shear strain. The result plots only show the ramp up portion of the first cycle where the crosshead was paused for photogrammetry pictures. The subsequent cycles where the crosshead was not paused have both the ramp up and ramp down portions of the loading included.

6.2.1 F-111 Nylon Bias Extension Testing

The F-111 Nylon bias extension shear stiffness behavior for the shear strain interval [0, 0.097] rad is shown in Figure 71 through Figure 73. Figure 71 shows the ramp up for the first load cycle of all samples tested. Figure 72 shows the shear stiffness results for the fifth load cycle. The first cycle load versus shear strain response during the ramp up for the Nylon had an initial non-linear region followed by a linear region. The first load cycle resulted in a shear strain set that was approximately 67% of the maximum induced shear strain of the cycle. The results for the fifth load cycle showed a predominantly linear response during the load ramp up. Figure 73 shows load cycles 2 through 5 for one of the samples tested. From this figure we see that subsequent cycling had no effect on the shear stiffness in this strain range. The load cycles do exhibit some degree of hysteresis in the stress-strain response.

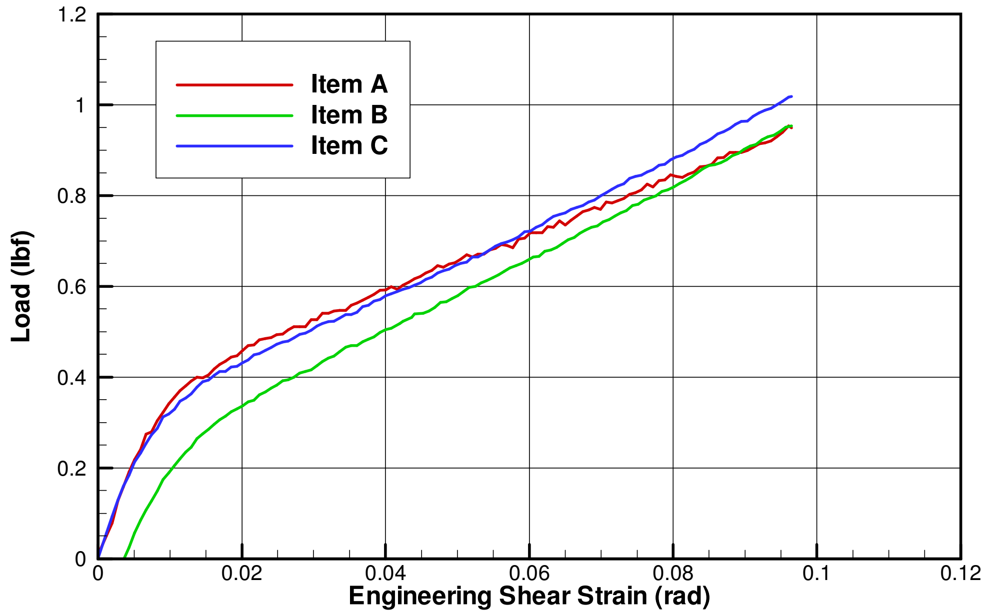

Figure 71: F-111 Nylon bias extension test, load ramp up cycle 1.

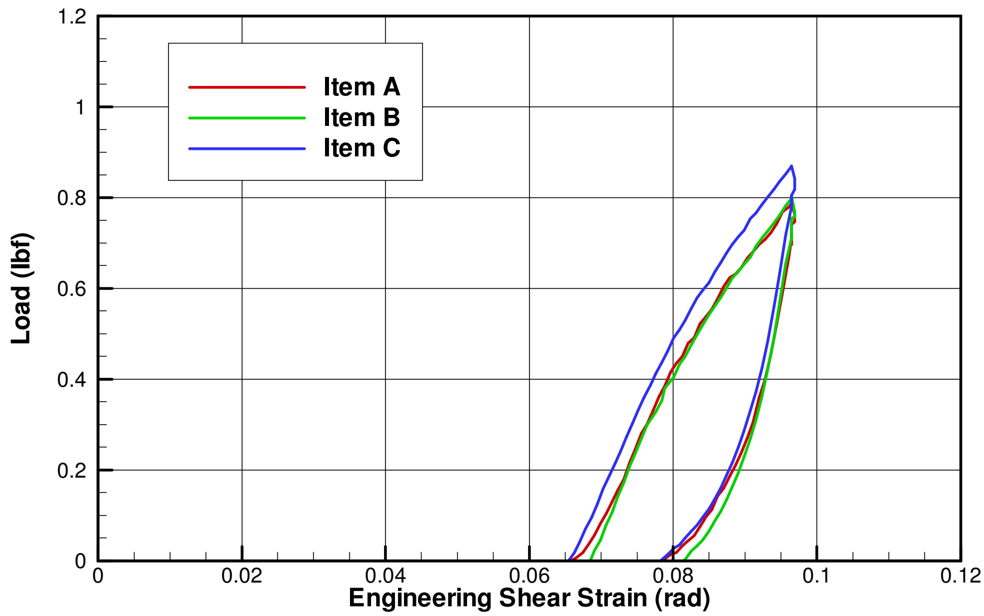

Figure 72: F-111 Nylon bias extension test, load cycle 5.

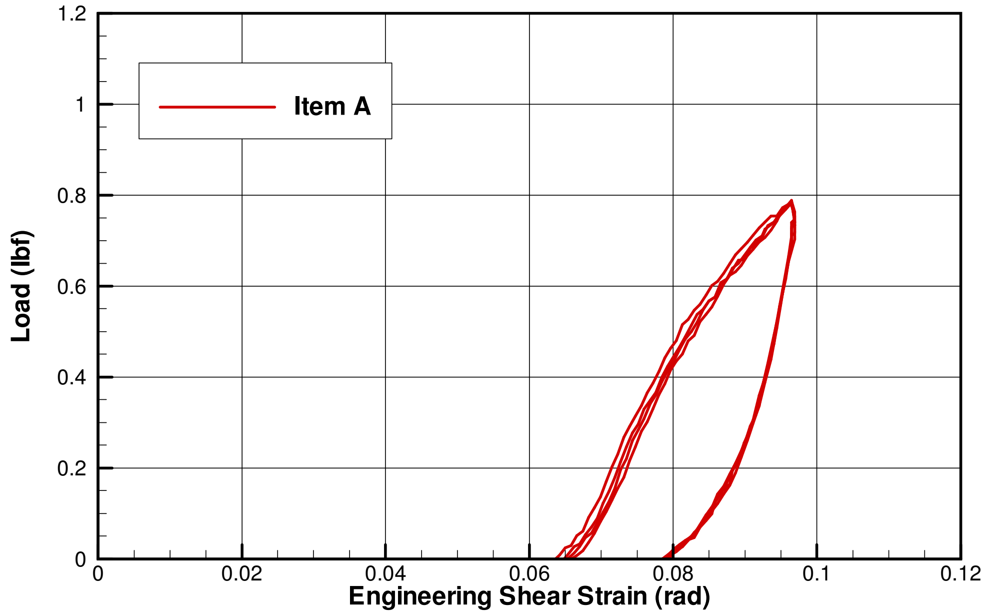

Figure 73: F-111 Nylon bias extension test, cycles 2 through 5.

6.2.2 HT1 Nomex Bias Extension Testing

The HT1 Nomex bias extension shear stiffness behavior for the shear strain interval [0, 0.097] rad is shown in Figure 74 through Figure 76. Figure 74 shows the ramp up for the first load cycle of all samples tested. Figure 75 shows the shear stiffness results for the fifth load cycle. The first cycle load versus shear strain response during the ramp up for the Nomex was predominantly linear. The first load cycle resulted in a shear strain set that was approximately 8% of the maximum induced shear strain of the cycle. The results for the fifth load cycle showed a greater degree of non-linearity during the load ramp up. Figure 76 shows load cycles 2 through 5 for one of the samples tested. From this figure we see that subsequent cycling had no effect on the shear stiffness in this strain range. The load cycles do exhibit some degree of hysteresis in the stress-strain response.

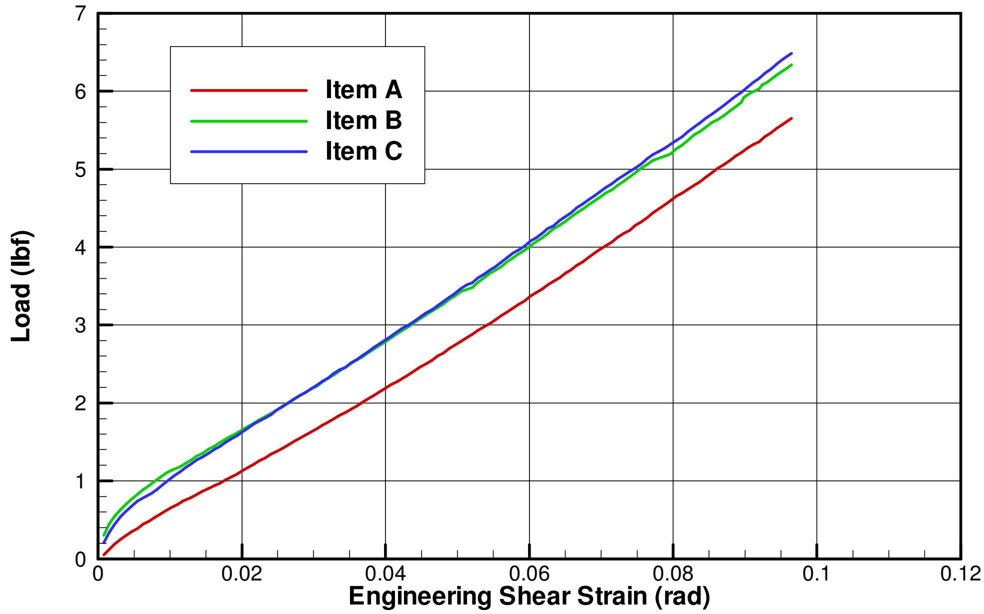

Figure 74: HT1 Nomex bias extension test, load ramp up cycle 1.

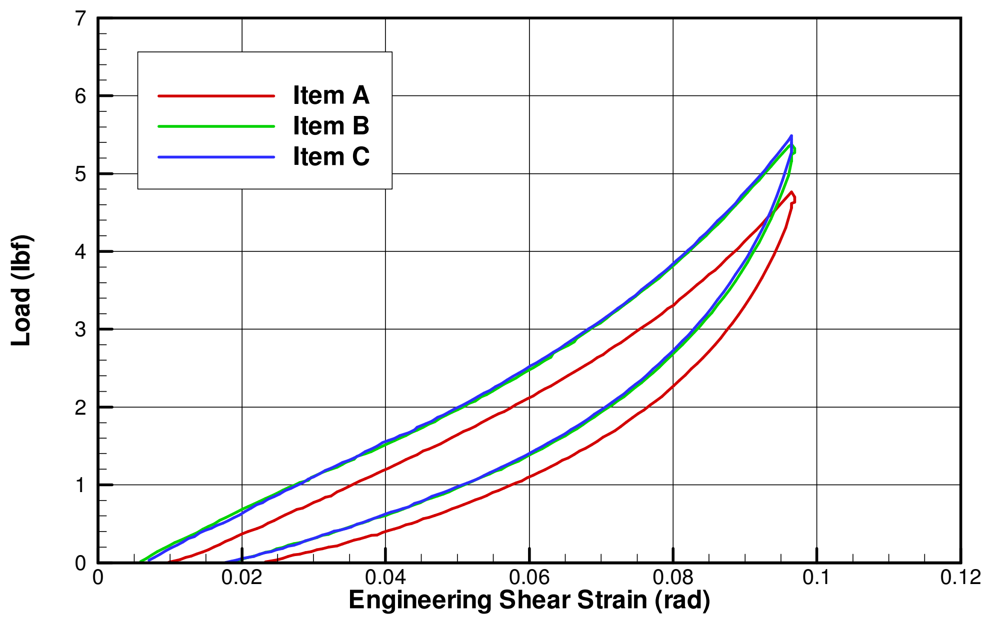

Figure 75: HT1 Nomex bias extension test, load cycle 5.

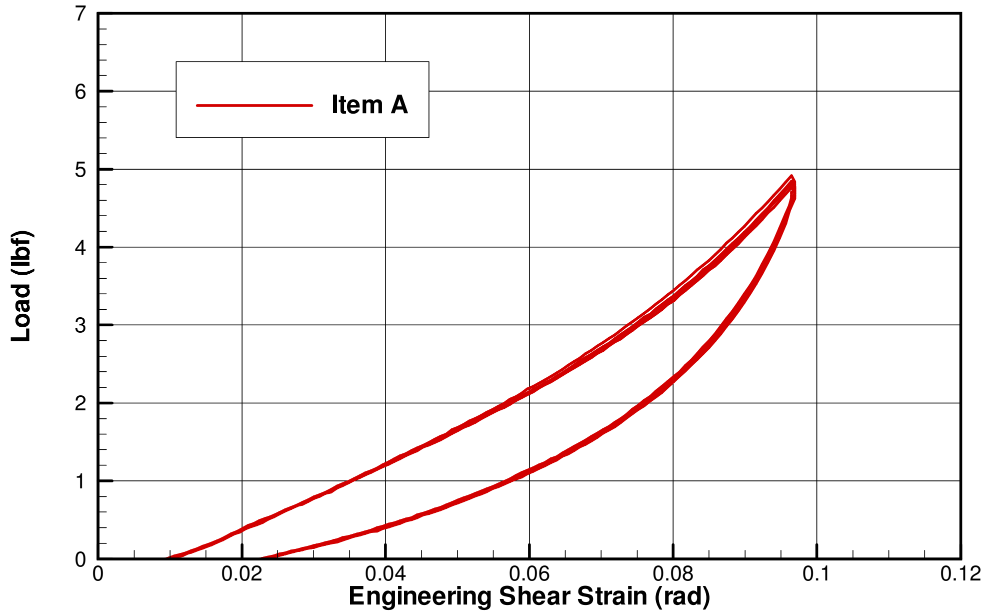

Figure 76: HT1 Nomex bias extension test, cycles 2 through 5.

6.2.3 200 Denier Kevlar Bias Extension Testing

The 200 denier Kevlar bias extension shear stiffness behavior for the shear strain interval [0, 0.097] rad is shown in Figure 77 through Figure 79. Figure 77 shows the ramp up for the first load cycle of all samples tested. Figure 78 shows the shear stiffness results for the fifth load cycle. The first cycle load versus shear strain response during the ramp up for the 200 denier Kevlar was predominantly linear. The first load cycle resulted in a shear strain set that was approximately 10% of the maximum induced shear strain of the cycle. Figure 79 shows load cycles 2 through 5 for one of the samples tested. From this figure we see that subsequent cycling had no effect on the shear stiffness in this strain range. The load cycles do exhibit some degree of hysteresis in the stress-strain response.

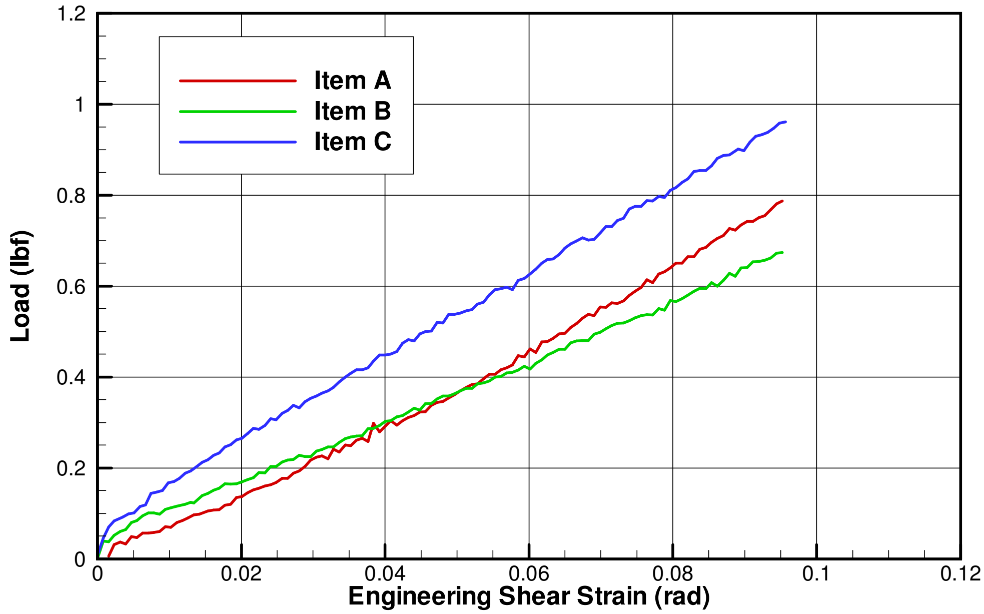

Figure 77: 200 denier Kevlar bias extension test, load ramp up cycle 1.

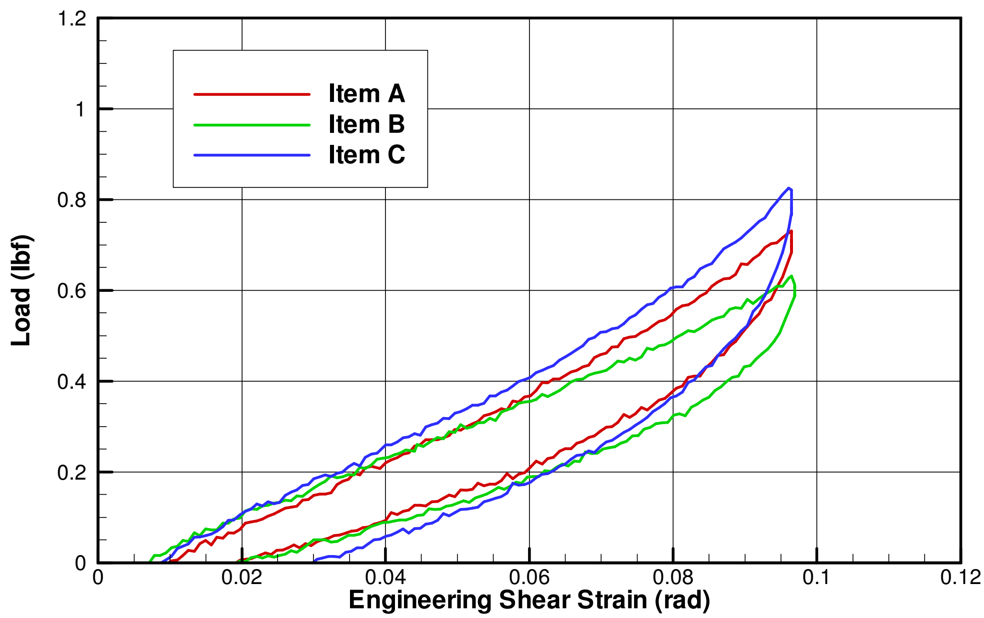

Figure 78: 200 denier Kevlar bias extension test, load cycle 5.

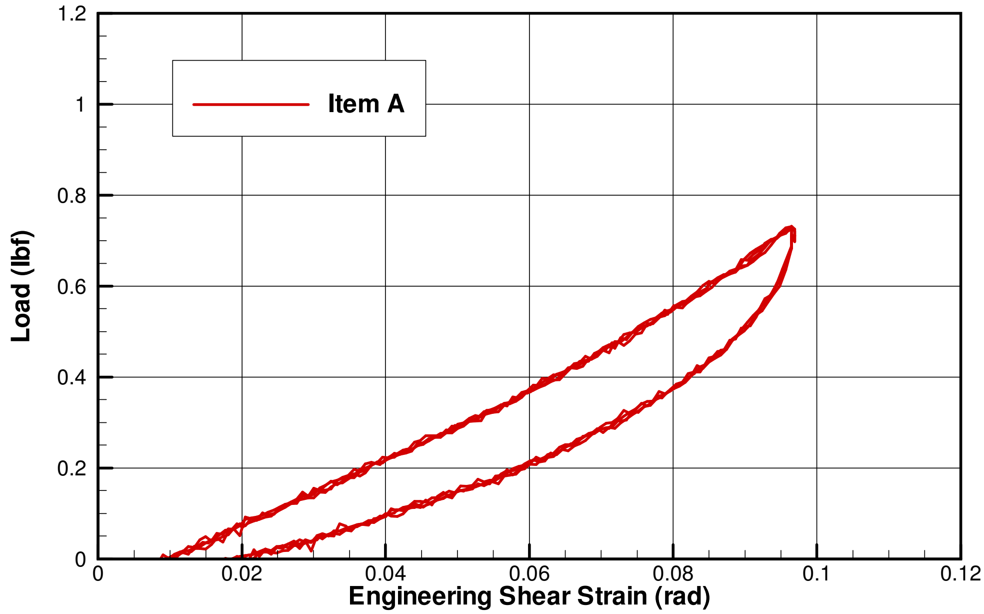

Figure 79: 200 denier Kevlar bias extension test, cycles 2 through 5.

6.2.4 840 Denier Kevlar Bias Extension Testing

The 840 denier Kevlar bias extension shear stiffness behavior for the shear strain interval [0, 0.097] rad is shown in Figure 80 through Figure 82. Figure 80 shows the ramp up for the first load cycle of all samples tested. Figure 81 shows the shear stiffness results for the fifth load cycle. Similar to the Nomex and 200 denier Kevlar, the first cycle load versus shear strain response during the ramp up for the 840 denier Kevlar was predominantly linear. The first load cycle resulted in a shear strain set that was approximately 10% of the maximum induced shear strain of the cycle. Figure 82 shows load cycles 2 through 5 for one of the samples tested. From this figure we see that subsequent cycling had no effect on the shear stiffness in this strain range. The load cycles do exhibit some degree of hysteresis in the stress-strain response.

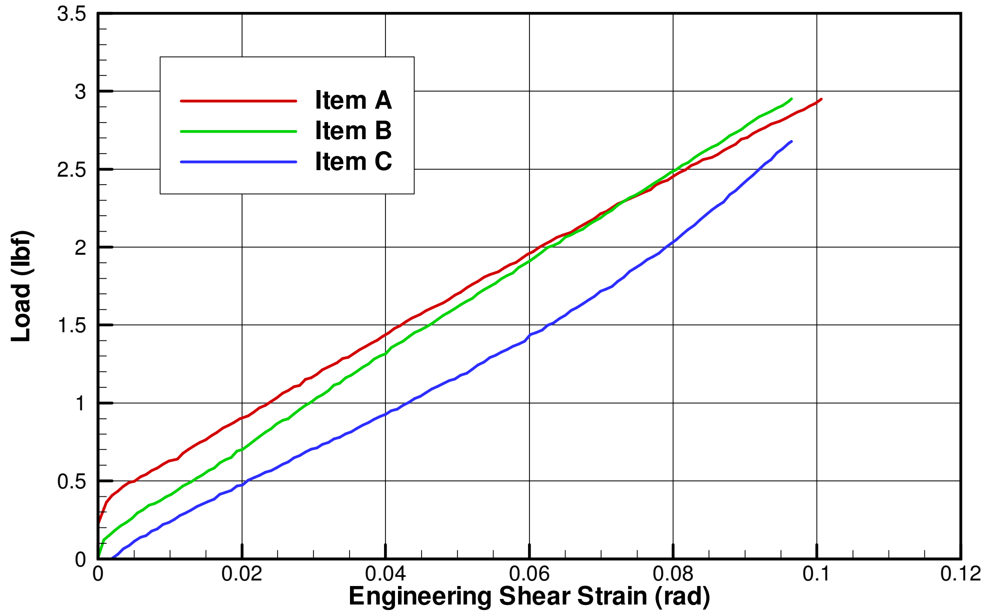

Figure 80: 840 denier Kevlar bias extension test, load ramp up cycle 1.

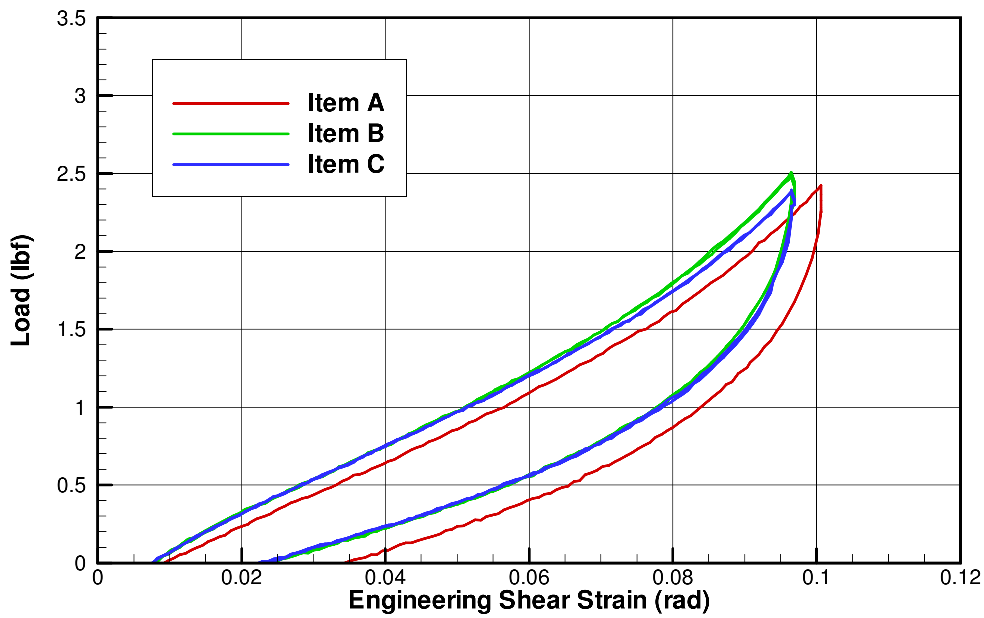

Figure 81: 840 denier Kevlar bias extension test, load cycle 5.

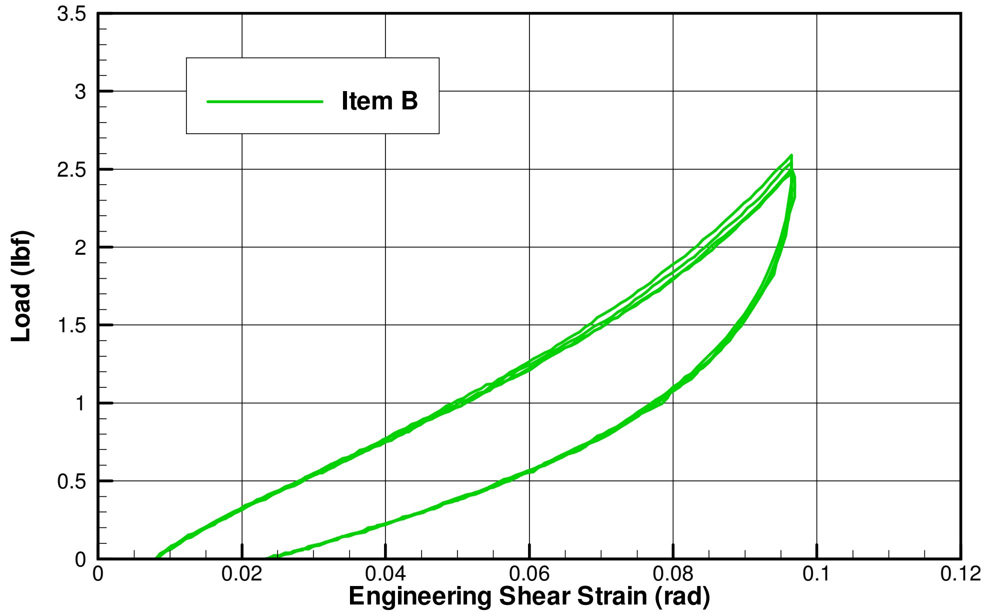

Figure 82: 840 denier Kevlar bias extension test, cycles 2 through 5.

6.3 Inflated Cylinder Testing

Inflated cylinder torsion test results are presented in the next two sub sections for the HT1 Nomex and 200 Denier Kevlar materials. During the experimental program problems developed with the F-111 Nylon and 840 denier Kevlar materials. The F-111 material tested as part of the Isotensoid program had a very light coating applied as discussed in Section 3.4. As a result of the coating problems discussed in this section we were not able to coat the F-111 material for this task. Without the coating, the F-111 Nylon cylinders could not hold pressure in the testing. The 840 denier Kevlar cylinders presented a problem of excess skew in the weave of the fabric. Under just the influence of the inflation pressure the cylinders rotated as much as 20 degrees. This rotation put an offset in the data such that only a small clockwise rotation could be made before the fixture hardware would bottom out. As a result, using this data would most likely misrepresent the properties of the material. The numerical data for these 840 denier Kevlar tests has been provided to the customer but shear stress-strain data is not plotted in this report.

The graphs in this section plot shear stress versus shear strain in the material. End cap rotation was converted into engineering shear strain using measurements of the cylinder circumference and length. This was calculated as $\gamma = \frac{r\phi}{L}$ where ϕ = twist angle, r = radius of cylinder, and L = length of cylinder. Applied torque was converted into shear stress using $\tau = \frac{Tr}{J}$ where T = applied torque, r = radius of cylinder, and J = cylinder polar moment of inertia. For the test cylinder, $J = 2\pi r^3$.

Table 7 details the manual measurements made during cylinder testing for circumference and length. With the inflation load we get a hoop and axial preload state which has the effect of increasing the shear stiffness. Testing was conducted at inflation pressures of 1.0 and 7.0 psi.

Table 8 details the hoop stress preload states for these two inflation pressures. During the 7.0 psi testing the torsion cycling resulted in increasing the leakage of the test article. As the leakage increased the pressure fell below 7.0 psi so that a uniform preload state was not maintained. These pressure changes are not shown in the shear stress-strain plots, but are included in the time history data provided to the customer.

Table 7: Manual inflated cylinder measurements.

	Inflation Pressure (psig)	
Measurement	**1.0**	**7.0**
Circumference (inch)		
200 denier Kevlar		
Item A	24.2	24.3
Item B	24.2	24.3
Item C	24.3	24.3
Nomex		
Item A	24.6	25.0
Item B	24.6	25.0
Item C	24.5	24.8
Length (inch)		
200 denier Kevlar		
Item A	19.6	-
Item B	19.6	-
Item C	19.5	-
Nomex		
Item A	19.5	-
Item B	19.7	-
Item C	19.6	-

Table 8: Inflated cylinder preload states.

	Nominal Hoop Stress (lbf/in)	
Test Item	**1 psig**	**7 psig**
200 denier Kevlar		
Item A	3.85	27.06
Item B	3.85	27.11
Item C	3.86	27.06
Nomex		
Item A	3.91	27.85
Item B	3.92	27.85
Item C	3.90	27.63

6.3.1 HT1 Nomex Inflated Cylinder Testing

Figure 83 shows the time history data for the HT1 Nomex cylinder identified as Item B. Between 0.0 and 1000 seconds torque testing was conducted at an inflation pressure of 1.0 psi. From time 1000 to 1600 torque testing was conducted at an inflation pressure of 7.0 psi. The full +/- 70 degree twist angle range of the fixture was used in both cases. Figure 84 shows the shear stress-strain data that was calculated from the torque and twist angle measurements. We see a significant increase in the shear stiffness when changing the pressure from 1.0 to 7.0 psi. The data for test articles Item A and Item C are included in the data set provided to the customer.

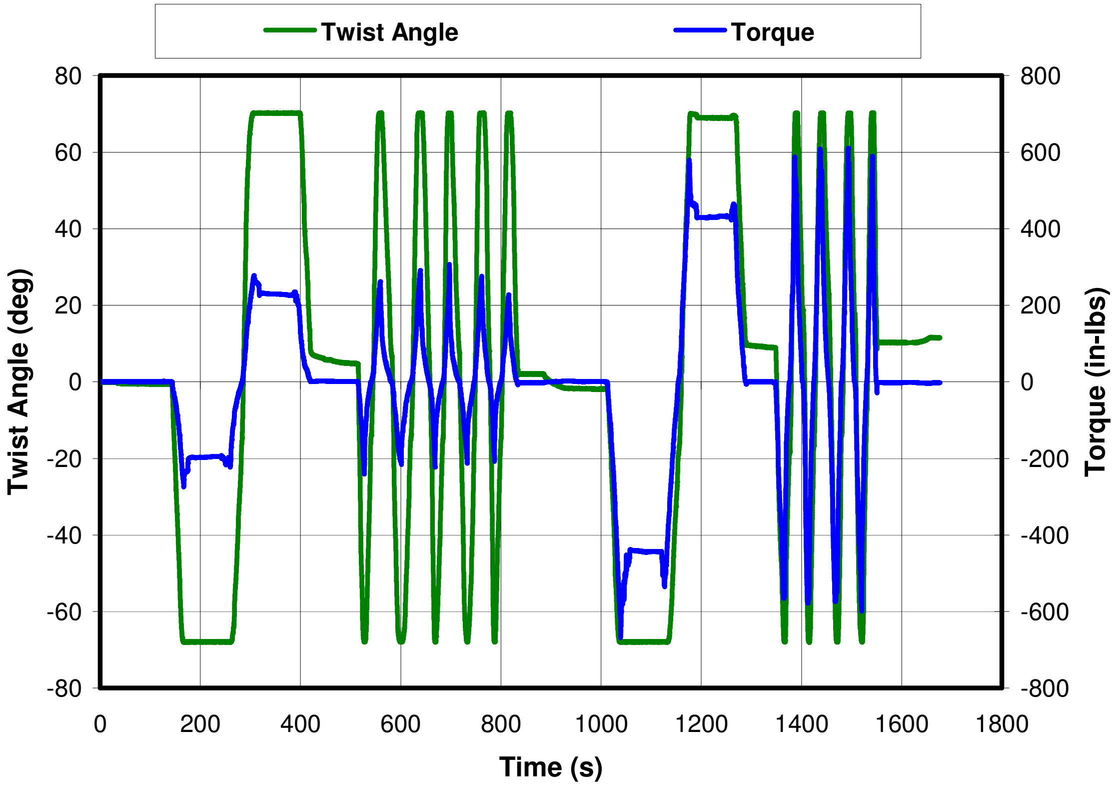

Figure 83: HT1 Nomex inflated cylinder test, Item B time history.

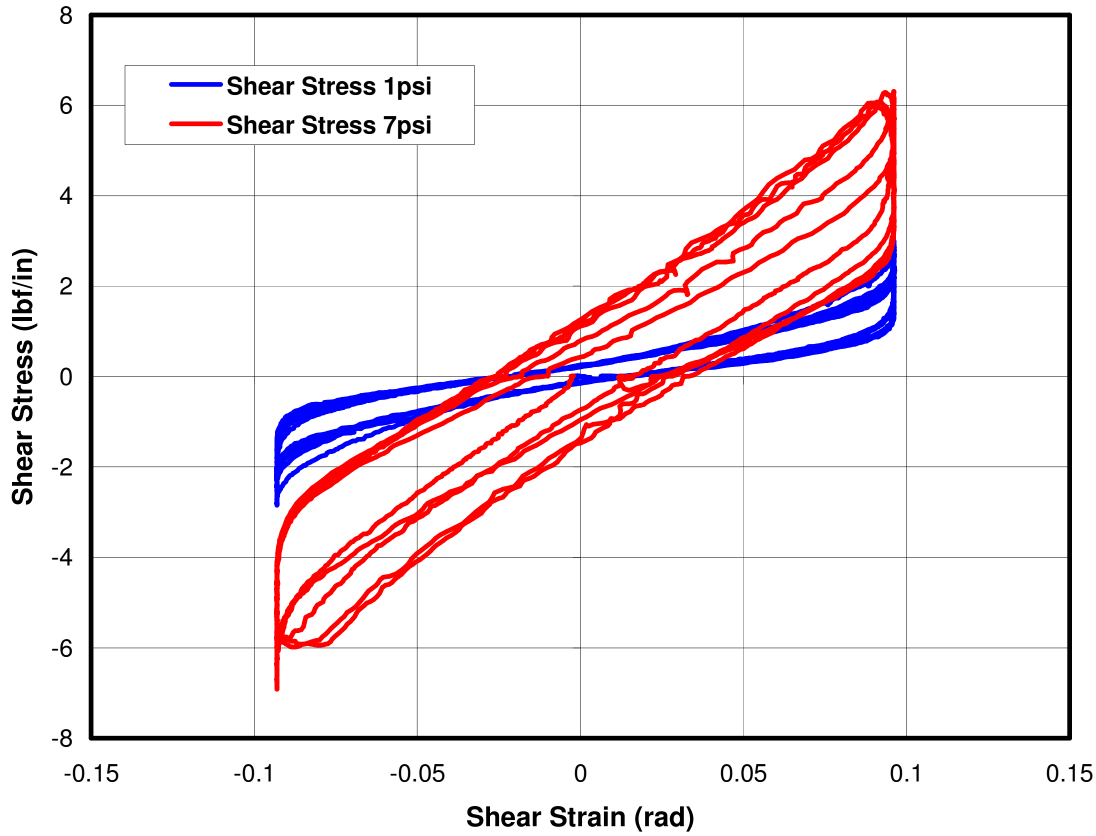

Figure 84: HT1 Nomex inflated cylinder test, Item B shear stress-strain.

6.3.2 200 Denier Inflated Cylinder Testing

Figure 85 shows the time history data for the 200 denier Kevlar cylinder identified as Item B. Between 0.0 and 1000 seconds torque testing was conducted at an inflation pressure of 1.0 psi. From time 1500 to 2500 torque testing was conducted at an inflation pressure of 7.0 psi. The full +/- 70 degree twist angle range of the fixture was used in both cases. Figure 86 shows the calculated shear stress strain data that was calculated from the torque and twist angle measurements. We see a significant increase in the shear stiffness when changing the pressure from 1.0 to 7.0 psi. The data for test articles Item A and Item C are included in the data set provided to the customer.

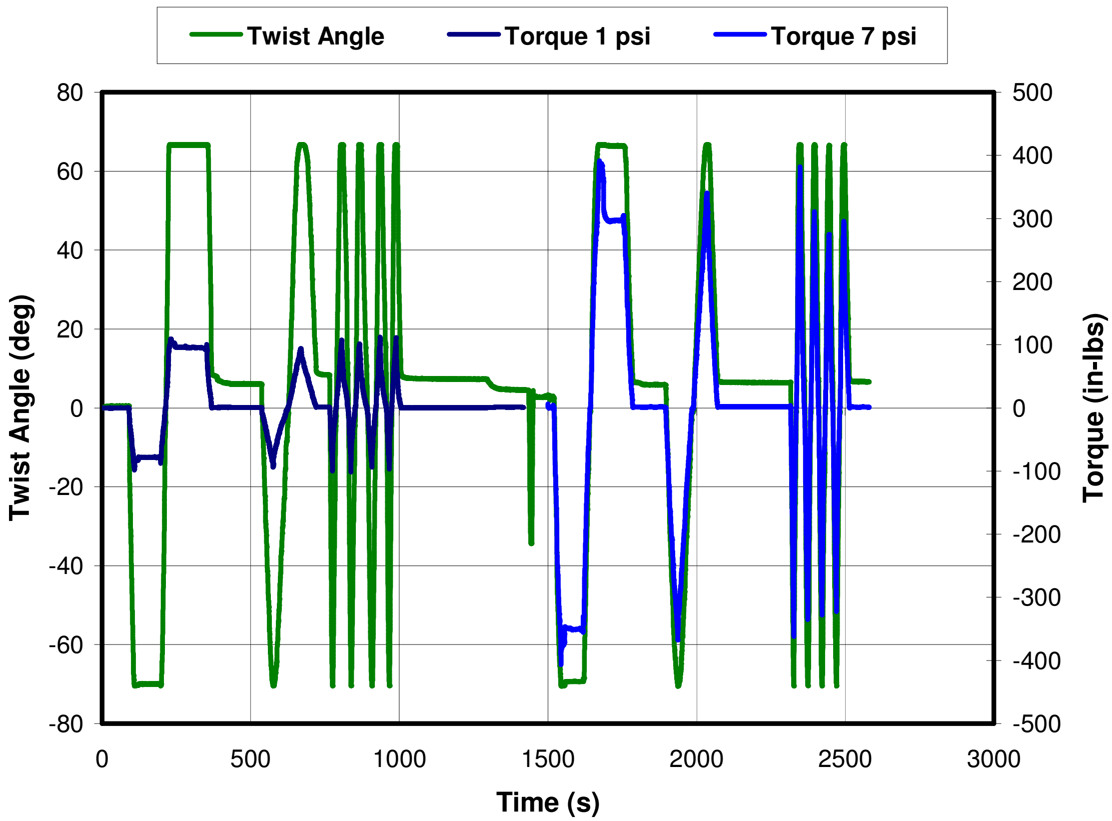

Figure 85: 200 denier Kevlar inflated cylinder test, Item B time history.

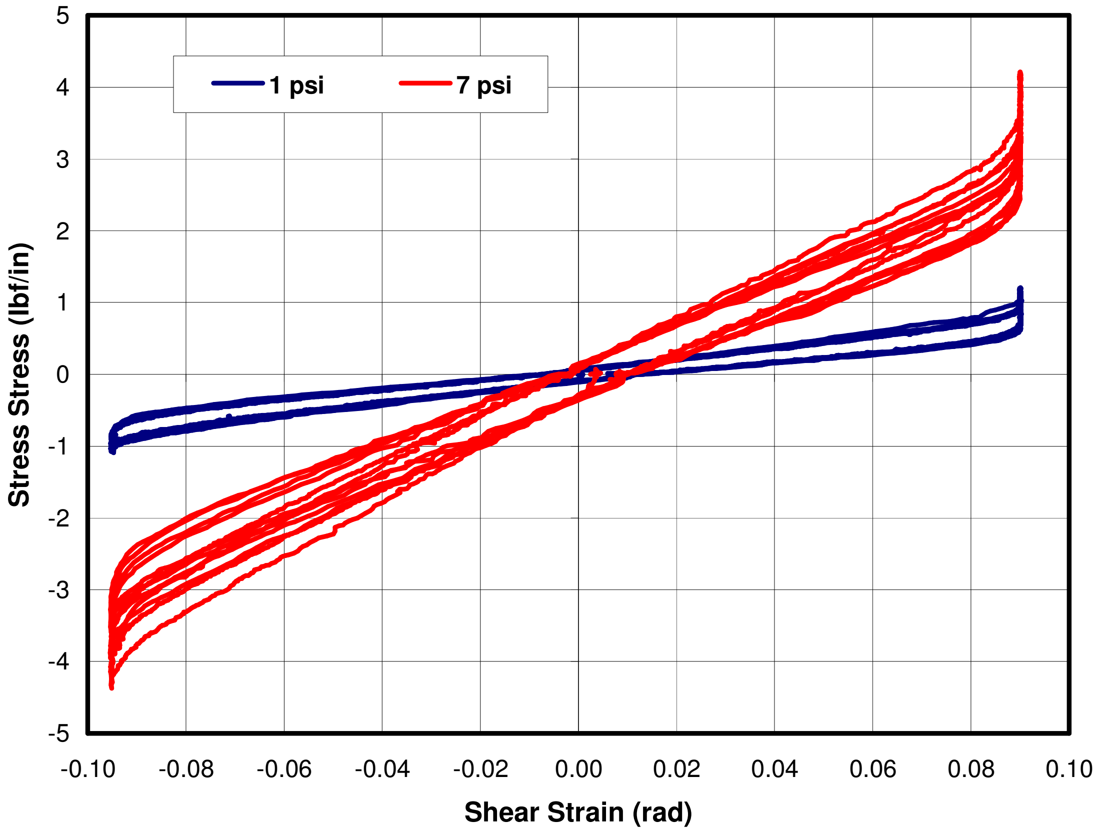

Figure 86: 200 denier Kevlar inflated cylinder test, Item B shear stress-strain.

6.4 Test Recommendations

Based on the material testing and data taken throughout this study, several recommendations for future work were compiled for each test type. This section details the lessons learned and recommendations for future test phases.

Uni-axial testing in this program addressed measurements of hysteresis and strain sets after loading. An additional measurement recommended for future uni-axial testing would be the degree to which the observed strain set is permanent. Samples would have a gauge length marked on them in the axial and lateral directions. After the samples are removed from the INSTRON, the axial and lateral gauge length would be measured as a function of time. This information would be important to better understand the effect of break in cycling of the samples.

For the trellis frame testing, it should be noted that samples were installed on the trellis frame apparatus without any initial tension, per the test procedure. It was difficult to repeatedly install the samples without the presence of some slack in the setup. Ideally, all the points would be planar at the beginning of the test trellis frame shear test. The presence of the slack resulted in out of plane effects that should be able to be quantified once the photogrammetry data is post processed. The presence of this slack also made the no load photogrammetry measurements quite challenging since in the state of slack the sample could be easily be due to small amounts in the out of plane direction. For future efforts with this fixture, some type of tensioning frame is recommended to develop a repeatable minimum load taut condition prior to loading the frame.

The inflated cylinder test articles clearly exhibited circumference changes as the cylinders were torqued. The current procedure could only accommodate manual measurement of the circumference. It is recommended for future testing that a string potentiometer style device be used to measure the circumference in real time and that this data be recorded on the data acquisition system. This improvement would allow more data to be gathered in less time. It would also eliminate the need lock in a specific twist angle while the measurements are conducted.

While conducting the INSTRON testing for the bias extension and trellis frame test samples, the INSTRON crosshead was paused and held constant so that photogrammetry pictures could be taken. A single camera was used and had to be moved between the three planned camera positions. This procedure had many disadvantages relative to accuracy and the labor time to complete the test. While a strain state was locked in, the load dropped off significantly due to inelastic effects that were not desired. This action of pausing the crosshead also was problematic for the INSTRON itself. The INSTRON software had the tendency to crash after a pause interval. A sufficient number of photogrammetry cameras are now available at ILC such that the testing can be conducted without any pauses at all. This improvement will shorten test times and increase the consistency of the trellis frame shear test results.

7. Summary

Textile material load versus elongation characteristics have been experimentally determined for the PAI-DAE program Flexible Material Systems Testing task. This testing was carried out for a set of four materials that have been considered for inflatable aerodynamic decelerators. Uni-axial strip tensile testing was implemented to measure the normal stress-strain behavior of the materials. Three test procedures were implemented to measure the shear stress-strain behavior of the materials. Follow on work in this area could include the following:

- Post processing and analysis of the photogrammetry data taken during the bias extension and picture frame shear testing.
- Review of the macro photography data and correlate the observed weave shear angle with the shear strain calculated from the test data.
- Performance of the iterative curve fitting to establish experimental shear stress data for the bias extension testing.

The results for this work will enhance the predictive capability of inflatable aerodynamic decelerator finite element numerical models by providing this experimental data for the material law implementations. The results will also directly support a ground test program for inflatable decelerator material technology.

---

[i] Reference ASTM D297-93, 16.3 Density by Hydrostatic Method

[ii] Welch, Joseph V., "PAI-DAE Program – Experimental Mechanics Study, Stress-Strain Behavior of Isotensoid Woven Fabric Material," Final Report submitted to NASA Langley Research Center, February 18, 2010.

[iii] Harrison, P., Wiggers, J., Long, A.C., and Clifford. M.J., "Continuous Fiber Reinforced Composites – Determination of the In-plane Shear Stress Response to Shear Strain and Shear Strain Rate, Using the Picture-Frame Test," Internal Test Standard, Polymer Composites Research Group, University of Nottingham, 1st Edition, August 1, 2002.

[iv] Cao, J., et al., "Characterization of Mechanical Behavior of Woven Fabrics: Experimental Methods and Benchmark Results," Composites: Part A, pp 1037-1053, Elsevier, 2008.
[v] Cao, Jian and Peng, Xiongqi, "Bias Extension Test Standard," Advanced Materials Processing Laboratory, Department of Mechanical Engineering, Northwestern University, 8/2003.

REPORT DOCUMENTATION PAGE	*Form Approved* *OMB No. 0704-0188*

1. REPORT DATE *(DD-MM-YYYY)*	**2. REPORT TYPE**	**3. DATES COVERED** *(From - To)*
01- 10 - 2010	Contractor Report	

4. TITLE AND SUBTITLE
Flexible Material Systems Testing

5a. CONTRACT NUMBER
NNL09AC89D

5b. GRANT NUMBER

5c. PROGRAM ELEMENT NUMBER

6. AUTHOR(S)
Lin, John K.; Shook, Lauren S.; Ware, Joanne S.; Welch, Joseph V.

5d. PROJECT NUMBER

5e. TASK NUMBER

5f. WORK UNIT NUMBER
599489.02.07.07.21.21.01

7. PERFORMING ORGANIZATION NAME(S) AND ADDRESS(ES)
NASA Langley Research Center
Hampton, VA 23681-2199

8. PERFORMING ORGANIZATION REPORT NUMBER

9. SPONSORING/MONITORING AGENCY NAME(S) AND ADDRESS(ES)
National Aeronautics and Space Administration
Washington, DC 20546-0001

10. SPONSOR/MONITOR'S ACRONYM(S)
NASA

11. SPONSOR/MONITOR'S REPORT NUMBER(S)
NASA/CR-2010-216854

12. DISTRIBUTION/AVAILABILITY STATEMENT
Unclassified - Unlimited
Subject Category 23
Availability: NASA CASI (443) 757-5802

13. SUPPLEMENTARY NOTES
Final Report
Langley Technical Monitor: Charles J. Player

14. ABSTRACT
An experimental program has been undertaken to better characterize the stress-strain characteristics of flexible material systems to support a NASA ground test program for inflatable decelerator material technology. A goal of the current study is to investigate experimental methods for the characterization of coated woven material stiffness. This type of experimental mechanics data would eventually be used to define the material inputs of fluid-structure interaction simulation models. The test methodologies chosen for this stress-strain characterization are presented along with the experimental results.

15. SUBJECT TERMS
Fabric; Flexible materials; Inflatable decelerator; Stress-strain

16. SECURITY CLASSIFICATION OF:			**17. LIMITATION OF ABSTRACT**	**18. NUMBER OF PAGES**	**19a. NAME OF RESPONSIBLE PERSON**
a. REPORT	**b. ABSTRACT**	**c. THIS PAGE**			STI Help Desk (email: help@sti.nasa.gov)
					19b. TELEPHONE NUMBER *(Include area code)*
U	U	U	UU	74	(443) 757-5802